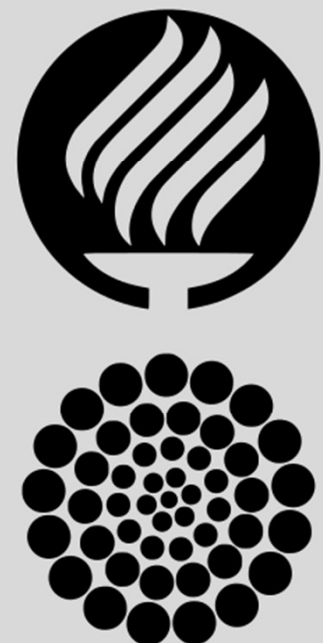


Fabrication of graphitic-carbon suspended nanowires through mechano-electrospinning of photo-crosslinkable polymers



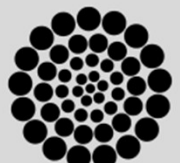
Osamu Katagiri-Tanaka
A01212611@itesm.mx

Principal Advisor: **Dr. Héctor Alán Aguirre Soto**
Co-advisor and Director of Program: **Dra. Dora Iliana Medina Medina**

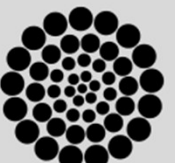
25 Nov 2020

Agenda

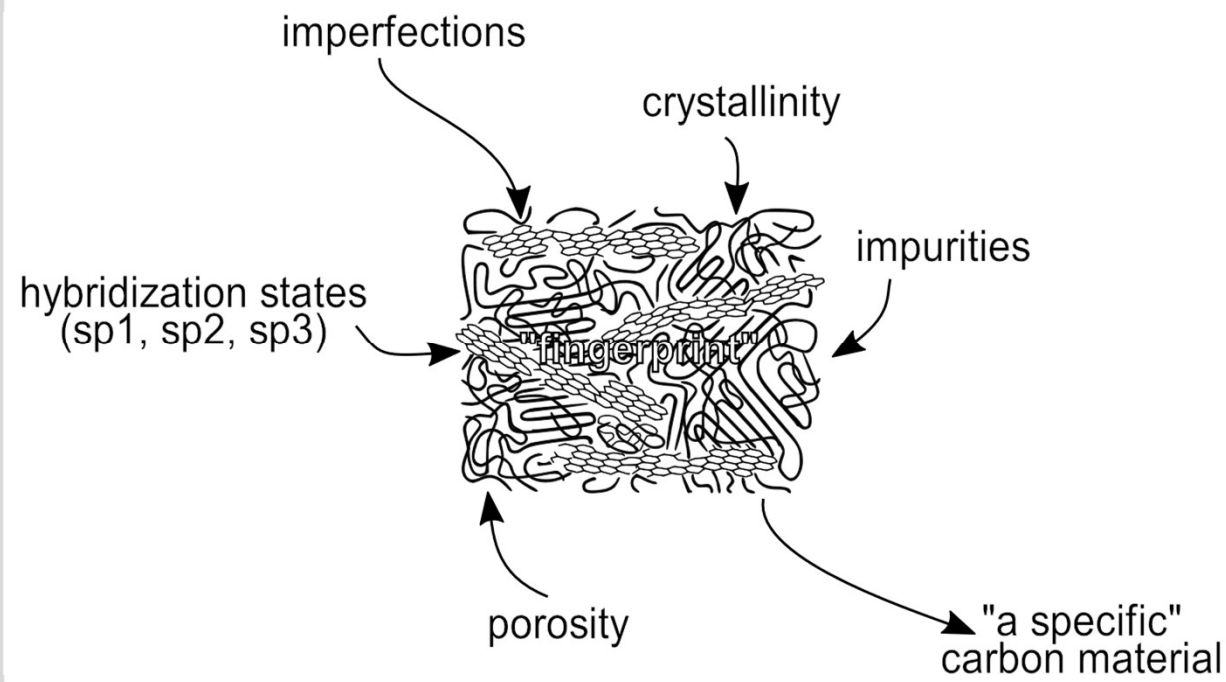
- Motivation & Problem Statement : 10 min
- Objectives : 3 min
- NFES literature review : 10 min
- Rheology Analyses : 10 min
- Fabrication & Characterization : 5 min
- Conclusions & Future Work : 3 min



Motivation & Problem Statement



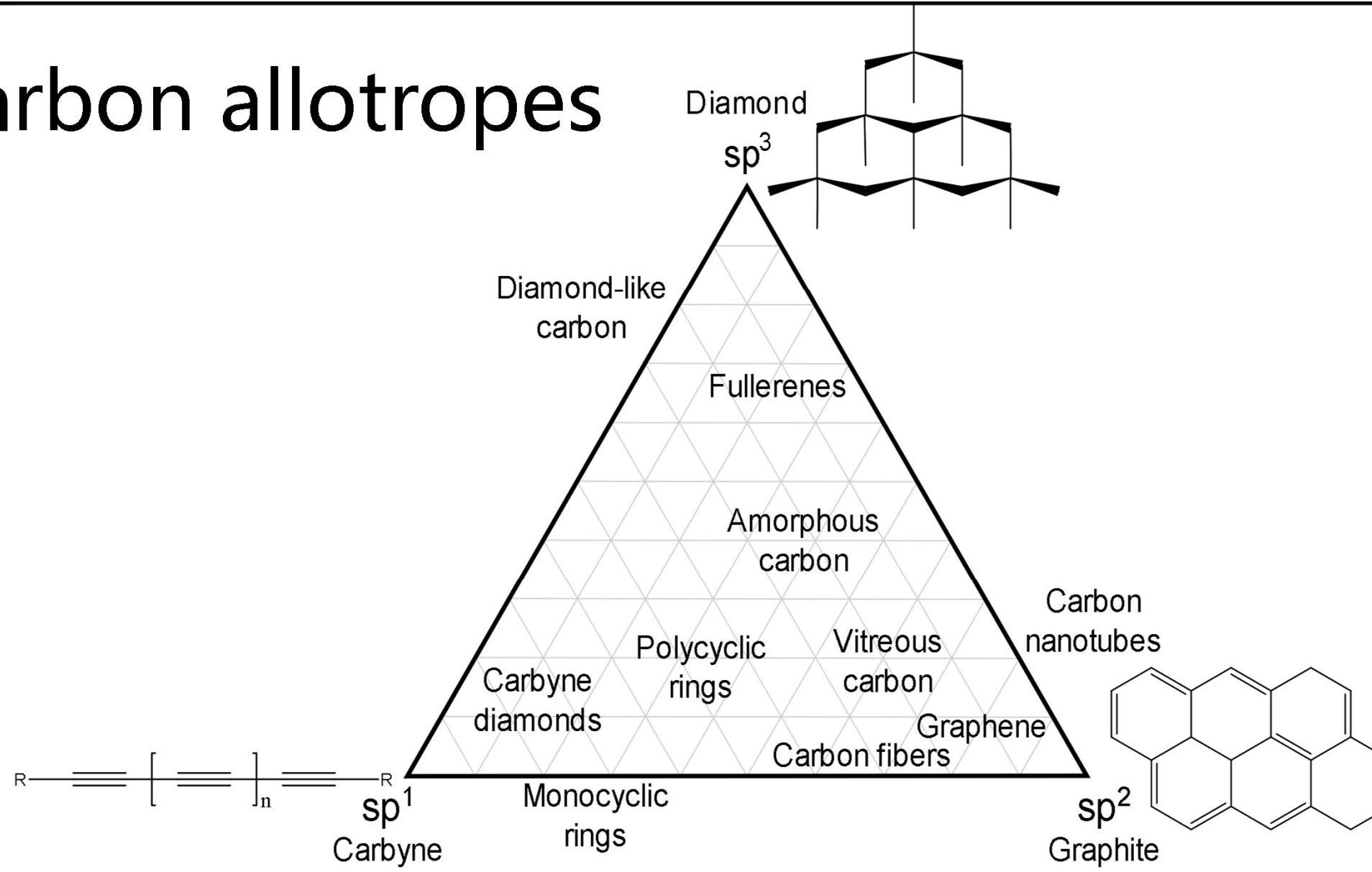
Carbon Based Nanomaterials (CBNs)



The crystallite size, molecular arrangement, and anisotropy determine the material's properties.

The interminable collection of CBNs range from soft, conductive lubricants to very hard, low conductivity solids; and from black colour, bulks to transparent, disordered thin films

Carbon allotropes



R.B. Heimann, S.E. Evsvukov, Y. Koga, Carbon allotropes: a suggested classification scheme based on valence orbital hybridization, *Carbon N. Y.* 35 (1997) 1654–1658.
[https://doi.org/10.1016/S0008-6223\(97\)82794-7](https://doi.org/10.1016/S0008-6223(97)82794-7).

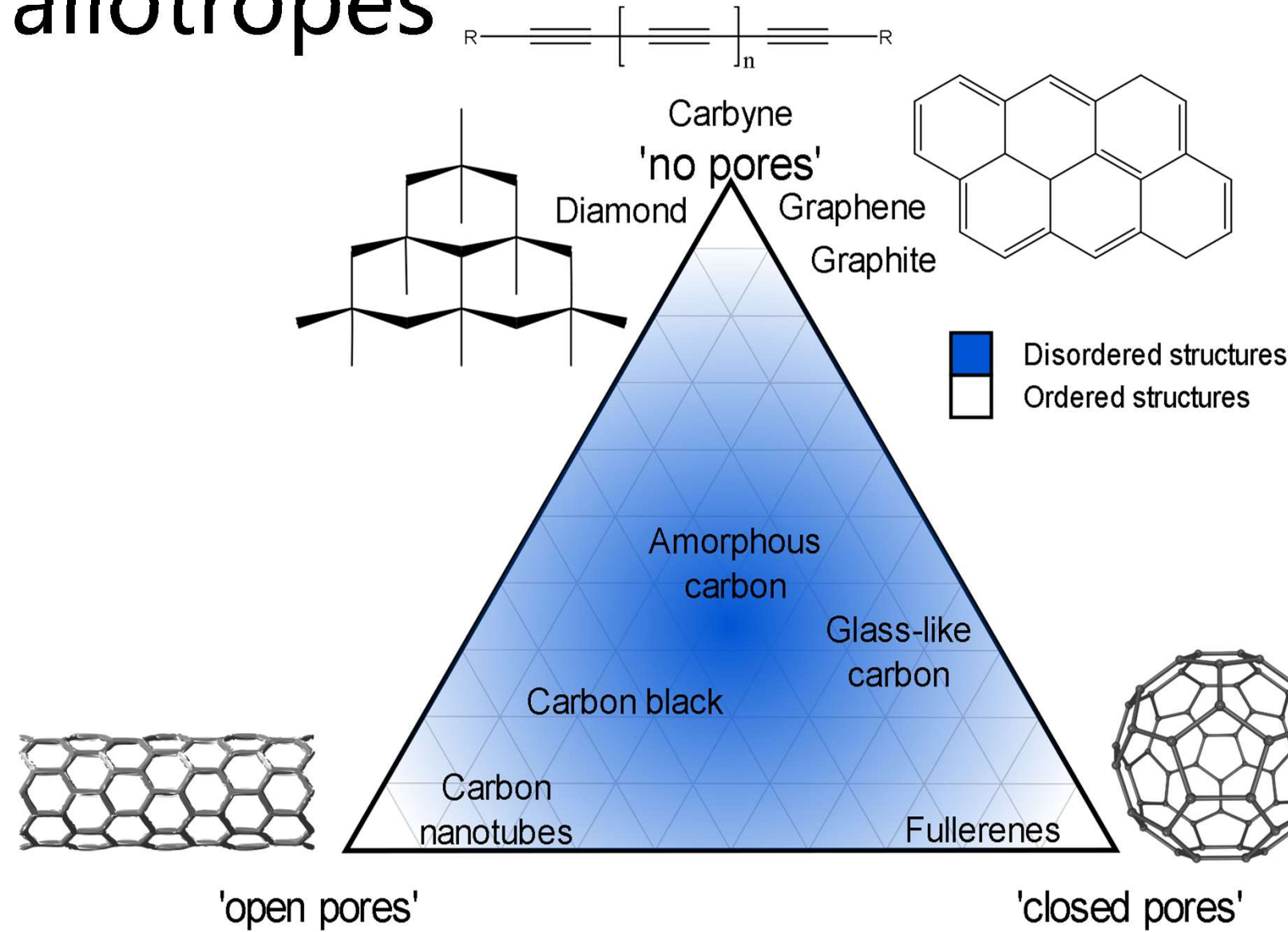
E.A. Belenkov, Classification of carbon structures, in: *Carbon Nanotub. Graphene*, Chelyabinsk State University, Chelyabinsk, Russia, 2003: p. 5.

M. Fedel, Blood compatibility of diamond-like carbon (DLC) coatings, in: *Diamond-Based Mater. Biomed. Appl.*, Elsevier, 2013: pp. 71–102. <https://doi.org/10.1533/9780857093516.1.71>.

M. Razeghi, *Fundamentals of Solid State Engineering*, Springer International Publishing, Cham, 2019. <https://doi.org/10.1007/978-3-319-75708-7>.

K. Alstrup Jensen, J. Bøgelund, P. Jackson, N. Raun Jacobsen, R. Birkedal, P. Axel Clausen, A. Thoustrup Saber, H. Wallin, U. Birgitte Vogel, *Carbon nanotubes - Types, products, market, and provisional assessment of the associated risks to man and the environment*, The Danish Environmental Protection Agency, 2015.

Carbon allotropes



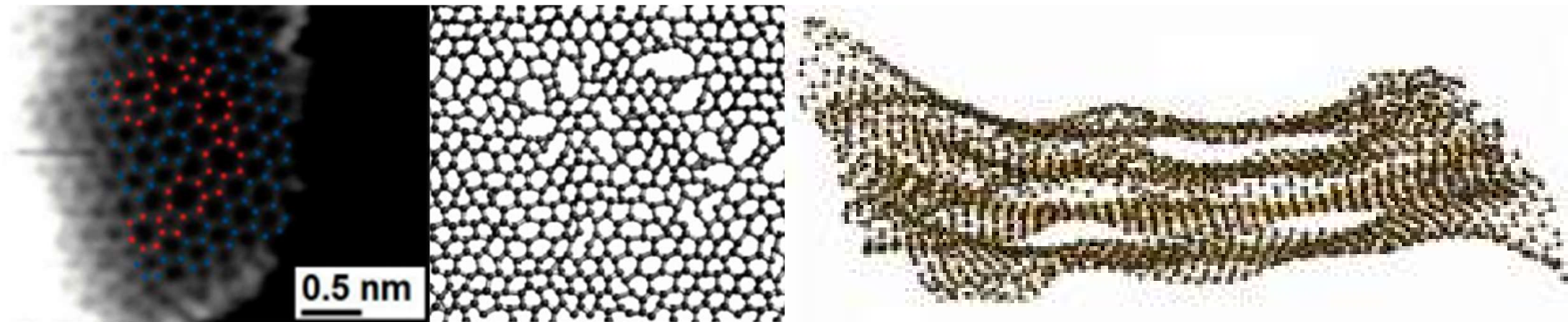
R.L. McCreery, Advanced Carbon Electrode Materials for Molecular Electrochemistry, Chem. Rev. 108 (2008) 2646–2687. <https://doi.org/10.1021/cr068076m>.

S. Beigi-boroujeni, O. Katagiri-tanaka, B. Cardenas-benitez, O. Sergio, A. Aguirre-soto, Pyrolytic Carbon from Novolac Epoxy Resin Compressed before Photocrosslinking and Pyrolysis, Mater. Today Proc. (2020).

Harry Marsh. Introduction to Carbon Science. Vol. 46. 1. Elsevier, Apr. 1989, p. 43. ISBN: 9780408038379. DOI: 10.1016/C2013-0-04111-4. URL: <https://linkinghub.elsevier.com/retrieve/pii/C20130041114>.

Pierson Hugh. Handbook of Carbon, Graphite, Diamonds and Fullerenes. Elsevier, 1994, p. 419. ISBN: 9780815513391.

Glass-like Carbon



Attractive for its electrochemical stability, thermal resistance, electrical conductivity, biocompatibility and is gas impermeable.

- It is used in the manufacture of semiconductors.

MicroChem's SU-8 & Tokai's recipe

Electrical resistivity, comparison:

highly oriented
pyrolytic graphite
(HOPG)

<
 $\times 10^3$

TOKAI Glassy
carbon

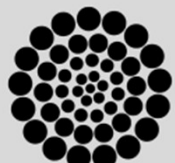


<
 $\times 4$

SU-8 glass-like
carbon



Tokai's recipe is a secret ...



MicroChem's SU-8 & Tokai's recipe

SU-8
glass-like
carbon
resistivity:

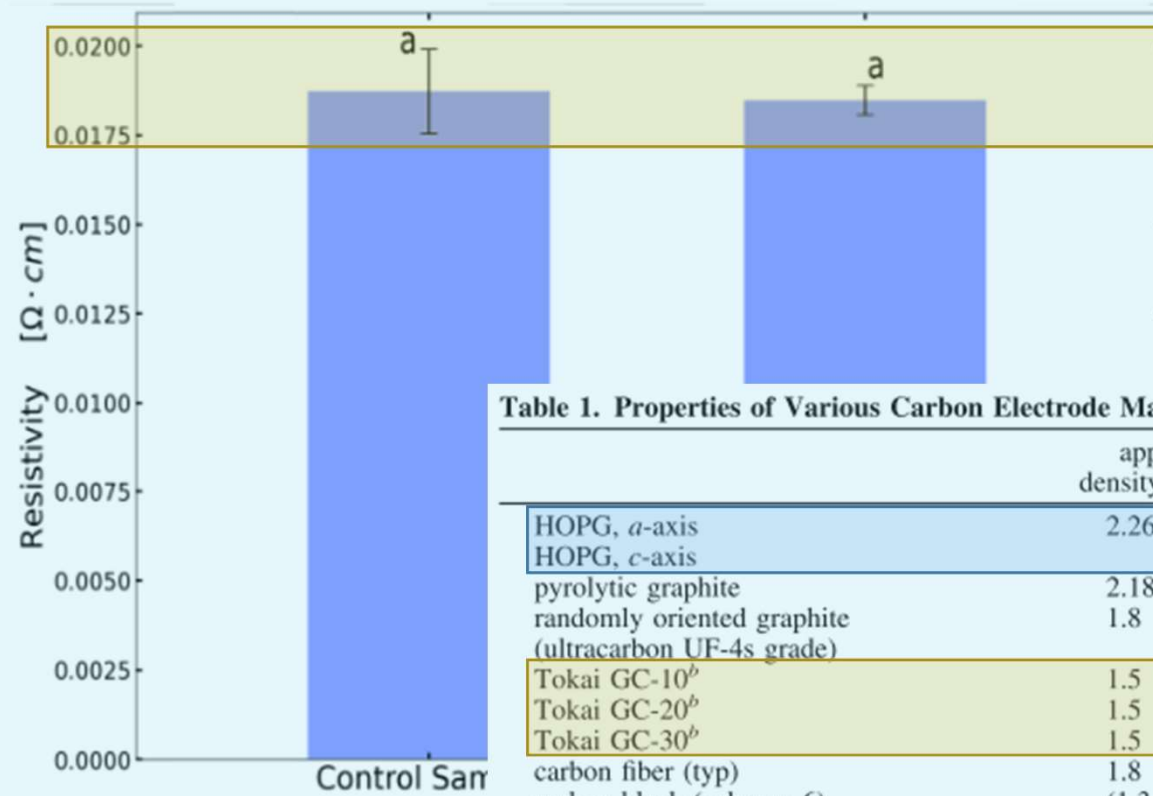


Figure 4. Bulk resistivity of carbon sheets derived from pyrolysis treatment as obtained from the fo

Table 1. Properties of Various Carbon Electrode Materials³

	apparent density (g/cm^3)	d_{002} (\AA)	ρ ($\Omega \cdot \text{cm}$)	L_a (\AA)	L_c (\AA)
HOPG, <i>a</i> -axis	2.26	3.354	4×10^{-5}	> 10000	
HOPG, <i>c</i> -axis			0.17		> 100000
pyrolytic graphite	2.18	3.34		1000 (typ) ^a	1000 (typ)
randomly oriented graphite (ultracarbon UF-4s grade)	1.8	3.35	1×10^{-3}	300 (typ)	500 (typ)
Tokai GC-10 ^b	1.5	3.49	4.5×10^{-3}	20 (typ)	-10
Tokai GC-20 ^b	1.5	3.48	4.2×10^{-3}	25 (typ)	12
Tokai GC-30 ^b	1.5	3.41	3.7×10^{-3}	55	70
carbon fiber (typ)	1.8	3.4	$(5-20) \times 10^{-4}$	> 100	40
carbon black (spheron 6)	(1.3–2.0) ^c	3.55	0.05	20	13
evaporated a-C	-2.0	>3.4	$\sim 10^3$	~ 10	~ 10
a-C:H	1.4–1.8		$10^7 - 10^{16}$		
pyrolyzed photoresist film (PFF)			0.006 ¹⁴⁹		
boron-doped diamond			0.05–0.5 ^d		
N-doped amorphous tetrahedral carbon			10–1000 ^e		

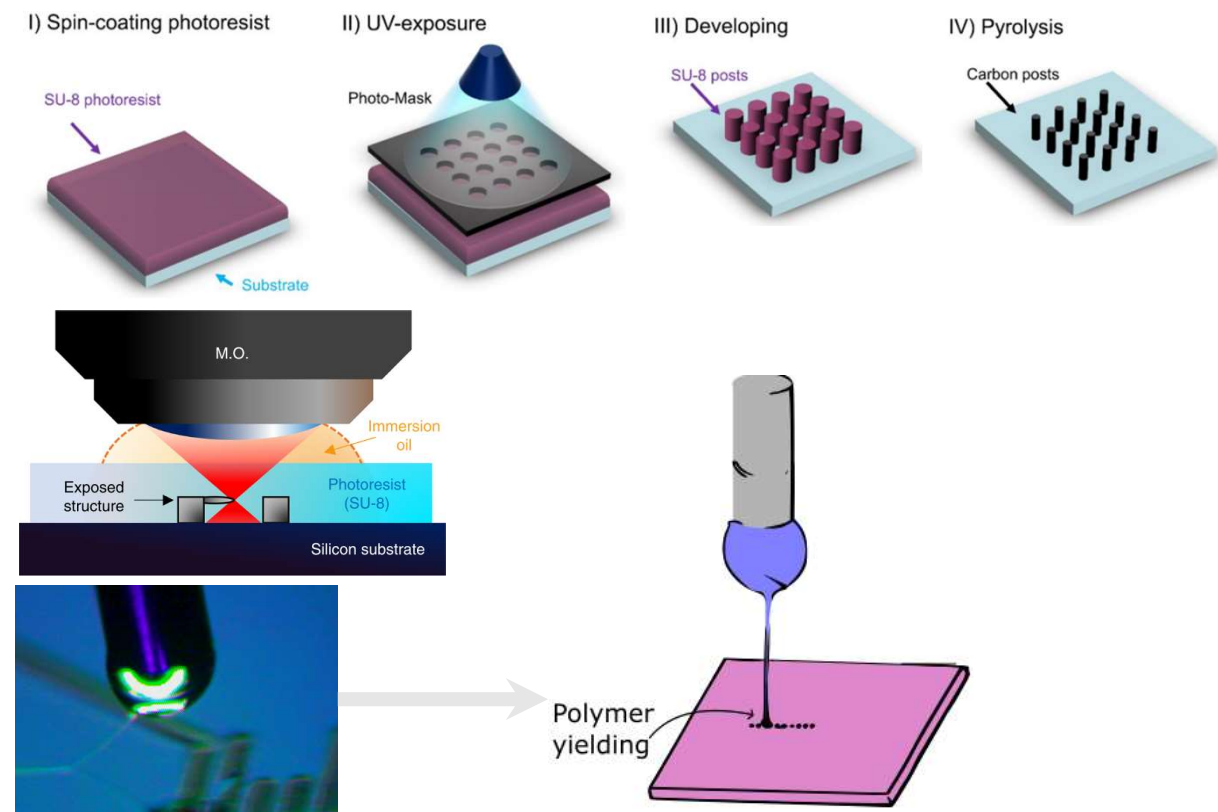
^a Entries marked "typ" may vary significantly with sample or preparation procedures. ^b Number refers to heat treatment temperatures, for example, GC-20 was treated at 2000 °C. ^c Depends on technique used to measure density. ^d Depends strongly on doping level. See ref 30. ^e See ref 35.

Current approaches

Photolithography Physical & Optical Limitations

Two-Photon Polymerization (TPP)
Slow (mm per sec) & **Expensive**

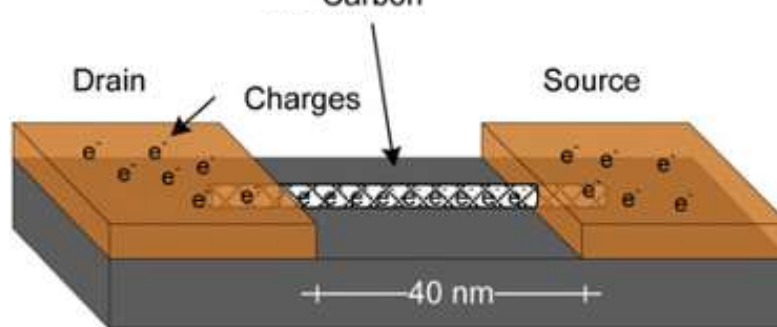
***Near-Field Electrosinning** (NFES)
Suspended Nanowires w/Spatial Control



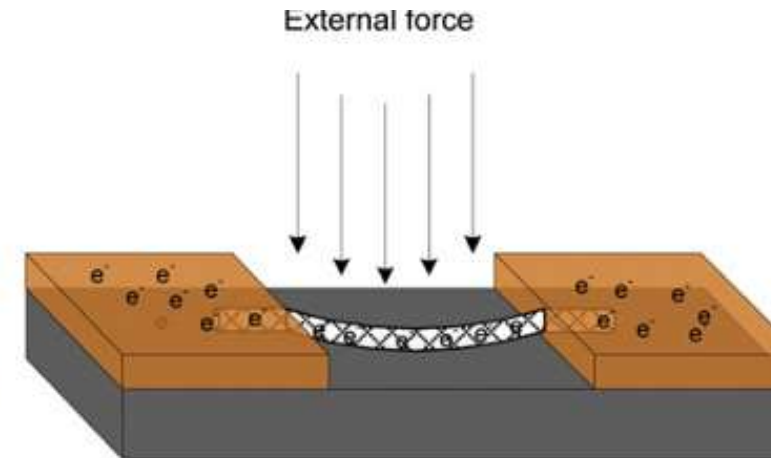
V. Galstyan, M. Bhandari, V. Sberveglieri, G. Sberveglieri, E. Comini, Metal Oxide Nanostructures in Food Applications: Quality Control and Packaging, Chemosensors. 6 (2018) 16. <https://doi.org/10.3390/chemosensors6020016>.

D. Kluge, J.C. Singer, B.R. Neugirg, J.W. Neubauer, H.-W. Schmidt, A. Fery, Top-down meets bottom-up: A comparison of the mechanical properties of melt electrospun and self-assembled 1,3,5-benzenetrisamide fibers, Polymer (Guildf). 53 (2012) 5754–5759. <https://doi.org/10.1016/j.polymer.2012.10.016>.

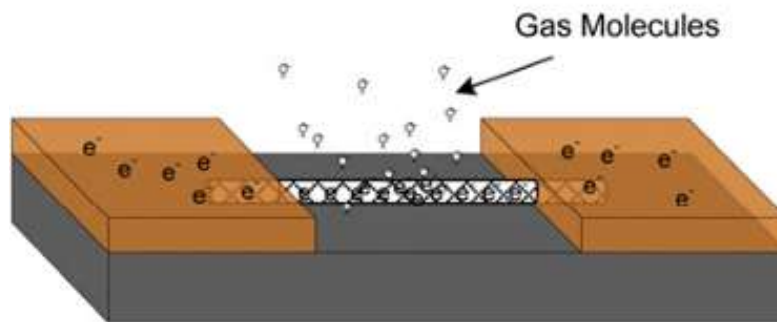
Glass-like Carbon NWs: Applications



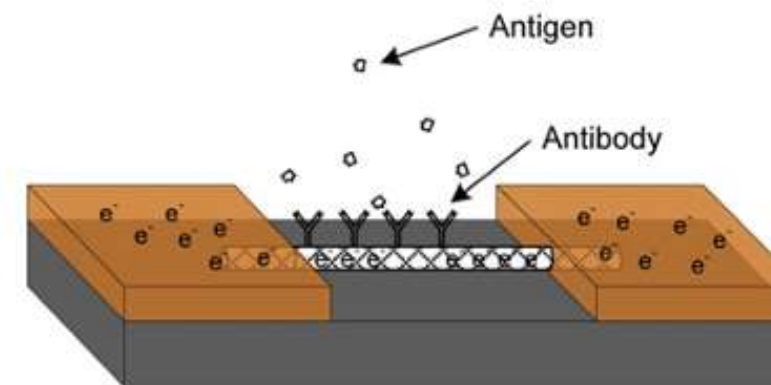
CNT-based FET transistor.



Physical nanosensor.



Chemical nanosensor.



Biological nanosensor.

V. Baudrit J, Recycling and Elimination of Wastes obtained from Agriculture by using Nanotechnology: Nanosensors, Int. J. Biosens. Bioelectron. 3 (2017) 368–375. <https://doi.org/10.15406/ijbsbe.2017.03.00084>.

R.L. McCreery, Advanced Carbon Electrode Materials for Molecular Electrochemistry, Chem. Rev. 108 (2008) 2646–2687. <https://doi.org/10.1021/cr068076m>.

G. Speranza, The Role of Functionalization in the Applications of Carbon Materials: An Overview, C — J. Carbon Res. 5 (2019) 84. <https://doi.org/10.3390/c5040084>.

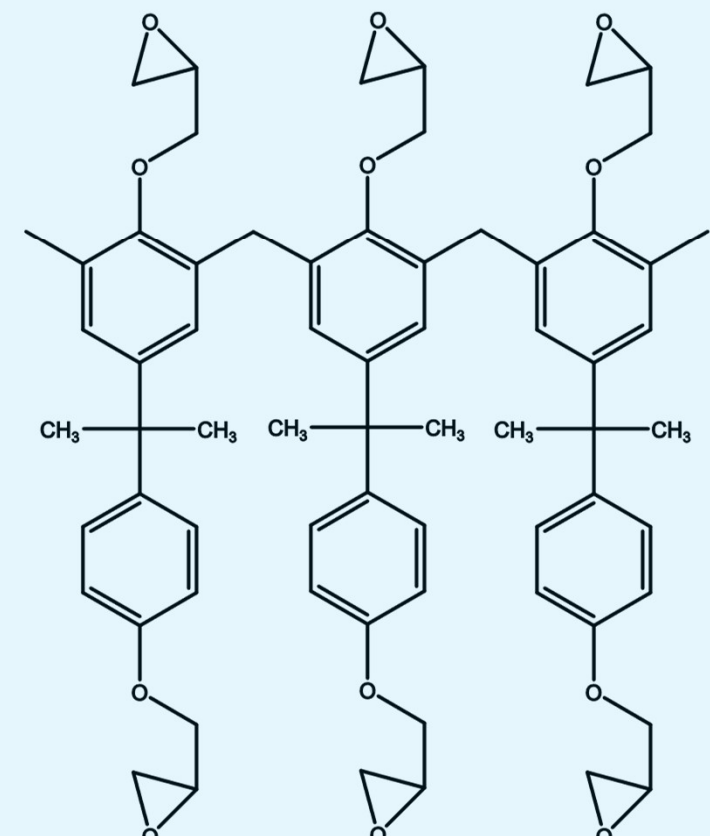
MicroChem's SU-8

Pyrolysis of SU8 is currently the typical method to produce glass-like carbon.

1. Polymer patterning through **photolithography**
2. Carbonization through **pyrolysis**

However, **photolithography generates waste** in the spin-coating and developing steps. Also, it presents **structural limitations**.

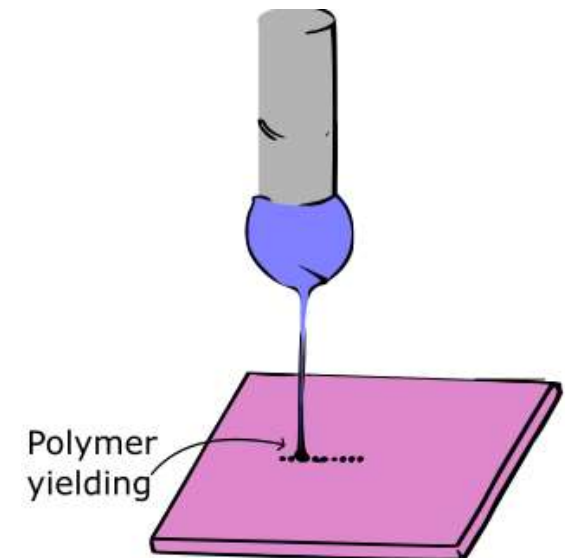
Limitations can be overcome with other fabrication techniques, such as **NFES**



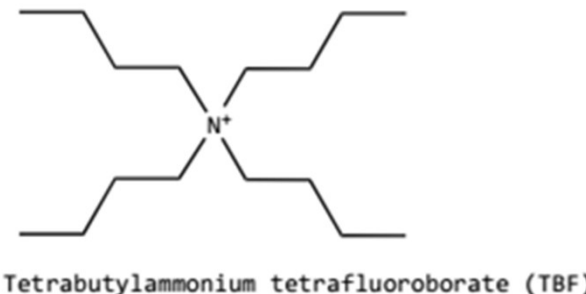
Structure of SU-8 after UV exposure

MicroChem's SU-8

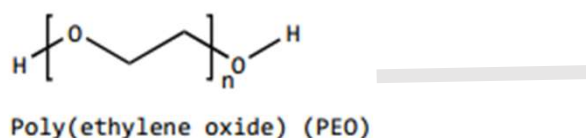
However, SU-8 **as is** is not electrospinnable
SU-8 does not have the right viscosity & solution conductivity.
SU-8 is design for photolithography.



SU-8 + TBF + PEO



→ To increase the **solution conductivity**



→ To provided the required **viscosity**

... both needed for **smooth PEO flow** during electrospinning

NFES Process Parameters

- Properties of an electrospun fiber depend on many parameters,
- and each parameter also depends on the polymer-solvent system.

Solution Parameters:

- Concentration
- Molecular weight
- Viscosity
- Electrical conductivity

Ambient Parameters:

- Humidity
- Temperature

Process Parameters:

- Applied Voltage
- Flow rate
- Working distance



The interdependence between the process and solution parameters presents a **challenge to predict the fiber morphology**.

Best Results so far by NFES (previous work)

Fiber yield rate of 81 %

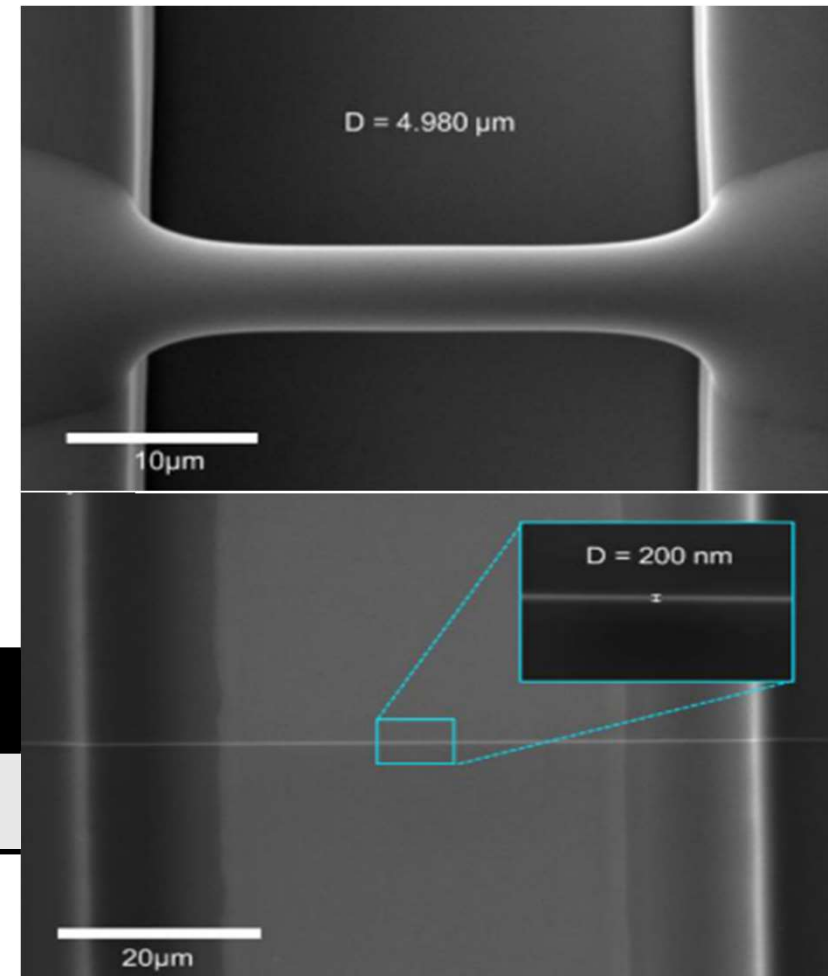
Fiber diameter before pyrolysis of $4.966 \mu\text{m}$

Fiber diameter after pyrolysis of 204 nm

Fiber length of $60.5 \pm 4.3 \mu\text{m}$

Fiber resistance from $407 \text{ K}\Omega$ to $1.727 \text{ M}\Omega$

wt% PEO	SU-8 2002 [mg]	PEO [mg]	TBF [mg]
0.25	2246	5.65	11.32

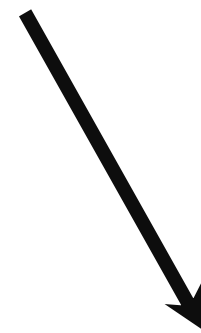


Methods: Implications of PEO

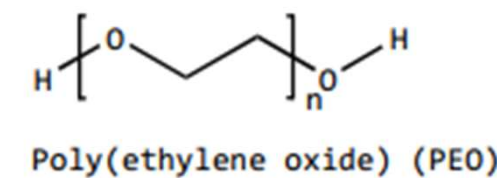
The **fiber yield rate** and **fiber conductivity** are impacted negatively as PEO introduces more oxygen to the solution



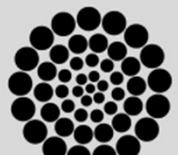
Some samples are destroyed during pyrolysis



High variance in the obtained conductivity across samples.



The addition of oxygen decreases the char yield.



Objectives

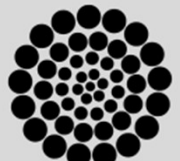


Objectives

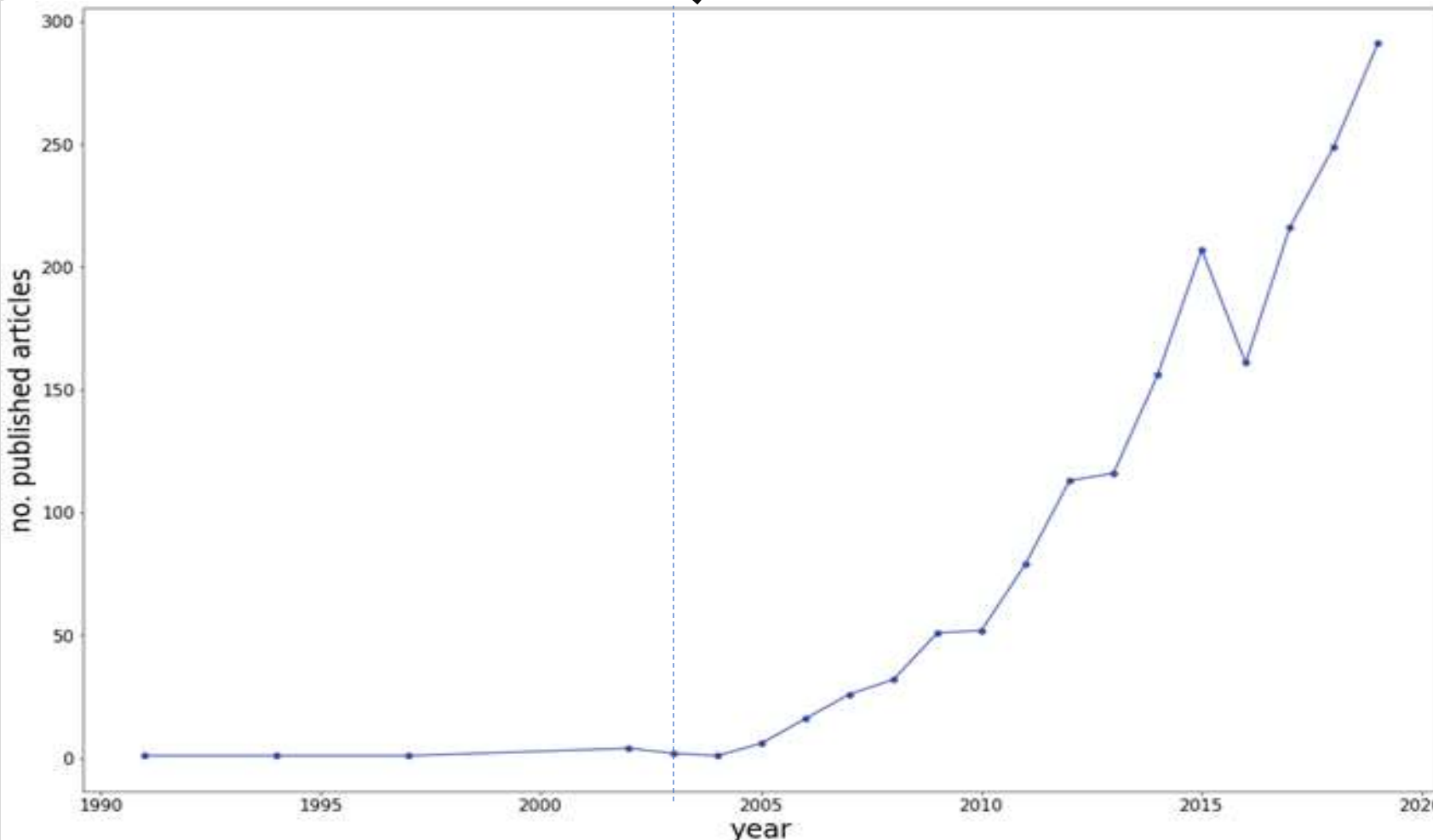
- General. Formulate polymer/solvent combinations that have the greatest potential to replace or modify the SU-8/PEO formulation for the fabrication of microscopic polymer fibers that may be converted to conductive suspended carbon nano-wires.
- Specific1. Learn how the diameter of the electrospun polymer fiber can be controlled by appropriate tuning of the **NFES parameters and solution properties**.
- Specific2. Through **rheological analyses**, determine if polymer solutions have comparative viscoelastic properties to those of the SU-8/PEO benchmark, and if they can be easily electrospun by NFES.
- Specific3. Propose **alternatives to the SU-8/PEO benchmark** formulation for the production of microscopic polymer fibers with potential for the fabrication of carbon nano-wires.

Specific Objective 1. Learn how the diameter of the electrospun polymer fiber can be controlled by appropriate tuning of the **NFES parameters and solution properties.**

NFES literature review



Methods: NFES literature (first NFES apparatus built in 2003 by J. Kameoka et al.)

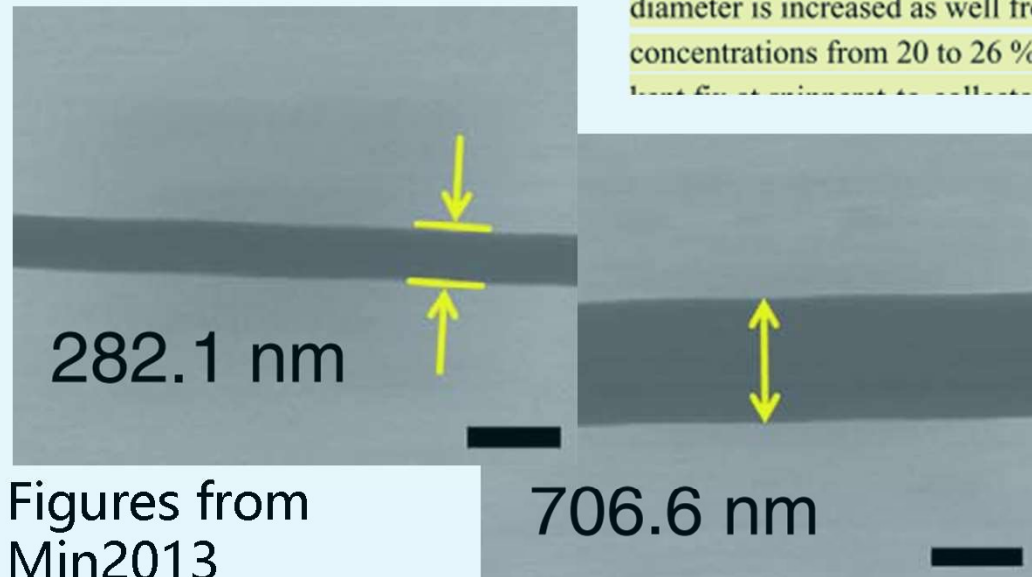


Thinnest fiber achieved by C. Chang et al. with ~50 nm in diameter. (PEO in water)

However, **fiber yield rate** was not reported

Methods: Data collection (analysis of NFES articles from 2003 to 2020)

The author mentions the process parameters and fiber properties within the article **in writing**.



Published in final edited form as:

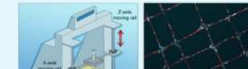
Adv Healthc Mater. 2017 October ; 6(19): . doi:10.1002/adhm.201700456.

Fattahi2017

3D Near-Field Electrospinning of Biomaterial Microfibers with Potential for Blended Microfiber-Cell Loaded Gel Composite Structures

PMMA microfibers. First, we varied the concentration of PMMA in nitromethane from 16 to 24 % (W/V) and observed as the PMMA concentration increased the polymer fiber diameter is increased as well from 1.86 ± 0.41 to 4.73 ± 1.40 μm corresponding to concentrations from 20 to 26 % (W/V, PMMA/nitromethane) while other parameters were

polymeric fibers in highly organized, controlled and reproducible manner. The research strategy described in this work offers several significant advantages including: 1) producing precise patterns of fibers on relatively large scale area with minimum material consumption, 2) ability to print in all three directions of X, Y and Z, 3) offering an inexpensive method with easy control over shape and orientation of fibers compared to other available methods, and 4) readily combines with other pre-patterned nanostructures or microstructures such as gels (e.g. collagen gel) to create multi-material composites.



Methods: Data collection (analysis of NFES articles from 2003 to 2020)

The author provides the data in **plots and graphs**.

WebPlotDigitalizer (<https://github.com/ankitrohatgi/WebPlotDigitizer>):

panels a to c when the voltage is switched from 400 to 200 V in steps of 100 V. The light against the smooth Si surface. X-Y stage speed is 40 mm/s.

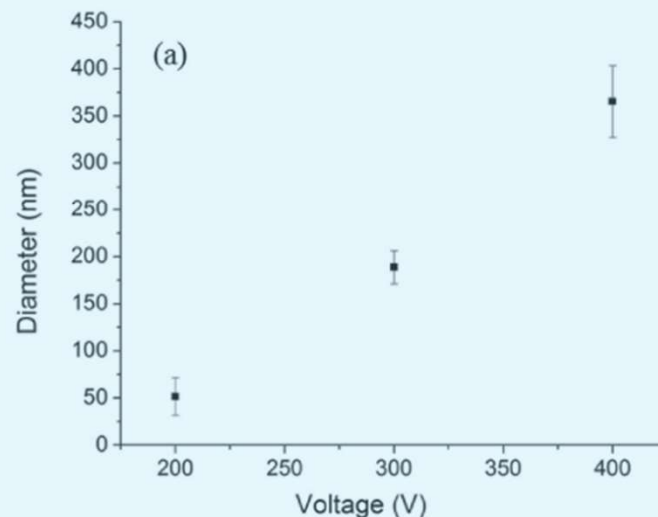
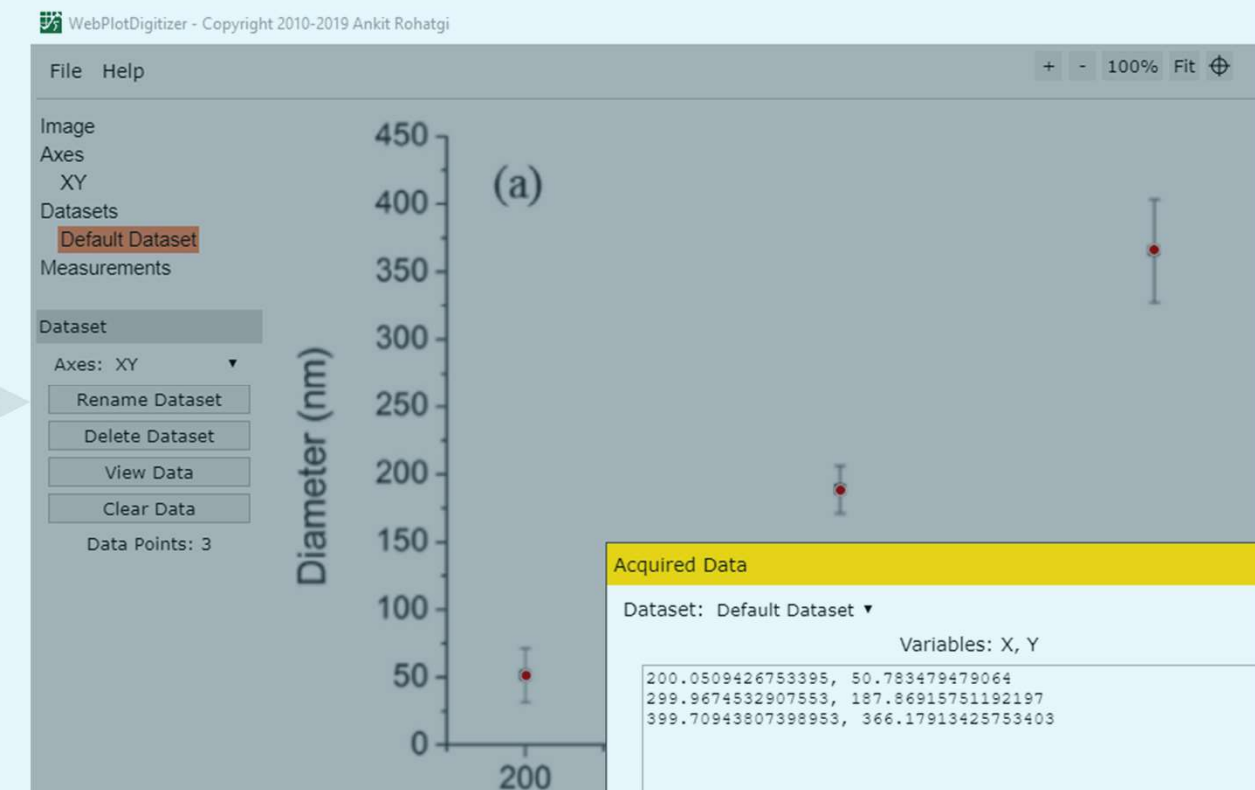


Figure 6. Correlation between nanofiber thickness and voltage applied between electrodes.

M.J. Madou, D. Dunn-Rankin, L. Kulinsky, A. Mirsepassi, G.S. Bisht, S. Oh, G. Canton, Controlled Continuous Patterning of Polymeric Nanofibers on Three-Dimensional Substrates Using Low-Voltage Near-Field Electrospinning, *Nano Lett.* 11 (2011) 1831–1837. <https://doi.org/10.1021/nl2006164>.

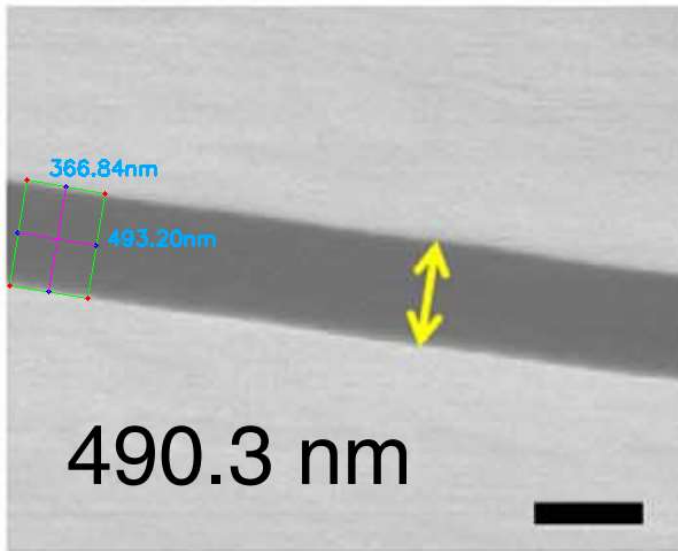


Applied voltage vs. fiber diameter by Madou2011

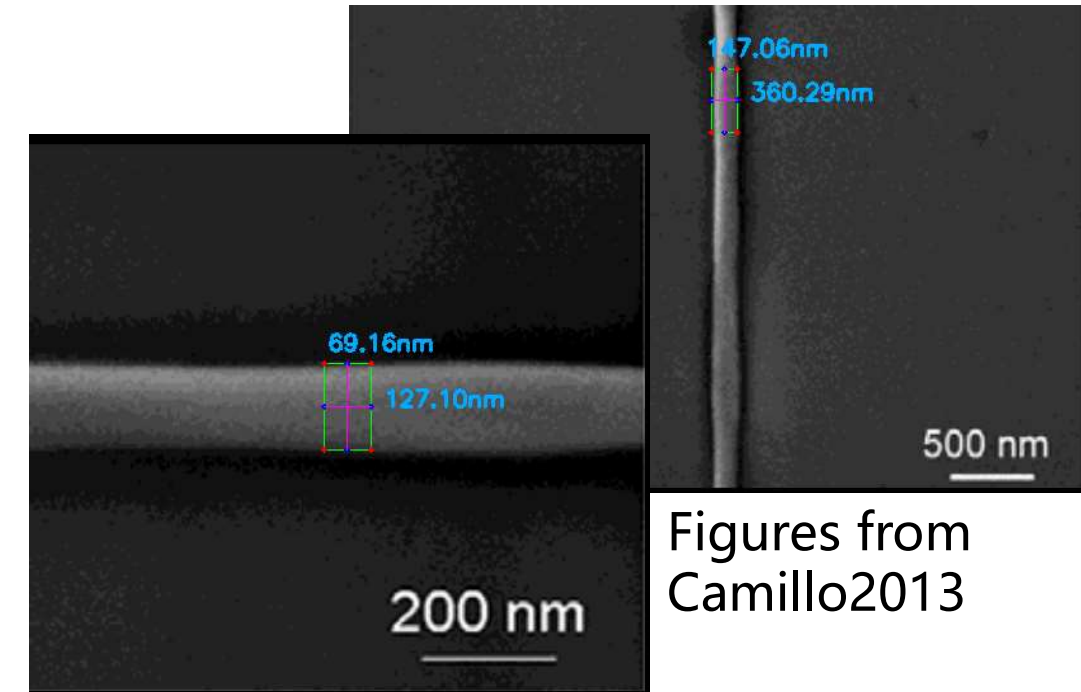
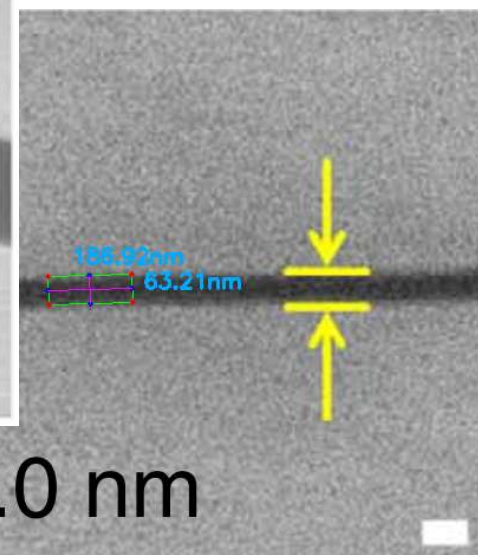
Methods: Data collection (analysis of NFES articles from 2003 to 2020)

The author does not mention the fiber diameter in writing but provides a **EM characterization**.

Python Image Analysis (with a 3.2% error in



Figures from Min2013

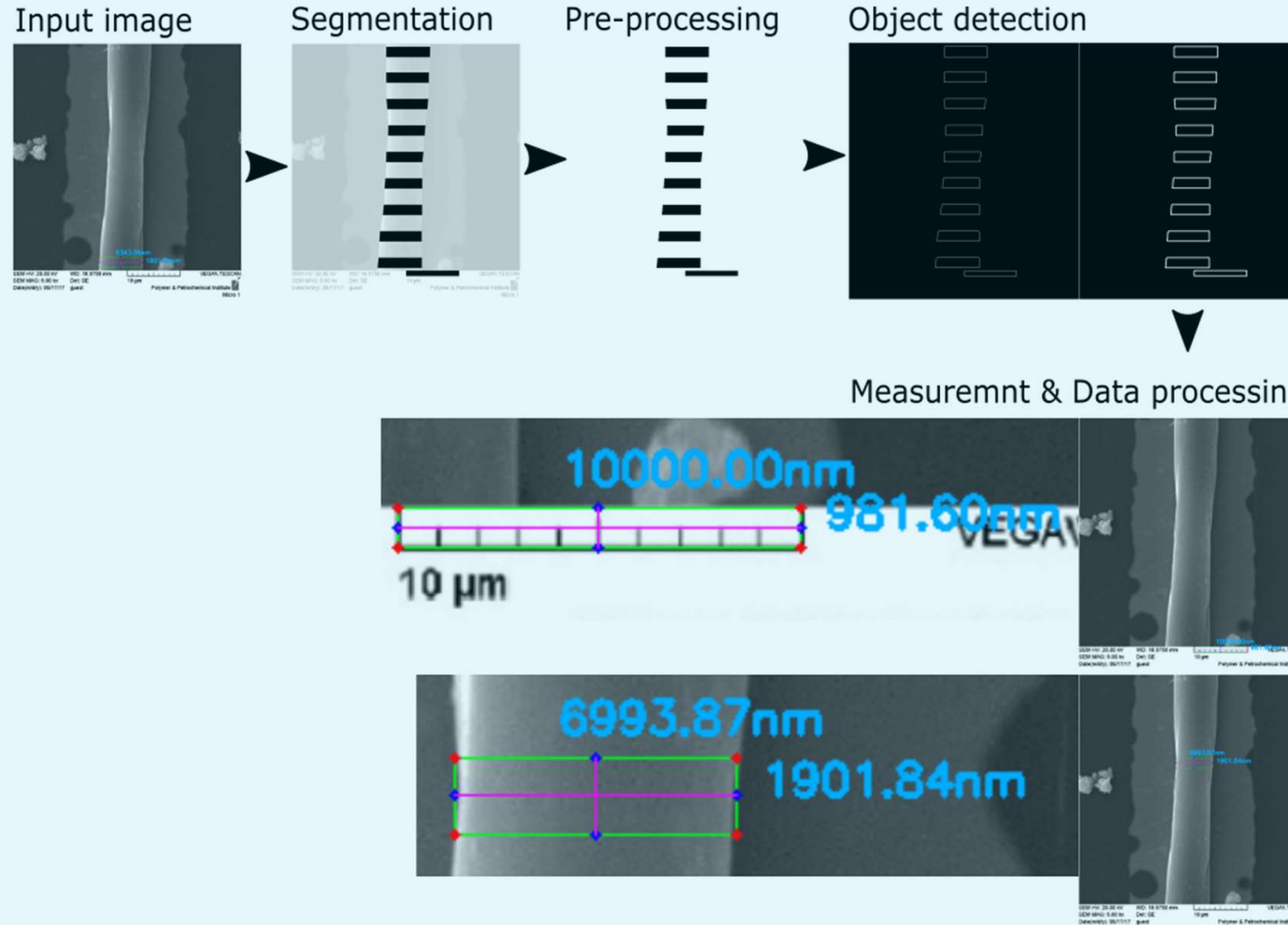


Figures from
Camillo2013

S.-Y. Min, T.-S. Kim, B.J. Kim, H. Cho, Y.-Y. Noh, H. Yang, J.H. Cho, T.-W. Lee, Large-scale organic nanowire lithography and electronics, Nat. Commun. 4 (2013) 1773. <https://doi.org/10.1038/ncomms2785..>
<https://github.com/katagirimx/OpenCV-image-measuring>
D. Di Camillo, V. Fasano, F. Ruggieri, S. Santucci, L. Lozzi, A. Camposeo, D. Pisignano, Near-field electrospinning of conjugated polymer light-emitting nanofibers, Nanoscale. 5 (2013) 11637–11642.
<https://doi.org/10.1039/C3NR03094F>.

Methods: Data collection (analysis of NFES articles from 2003 to 2020)

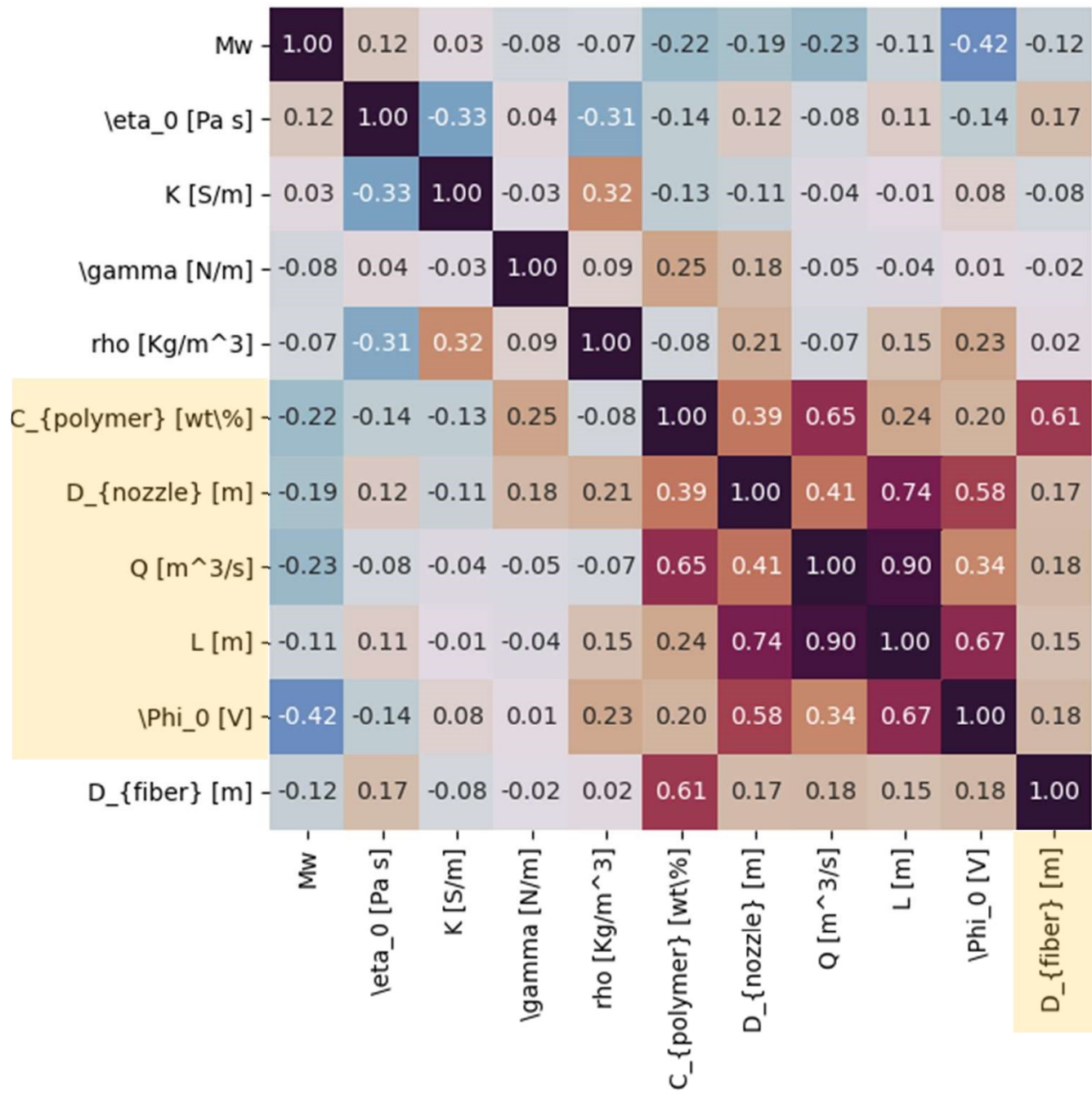
The author does not mention the fiber diameter in writing but provides a **EM characterization**.



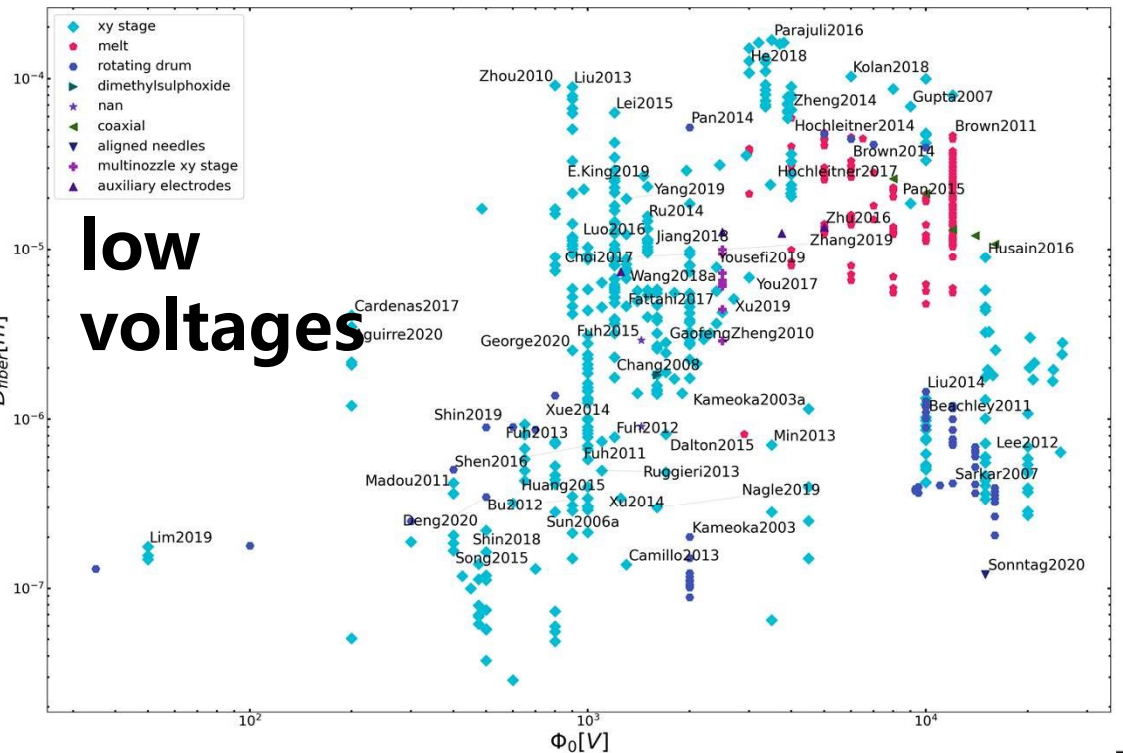
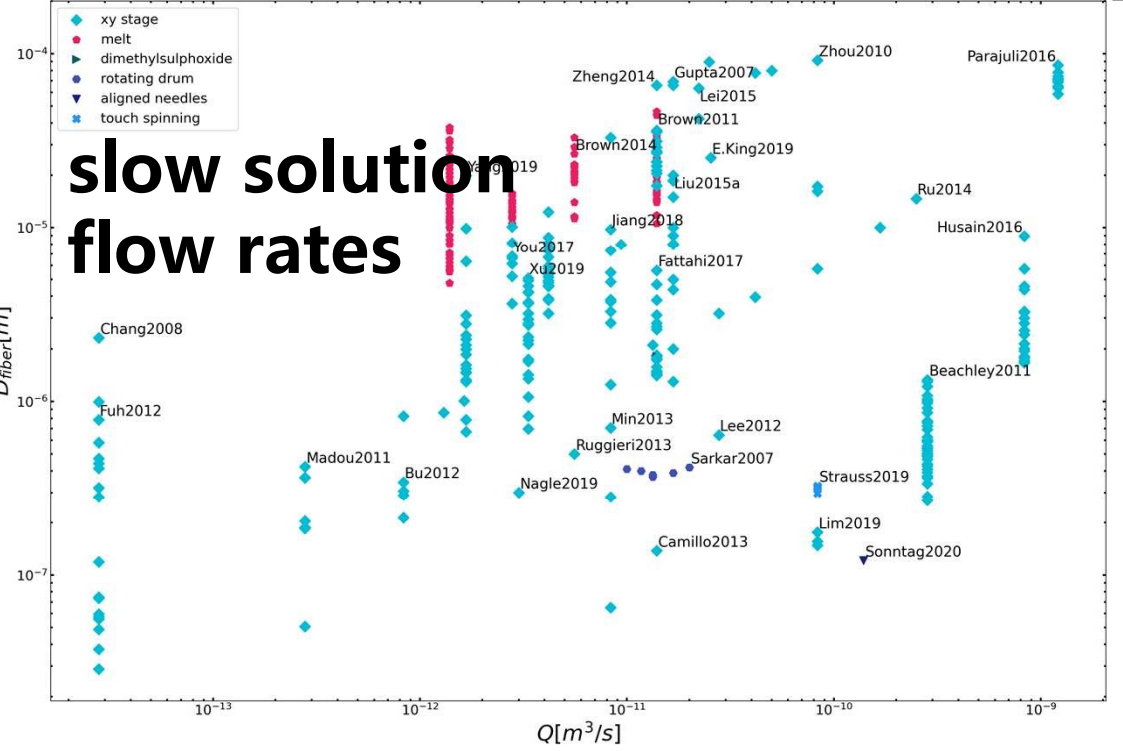
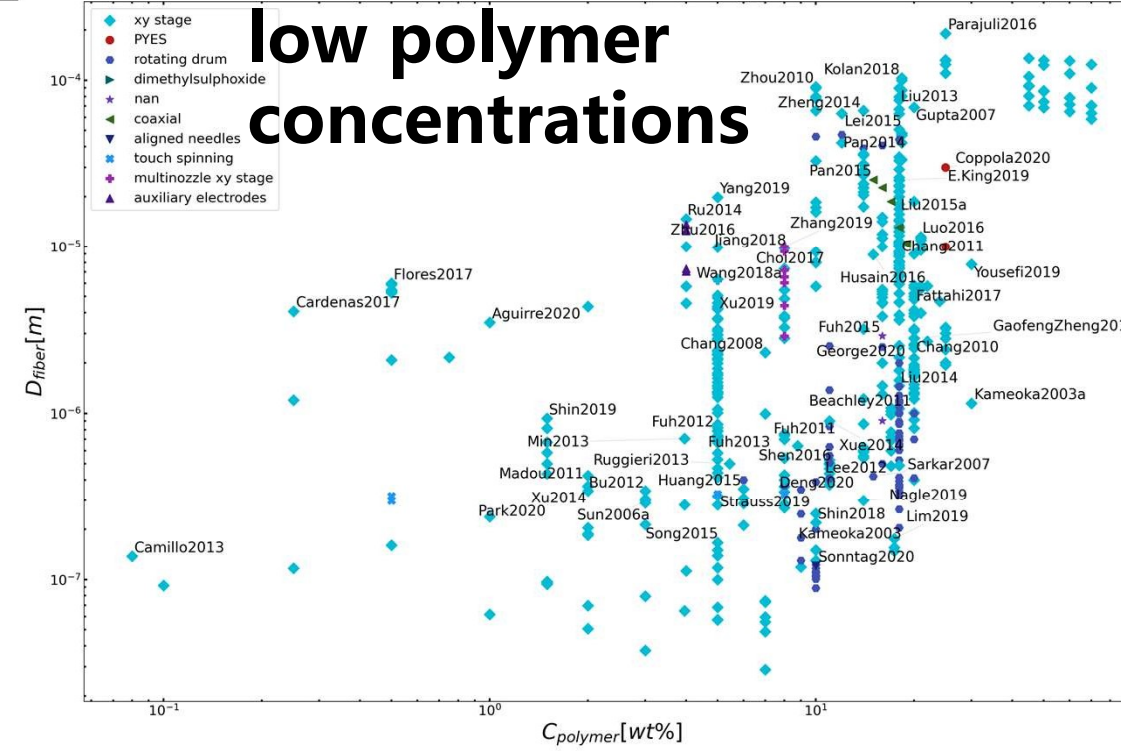
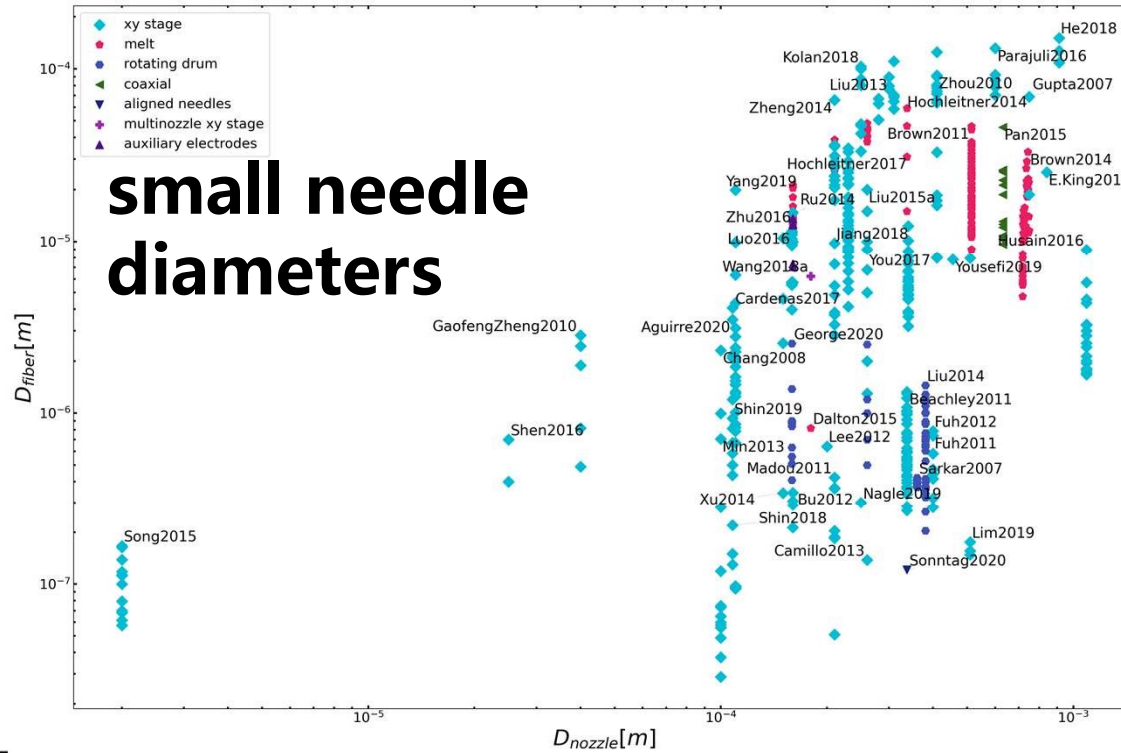
Conclusion 1.1:

- Polymer Concentration,
- Nozzle Diameter,
- Solution Flow Rate,
- Working Distance,
- Applied Voltage

are the main drivers of the **final Fiber Diameter**

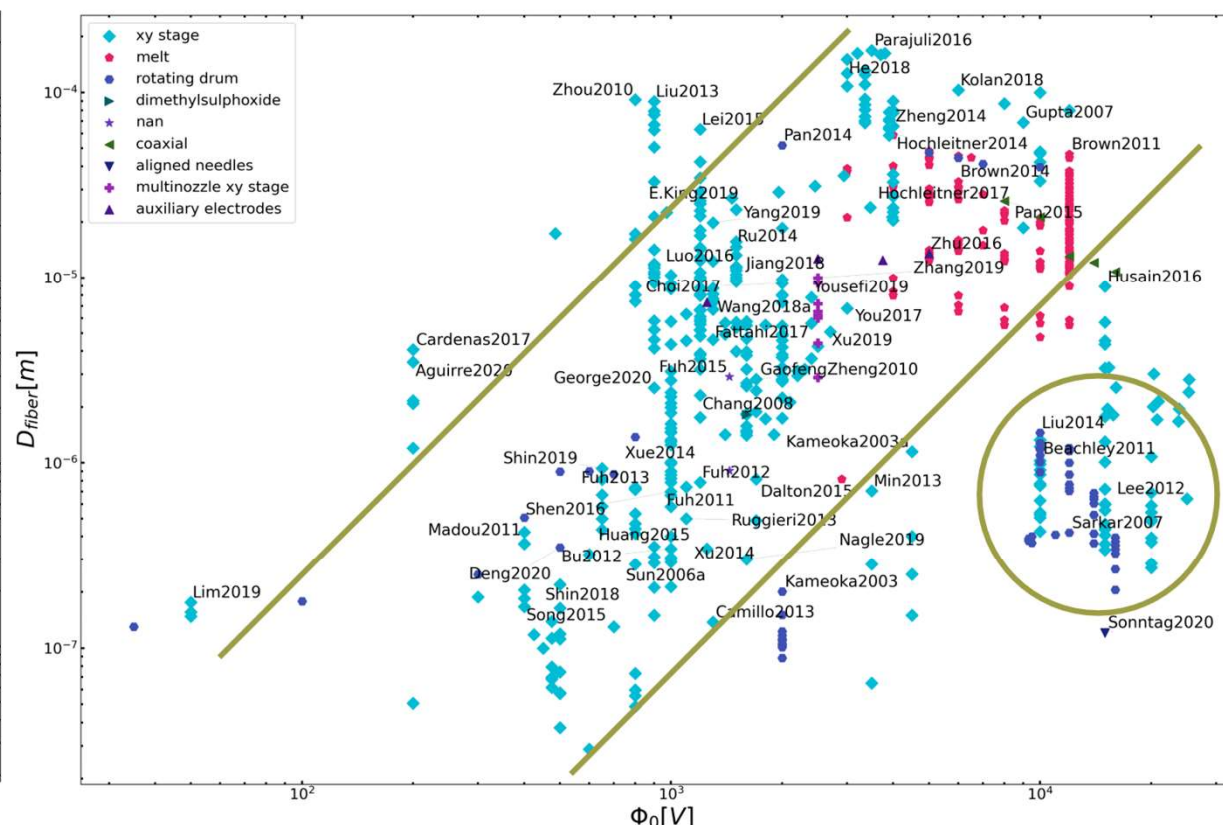
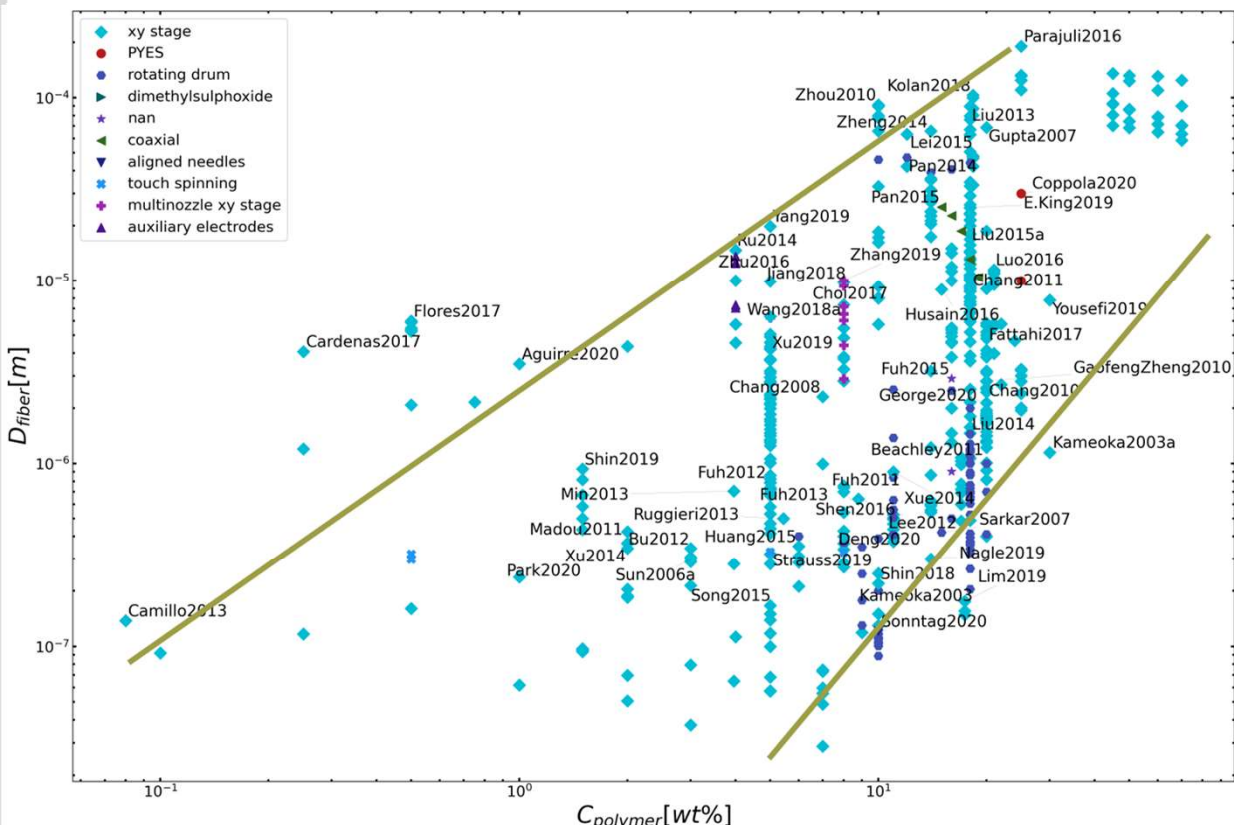


Conclusion 1.1: Process Parameters



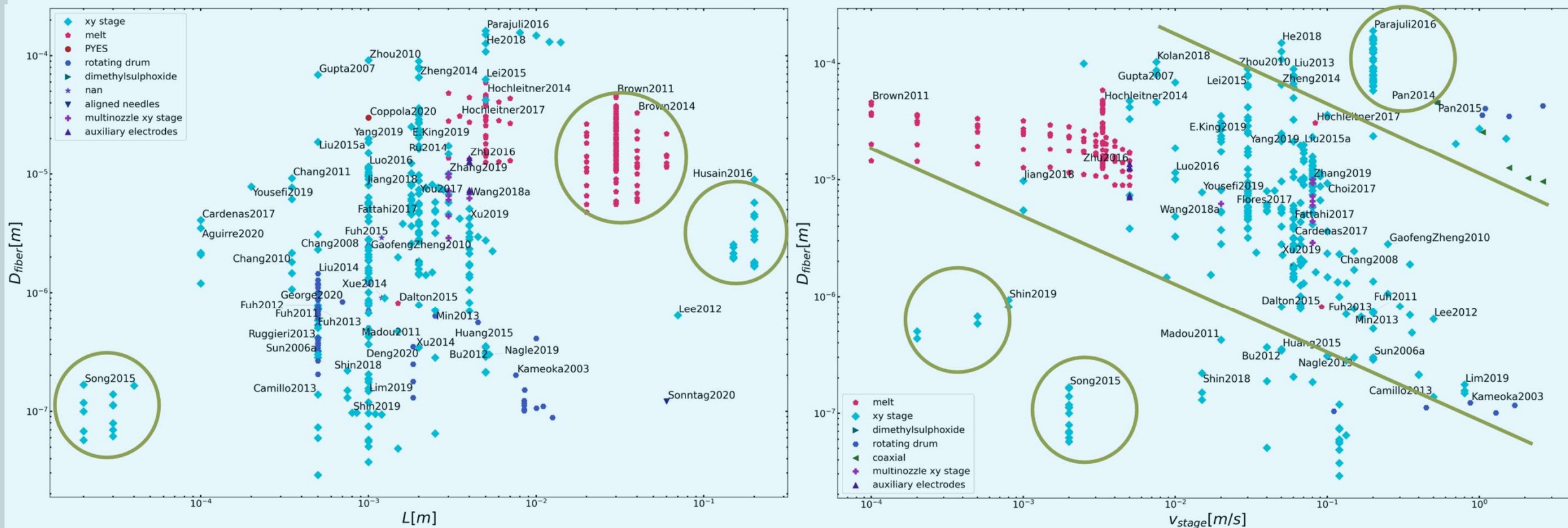
Conclusion 1.2: Let's focus on polymer concentration

Polymer concentration is the most reliable process parameter to control the morphology of electrospun fibers. (regardless the type of NFES process)



Conclusion 1.2: Let's focus on polymer concentration

Polymer concentration is the most reliable process parameter to control the morphology of electrospun fibers. (regardless the type of NFES process)



Diameter Prediction of Electrospun Fibers

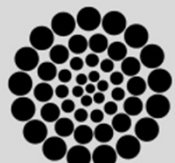
The fiber morphology not only depends on the process parameters, but also on the type of electrospinning process and on polymer-solvent system.

“[...] the fiber diameter **decreases** as the applied voltage **increases.**”
Helgeson et al.

“[...] **neither** the collecting distance nor the applied voltage **has large influences** on fiber diameter [...]”
Zhang et al.

“[...] while **decreasing** the voltage could also be used to **reduce** the average fiber diameter.”
Brown et al.

The existing **interdependence** between the process and solution parameters **adds complexity and ambiguity** to the effect of each parameter



Siddharth B. Gadkari. "Scaling analysis for electrospinning". In: SpringerPlus 3.1 (Dec. 2014), p. 705. ISSN: 2193-1801. DOI: 10.1186/2193-1801-3-705. URL <https://springerplus.springeropen.com/articles/10.1186/2193-1801-3-705>.

B. Zhang, F. Kang, J.-M. Tarascon, J.-K. Kim, Recent advances in electrospun carbon nanofibers and their application in electrochemical energy storage, Prog. Mater. Sci. 76 (2016) 319–380. <https://doi.org/10.1016/j.pmatsci.2015.08.002>.

M.E. Helgeson, K.N. Grammatikos, J.M. Deitzel, N.J. Wagner, Theory and kinematic measurements of the mechanics of stable electrospun polymer jets, Polymer (Guildf). 49 (2008) 2924–2936. <https://doi.org/10.1016/j.polymer.2008.04.025>.

T.D. Brown, F. Edin, N. Detta, A.D. Skelton, D.W. Hutmacher, P.D. Dalton, Melt electrospinning of poly(ϵ -caprolactone) scaffolds: Phenomenological observations associated with collection and direct writing, Mater. Sci. Eng. C. 45 (2014) 698–708. <https://doi.org/10.1016/j.msec.2014.07.034>.

Diameter Prediction of Electrospun Fibers

Helgeson and Wagner have presented an adimensional **analysis to predict the fiber diameter** with conservation equations of momentum, mass, electric charge and four dimensionless numbers:

Correlation between the electrostatic and viscous forces:

$$\Pi_1 = RePe\Psi = \frac{2\bar{\varepsilon}^2\Phi_0^2}{K\eta_0 L^2}$$

Ohnesorge number (jet behaviour and capillary rupture):

$$Oh = \frac{Re^2}{We} = \frac{\eta_0}{\sqrt{\rho\gamma R_{jet}}}$$



Helgeson get rid of known and/or hard to measure parameters, such as the initial jet velocity.

Diameter Prediction of Electrospun Fibers

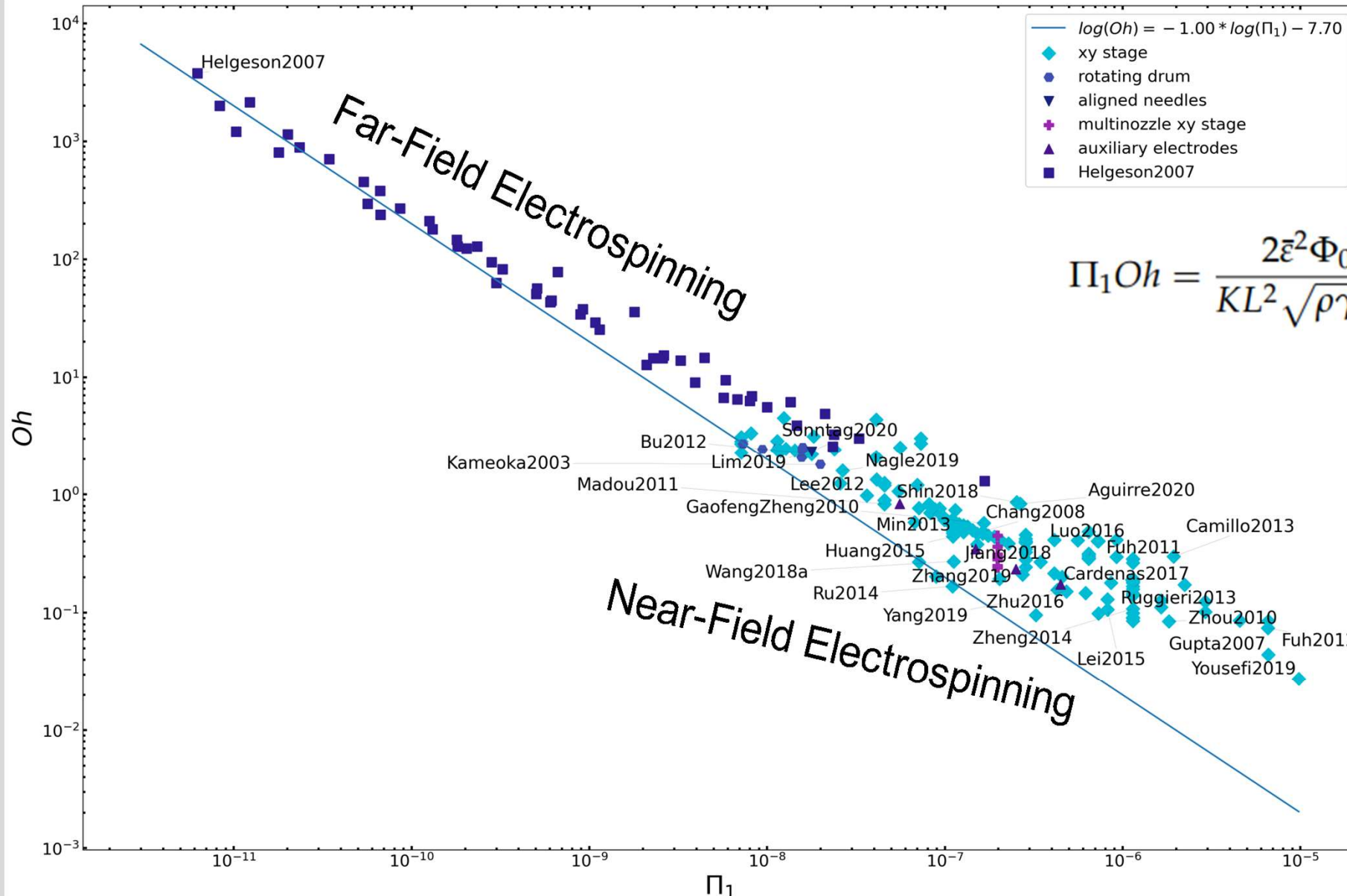
$$\text{Peclet number } Pe = \frac{2\bar{\varepsilon}v_0}{KR_0} \quad \text{Reynold number } Re = \frac{\rho v_0 R_0}{\eta_0} \quad \text{Weber number } We = \frac{\rho v_0^2 R_0}{\gamma}$$

$$\text{dimensionless electric field strength } \Psi = \frac{\bar{\varepsilon}E_0^2}{\rho v_0^2}$$

$$R_{jet} = R_f \sqrt{\frac{1}{w_s}}$$



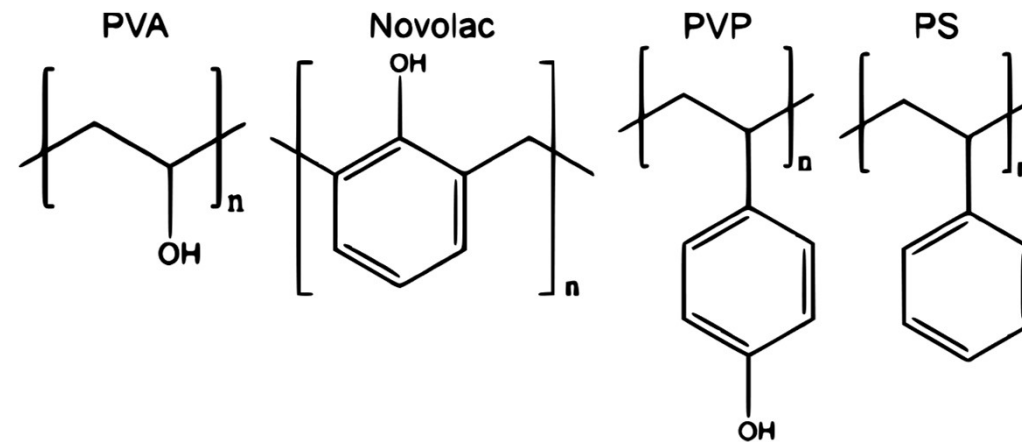
Diameter Prediction of Electrospun Fibers



$$\Pi_1 Oh = \frac{2\bar{\varepsilon}^2 \Phi_0^2}{KL^2 \sqrt{\rho \gamma R_{jet}}} = 2.5 \pm 0.2 \times 10^{-8}$$

Conclusion1.3: Selection of Polymer-Solvent combinations

Zhenan Bao et al. investigated the effect of the polymer chemical Structure of:

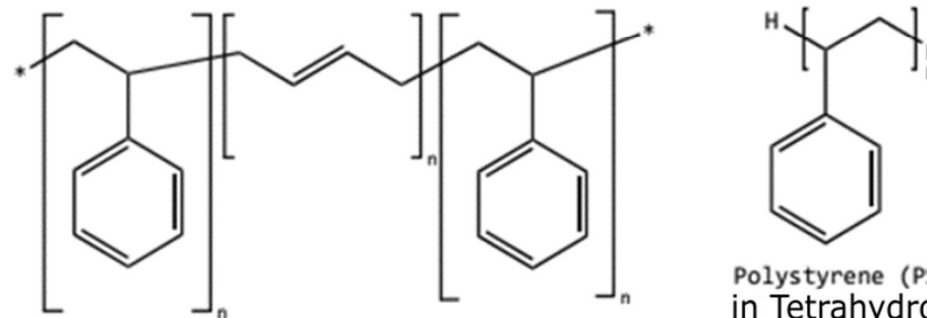


- higher **sp₂ carbon** content translates into higher graphitization degree and higher electrical conductivity
- polymers with **functional groups** are required for the creation of smooth and continuous fibers.

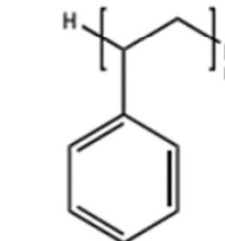


Conclusion1.3: Selection of Polymer-Solvent combinations

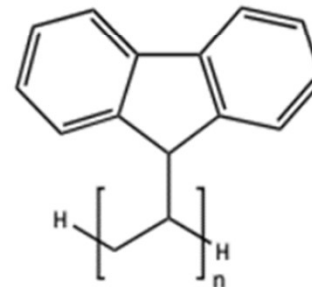
Polymers with **high carbon content relative to oxygen content**



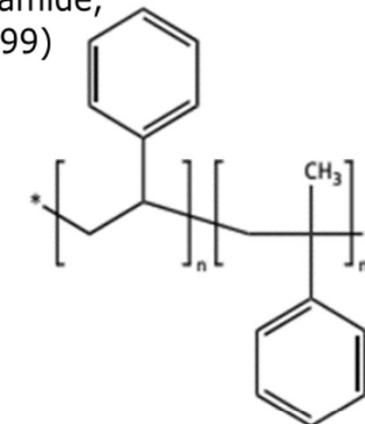
Poly(styrene-co-butadiene)
in Tetrahydrofuran, N,N-Dimethylformamide,
and 1-Methyl-2-Pyrrolidinone (Fong1999)



Polystyrene (PS)
in Tetrahydrofuran (Yousefi2019)



Poly(9-Vinyl Carbazole) (PVK)
in Chloroform (Min2013)



Poly(styrene-co-a-methylstyrene)
in N,N-Dimethylformamide (no records)

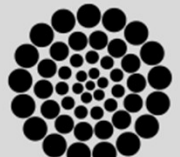
A.A. Yousefi, A.R. Mohebbi, S. Falahdoost Moghadam, S.A. Poursamar, L. Hao, Uniaxially aligned microwire networks for flexible transparent electrodes using a novel electrospinning set-up, Sol. Energy. 188 (2019) 1111–1117. <https://doi.org/10.1016/j.solener.2019.07.007>.

H. Fong, D.H. Reneker, Elastomeric nanofibers of styrene-butadiene-styrene triblock copolymer, J. Polym. Sci. Part B Polym. Phys. 37 (1999) 3488–3493. [https://doi.org/10.1002/\(SICI\)1099-0488\(19991215\)37:24<3488::AID-POLB9>3.0.CO;2-M](https://doi.org/10.1002/(SICI)1099-0488(19991215)37:24<3488::AID-POLB9>3.0.CO;2-M).

S.-Y. Min, T.-S. Kim, B.J. Kim, H. Cho, Y.-Y. Noh, H. Yang, J.H. Cho, T.-W. Lee, Large-scale organic nanowire lithography and electronics, Nat. Commun. 4 (2013) 1773. <https://doi.org/10.1038/ncomms2785>.

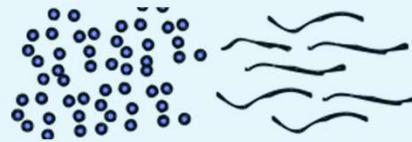
Specific Objective 2. Through **rheological analyses**, determine if polymer solutions have comparative viscoelastic properties to those of the SU-8/PEO benchmark, and if they can be easily electrospun by NFES.

Rheology Analyses



Literature claims

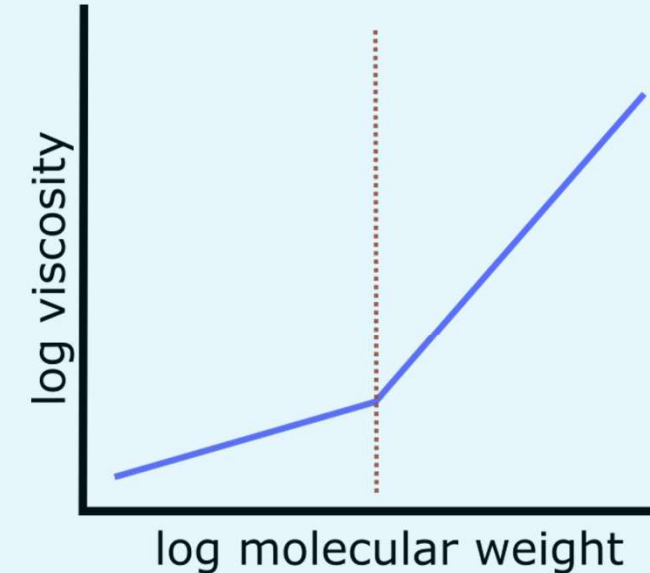
Under some critical concentration
NFES yields beads or small fibres



Over some critical concentration
NFES continuous fibres



Viscosity increases with molecular weight

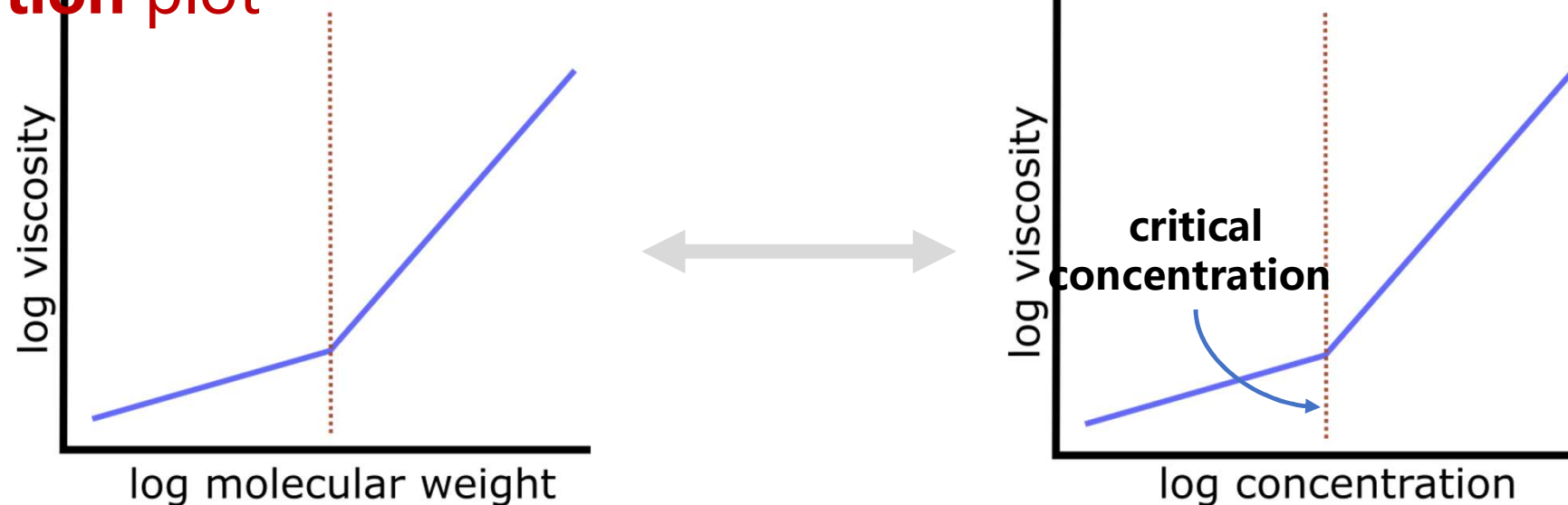


The general belief is that the molecular weight needs to be sufficient enough to create or induce **entanglements**

Literature claims

- As “electropinnability” is determined by the **polymer chain entanglement**,
- **chain entanglement** is controlled by *molecular weight*,
- increasing *molecular weight* increases viscosity, and
- viscosity is controlled by **polymer concentration**, then

The **critical/spinnable concentration** can be found in a **viscosity vs. concentration** plot



Methods: Sample Preparation (SU8-PEO)

Sample	Weight Percent <i>wt%</i>		
	SU-8	PEO	TBF
1	99.50	0.00	0.50
2	99.25	0.25	0.50
3	99.00	0.50	0.50
4	98.75	0.75	0.50
5	98.50	1.00	0.50
density [g/ml]	1.123		

3.0 ml samples
on a heating plate at 160 rpm and 60°C,
for 2 hours each.

A salt (TBF) was added to all the samples to
increase the electrical conductivity



Methods: Sample Preparation (PS & PSB)

Sample	Weight Percent <i>wt%</i>			Sample	Weight Percent <i>wt%</i>		
	THF	PS	TBF		NMP	PSB	TBF
6	99.25	0.25	0.50	14	98.50	1.00	0.50
7	94.50	5.00	0.50	15	95.50	4.00	0.50
8	89.50	10.00	0.50	16	91.50	8.00	0.50
9	84.50	15.00	0.50	17	87.50	12.00	0.50
10	79.50	20.00	0.50	density [g/ml]		1.027	
11	69.50	30.00	0.50				
12	64.50	35.00	0.50				
13	59.50	40.00	0.50				
density [g/ml]		0.888					

Methods: Sample Preparation (PSB & PSMS)

Sample	Weight Percent <i>wt%</i>				Sample	Weight Percent <i>wt%</i>		
	THF	DMF	PSB	TBF		DMF	PSMS	TBF
18	70.875	23.625	5.00	0.50	25	99.00	0.50	0.50
19	69.000	23.000	7.50	0.50	26	94.50	5.00	0.50
20	67.125	22.375	10.00	0.50	27	89.50	10.00	0.50
21	65.250	21.750	12.50	0.50	28	84.50	15.00	0.50
22	63.375	21.125	15.00	0.50	density [g/ml]		0.950	
23	59.625	19.875	20.00	0.50				
24	55.875	18.625	25.00	0.50				
density [g/ml]		0.888	0.950					

Methods: Sample Preparation (PVK & SU8-PVK)

Sample	Weight Percent wt%		
	CHL	PVK	TBF
29	99.50	0.00	0.50
30	99.49	0.01	0.50
31	84.50	15.00	0.50
32	79.50	20.00	0.50
33	69.50	30.00	0.50
density [g/ml]	1.492		

Sample	Weight Percent wt%		
	SU-8	PVK	TBF
34	99.50	0.00	0.50
35	99.495	0.005	0.50
36	98.75	0.75	0.50
37	94.50	5.00	0.50
38	79.50	20.00	0.50
density [g/ml]	1.123		

Methods: Rheology – Frequency Sweeps

Geometry:

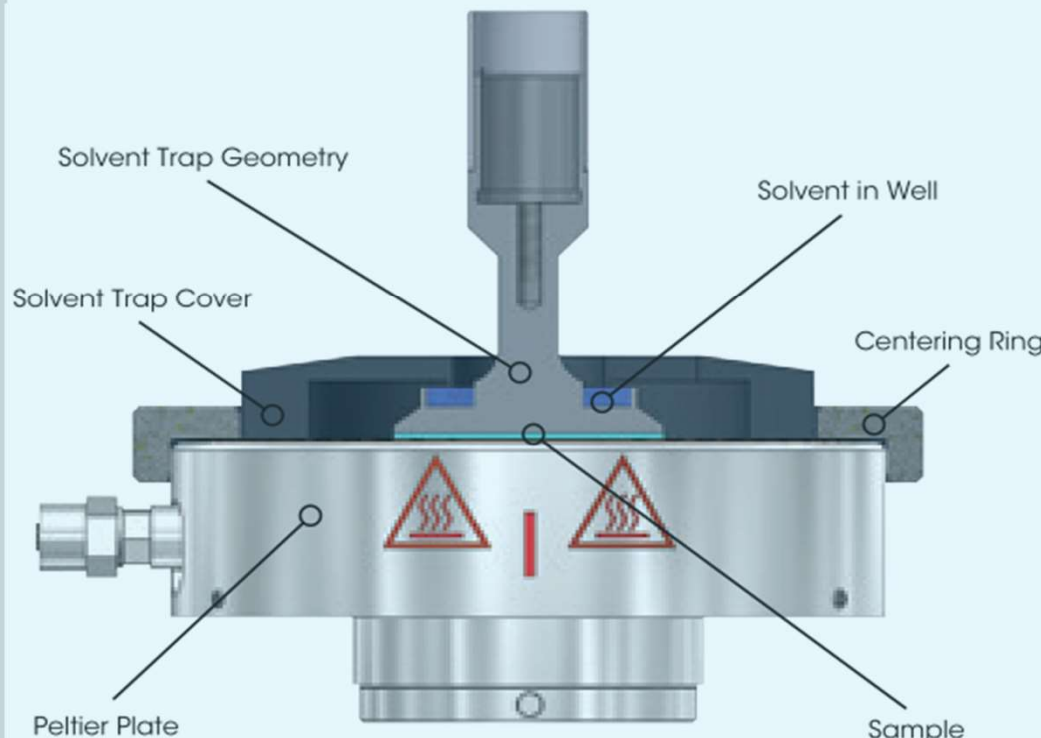
Steel cone plate, Peltier plate
(60.0 mm diameter, 0.9979° cone angle, 23 μm truncation)

Procedure:

Frequency sweep
(20°C, for 20 min
from 10^{-3} to 10^4 1/s shear rates)



Methods: Rheology – Instrumentation



Measured Parameter	Calculated Parameter
Torque	Stress
Angular displacement	Strain
Angular velocity	Shear rate

$$\text{Stress} = \text{Torque} [\text{N} \cdot \text{m}] \cdot \text{Stress constant}$$

$$\text{Strain} = \text{Angular displacement} [\text{rad}] \cdot \text{Strain constant}$$

$$\text{Shear rate} = \text{Angular velocity} \left[\frac{\text{rad}}{\text{s}} \right] \cdot \text{Strain constant}$$

$$\text{Viscosity} = \frac{\text{Stress}}{\text{Shear rate}}$$

$$\text{Young's Modulus} = \frac{\text{Stress}}{\text{Strain}}$$

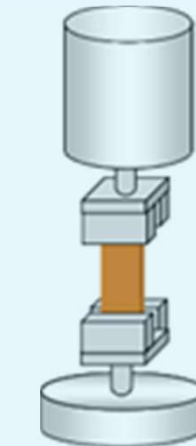
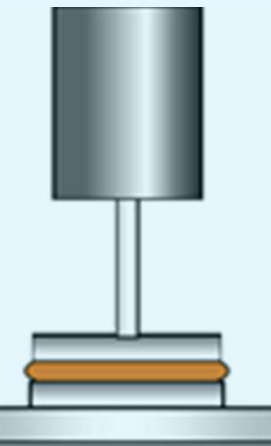
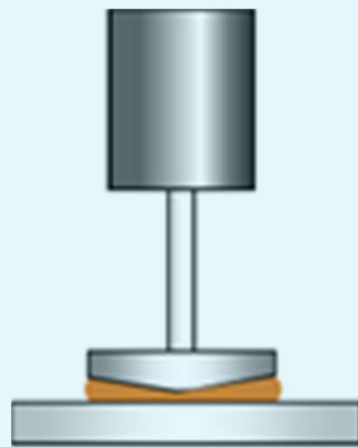
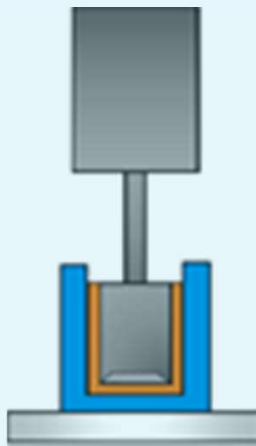
Discovery Hybrid Rheometers – TA Instruments, (n.d.). <https://www.tainstruments.com/products/rheology/discovery-hybrid-rheometers/> (accessed 18 May 2020).

Malvern Instruments Worldwide, Malvern Instruments White Paper - A Basic Introduction to Rheology Shear Flow, (2016) 1–20. <https://www.malvernpanalytical.com/en/learn/knowledge-center/whitepapers/WP160620BasicIntroRheology.html>.

Methods: Rheology – Geometry Selection

Geometry options:

Concentric Cylinders Cone and Plate Parallel Plate Torsion Rectangular

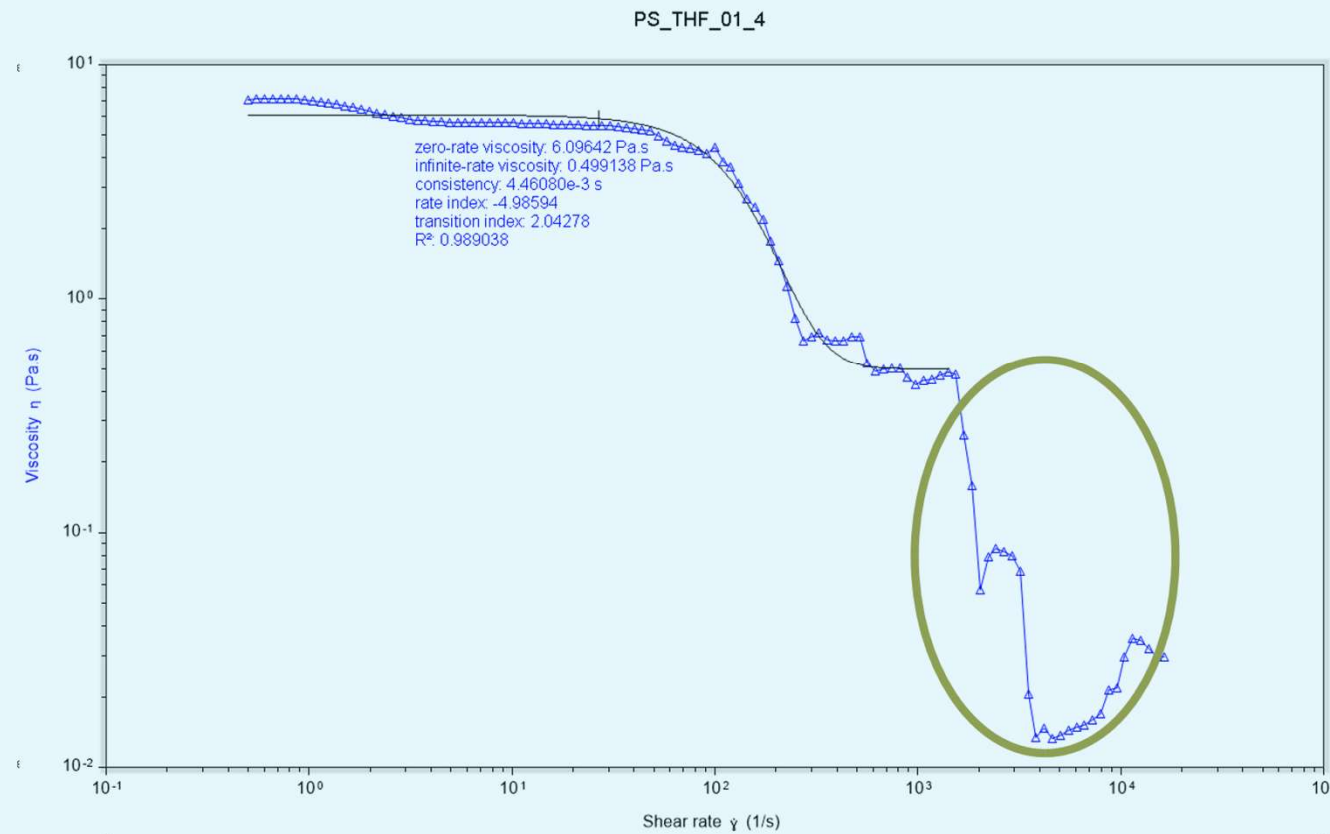


Very Low Viscosity

→ Solids

Methods: Rheology – Radial Migration Effect

High centrifugal stresses result in the sample being thrown out of the measuring area; a phenomenon known as 'radial migration effect'.

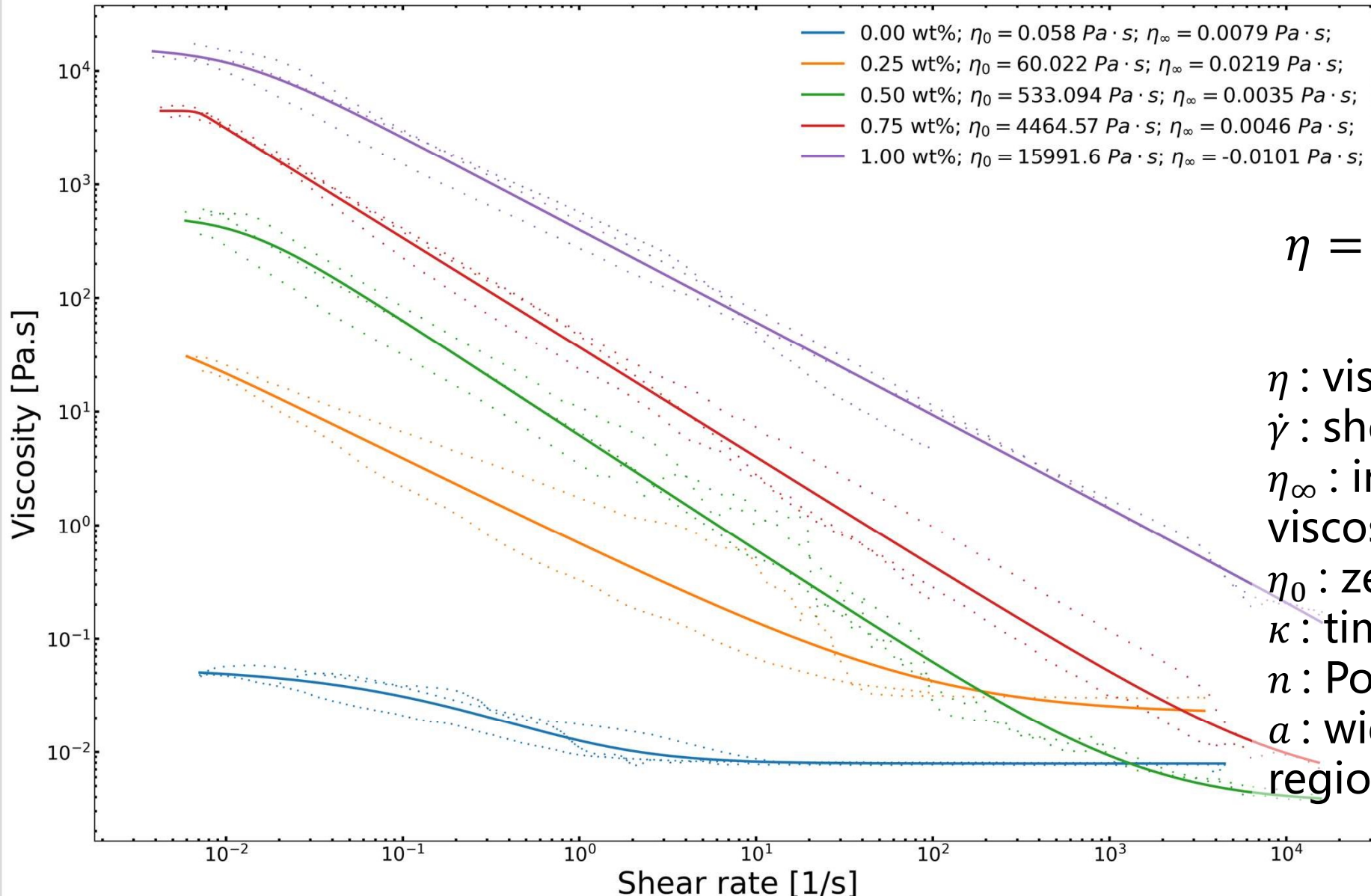


Once the 'radial migration effect' partially ejects the sample, the viscosity measurements are lower than expected due to a drop in torque.

R. W. Connelly and J. Greener. "High-Shear Viscometry with a Rotational Parallel-Disk Device". In: *Journal of Rheology* 29.2 (1985), pp. 209–226. ISSN: 0148-6055. DOI: 10.1122/1.549828.

Christopher J Pipe, Trushant S Majmudar, and Gareth H. McKinley. "High shear rate viscometry". In: *Rheologica Acta* 47.5-6 (July 2008), pp. 621–642. ISSN: 0035-4511. DOI: 10.1007/s00397-008-0268-1. URL: <http://link.springer.com/10.1007/s00397-008-0268-1>.

Methods: The Carreau-Yasuda Model



Methods: Other models:

Cross Model

$$\frac{\eta - b}{a - b} = \frac{1}{1 + (c\dot{\gamma})^d}$$

$$\eta = \frac{a - b}{1 + (c\dot{\gamma})^d} + b$$

where:

a = zero rate viscosity

b = infinite rate viscosity

c = consistency

d = rate index

Carreau Model

$$\frac{\eta - b}{a - b} = [1 + (c\dot{\gamma})^2]^{\frac{d-1}{2}}$$

$$\eta = \frac{a - b}{[1 + (c\dot{\gamma})^2]^{\frac{1-d}{2}}} + b$$

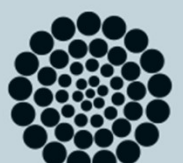
where:

a = zero rate viscosity

b = infinite rate viscosity

c = consistency

d = rate index



Methods: Other models:

Sisko

$$\eta = a + b\dot{\gamma}^{c-1}$$

where:

a = infinite rate viscosity

b = consistency

c = rate index

Williamson

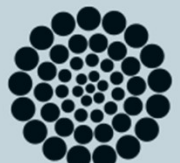
$$\eta = \frac{a}{1 + (b\dot{\gamma})^c}$$

where:

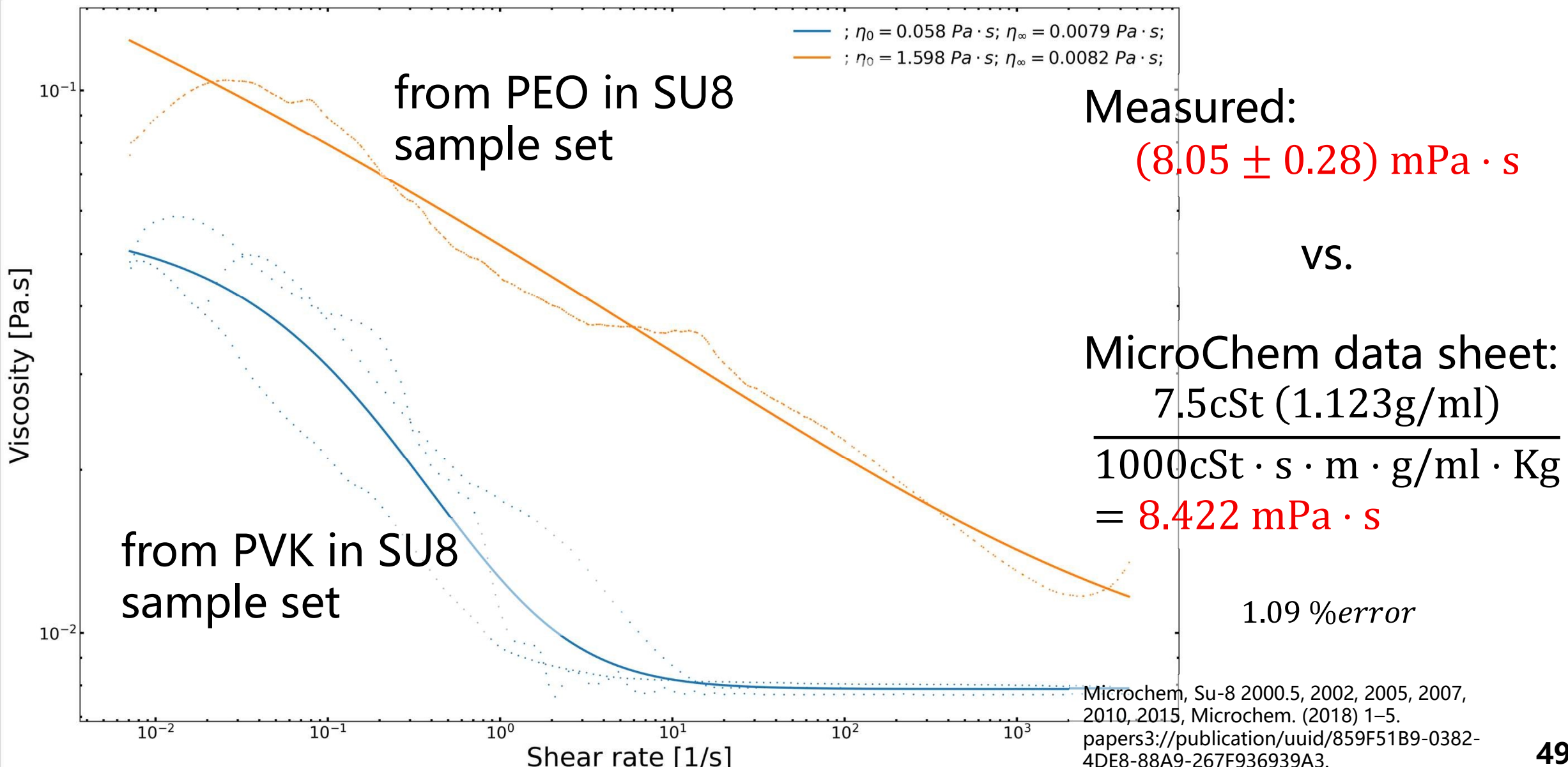
a = zero rate viscosity

b = consistency

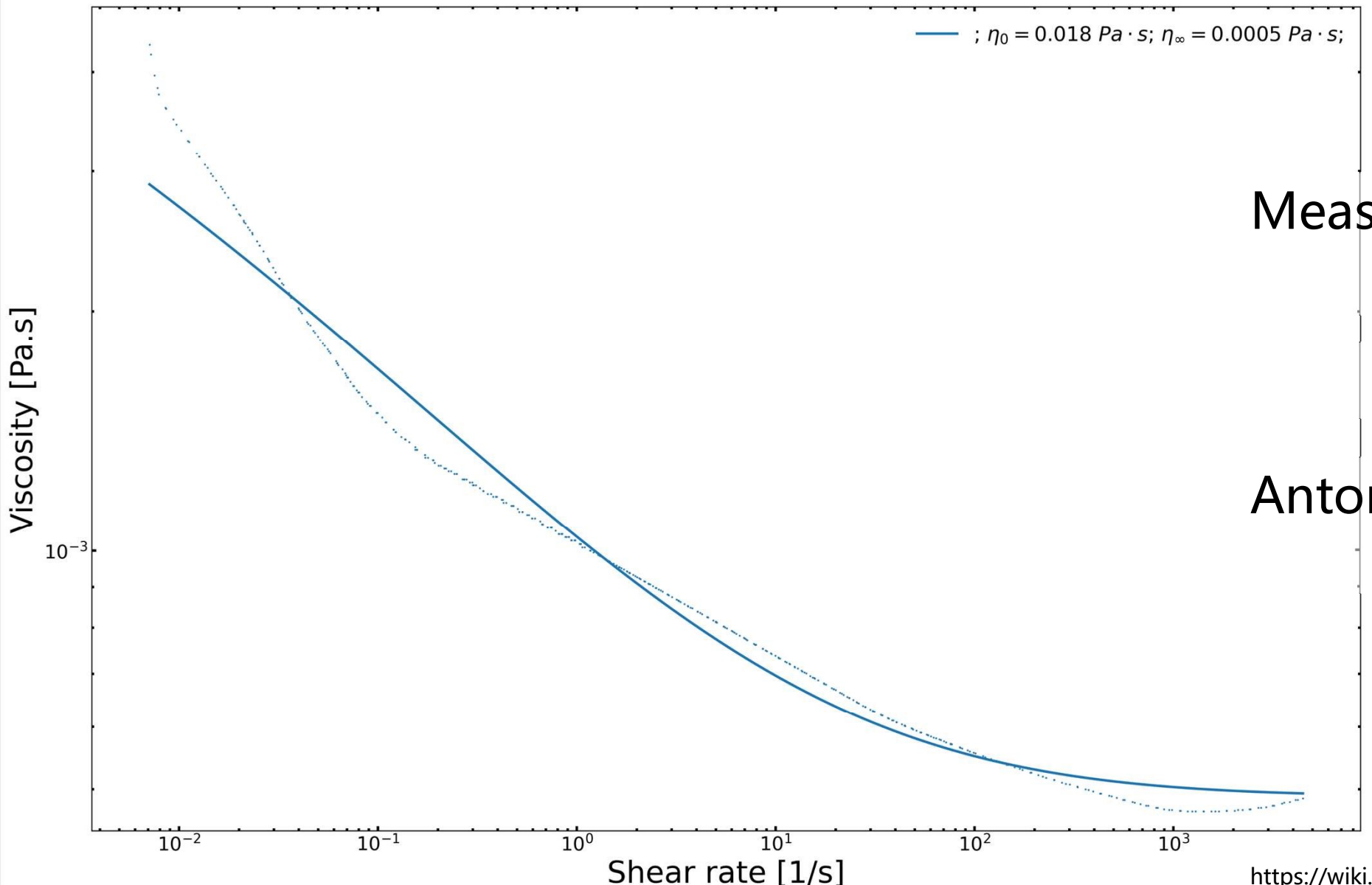
c = rate index

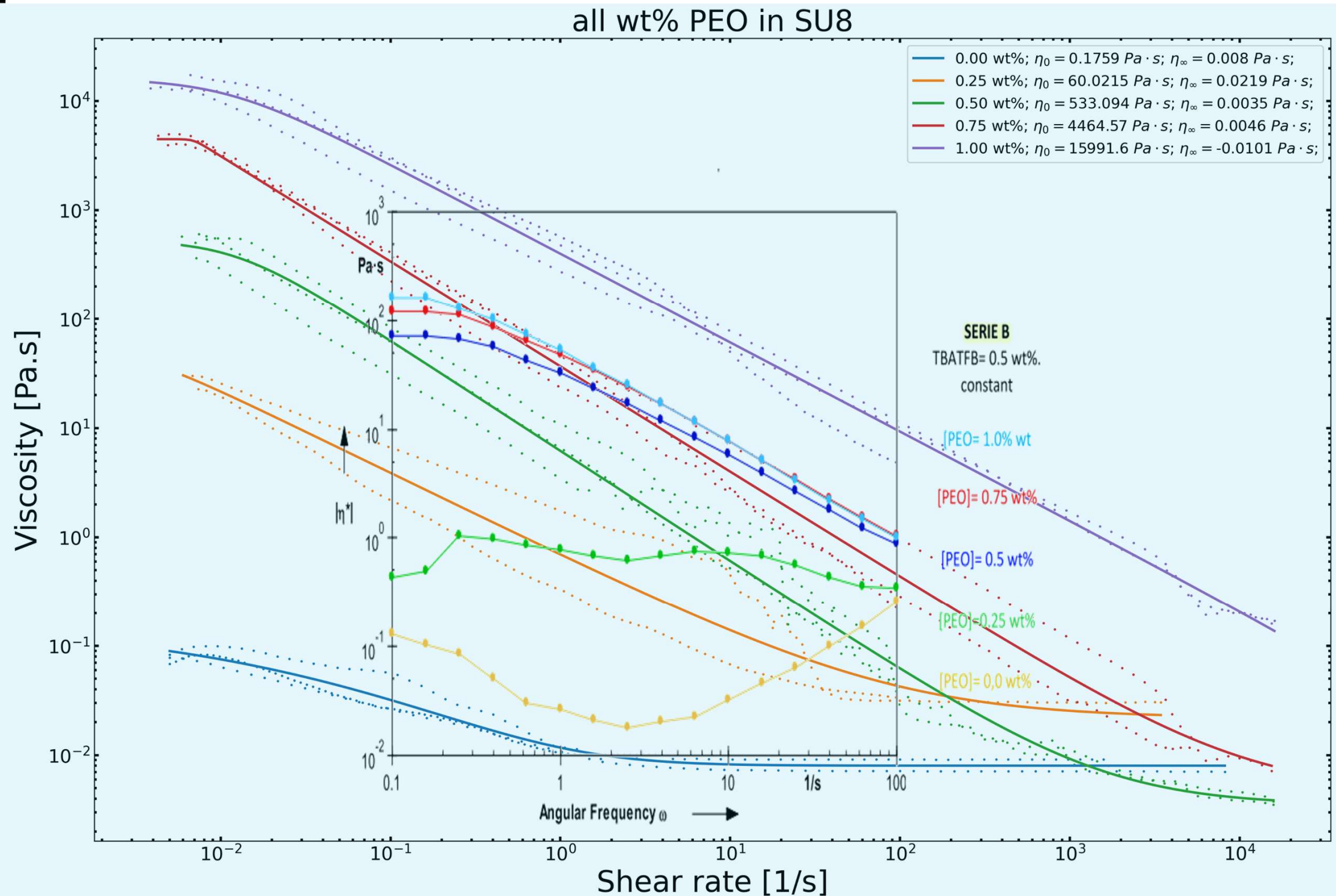


Methods: Rheology results validation for 0wt% PEO

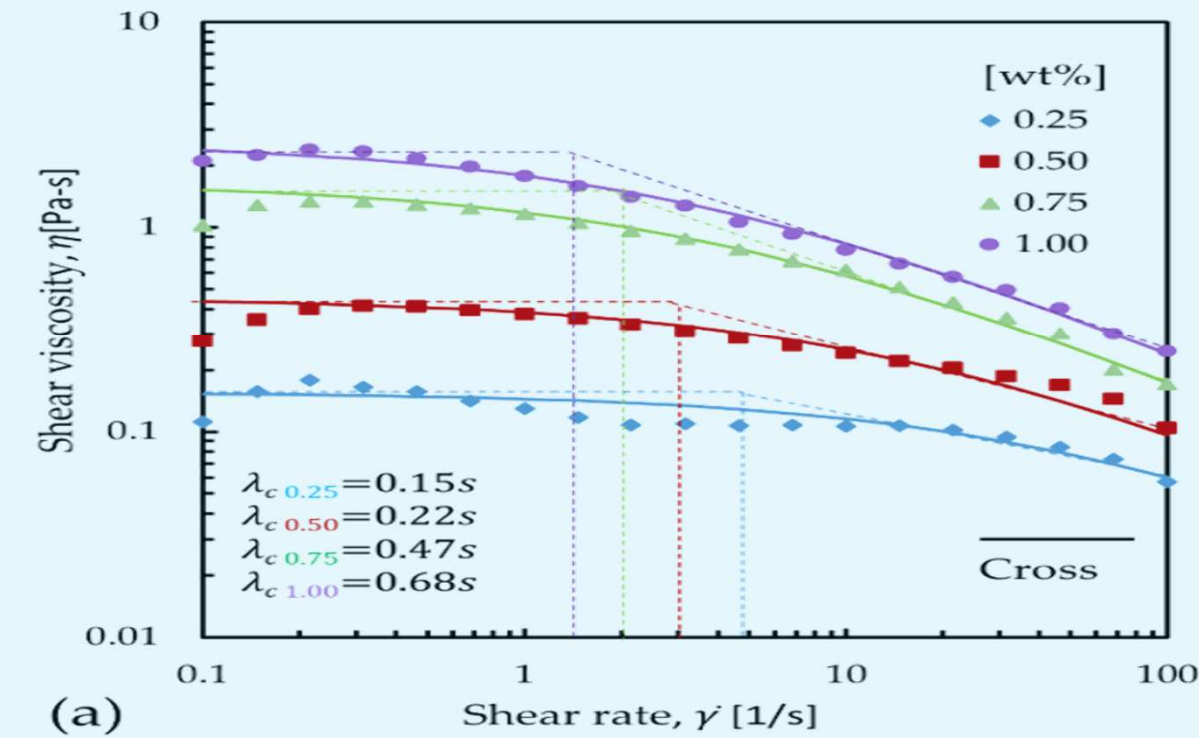
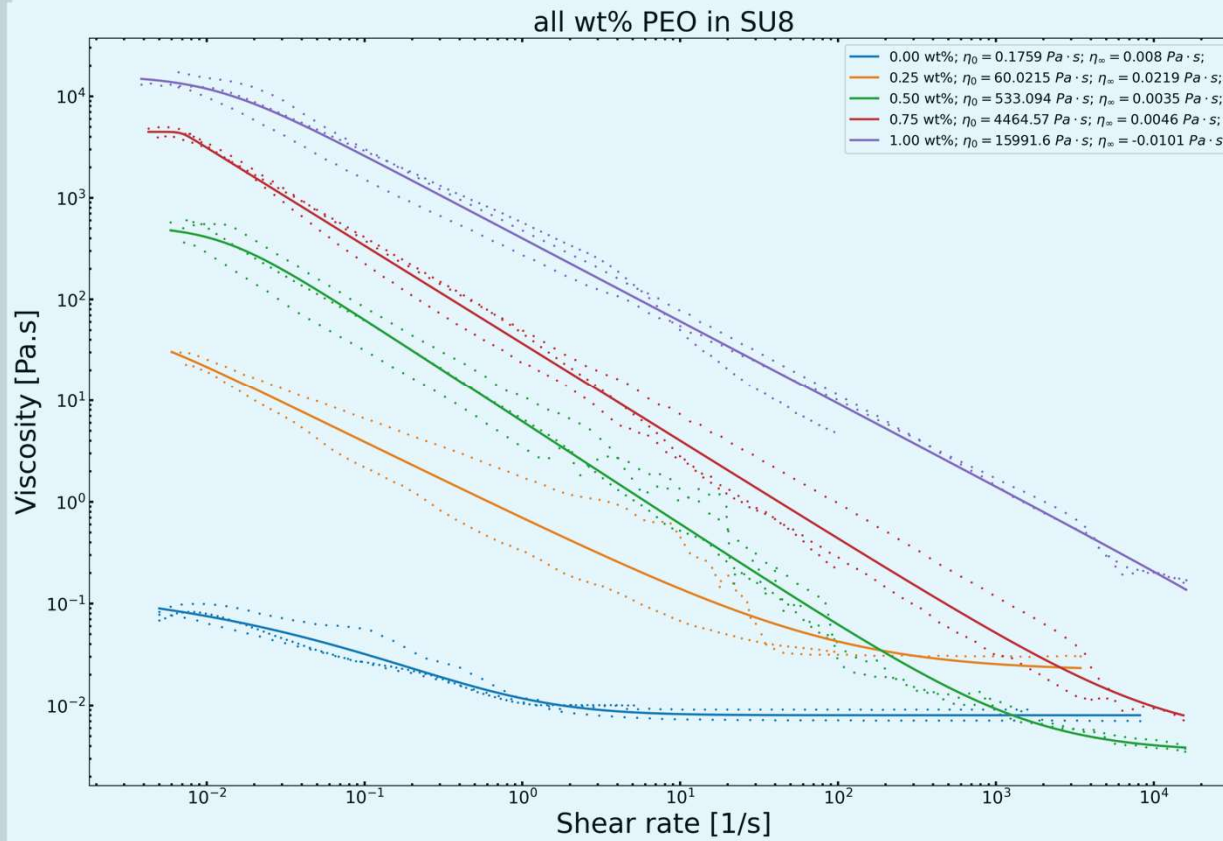


Methods: Rheology results validation for 0wt% PEO





Methods: Rheology results validation



Methods: Rheology results validation

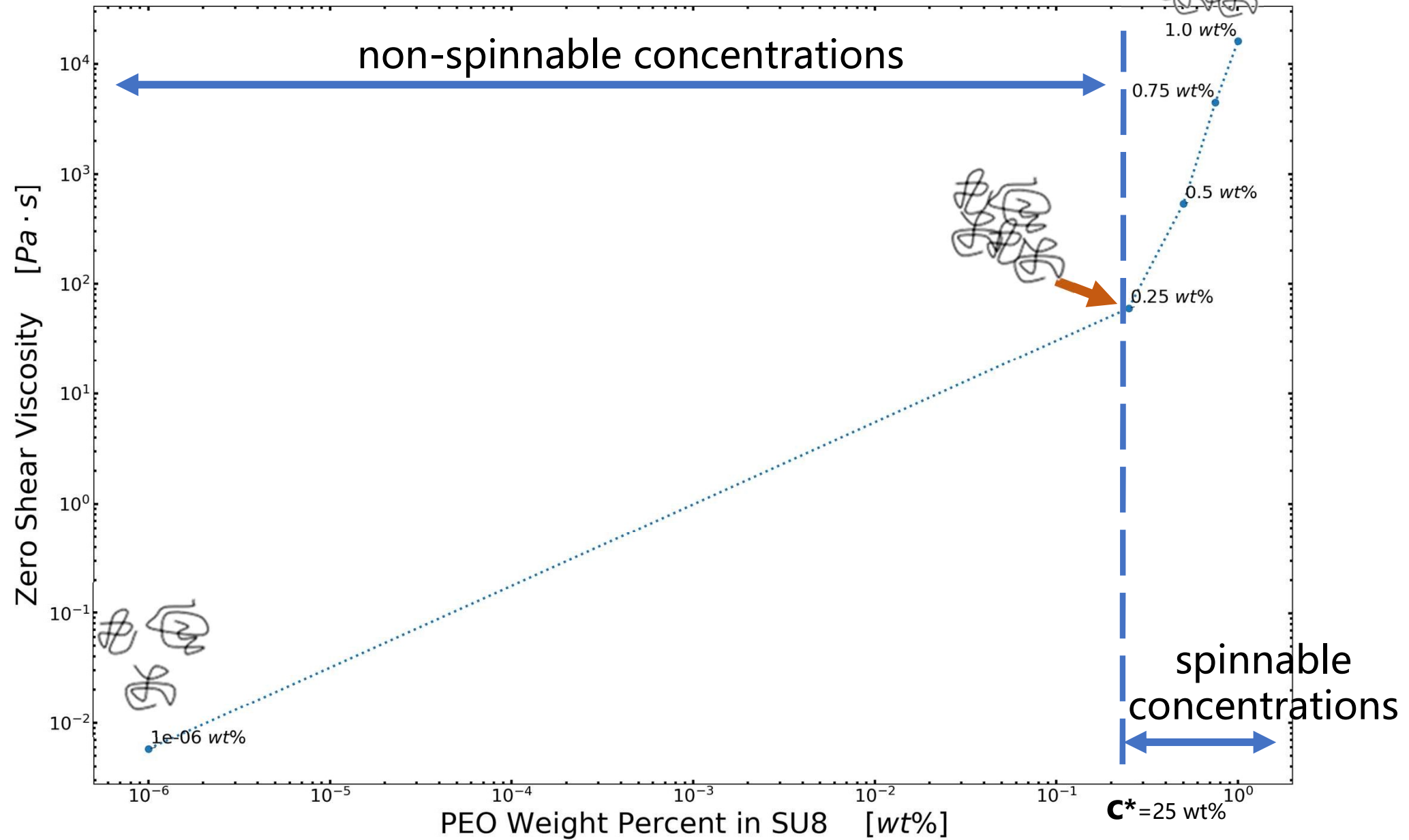
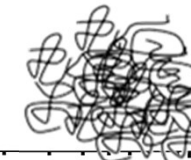
Sample	Weight Percent <i>wt%</i>		
	SU-8	PEO	TBF
1	99.50	0.00	0.50
2	99.25	0.25	0.50
3	99.00	0.50	0.50
4	98.75	0.75	0.50
5	98.50	1.00	0.50
density [g/ml]	1.123		

0.00 wt%; $\eta_0 = 0.058 \text{ Pa} \cdot \text{s}$; $\eta_\infty = 0.0079 \text{ Pa} \cdot \text{s}$;
0.25 wt%; $\eta_0 = 60.022 \text{ Pa} \cdot \text{s}$; $\eta_\infty = 0.0219 \text{ Pa} \cdot \text{s}$;
0.50 wt%; $\eta_0 = 533.094 \text{ Pa} \cdot \text{s}$; $\eta_\infty = 0.0035 \text{ Pa} \cdot \text{s}$;
0.75 wt%; $\eta_0 = 4464.57 \text{ Pa} \cdot \text{s}$; $\eta_\infty = 0.0046 \text{ Pa} \cdot \text{s}$;
1.00 wt%; $\eta_0 = 15991.6 \text{ Pa} \cdot \text{s}$; $\eta_\infty = -0.0101 \text{ Pa} \cdot \text{s}$;

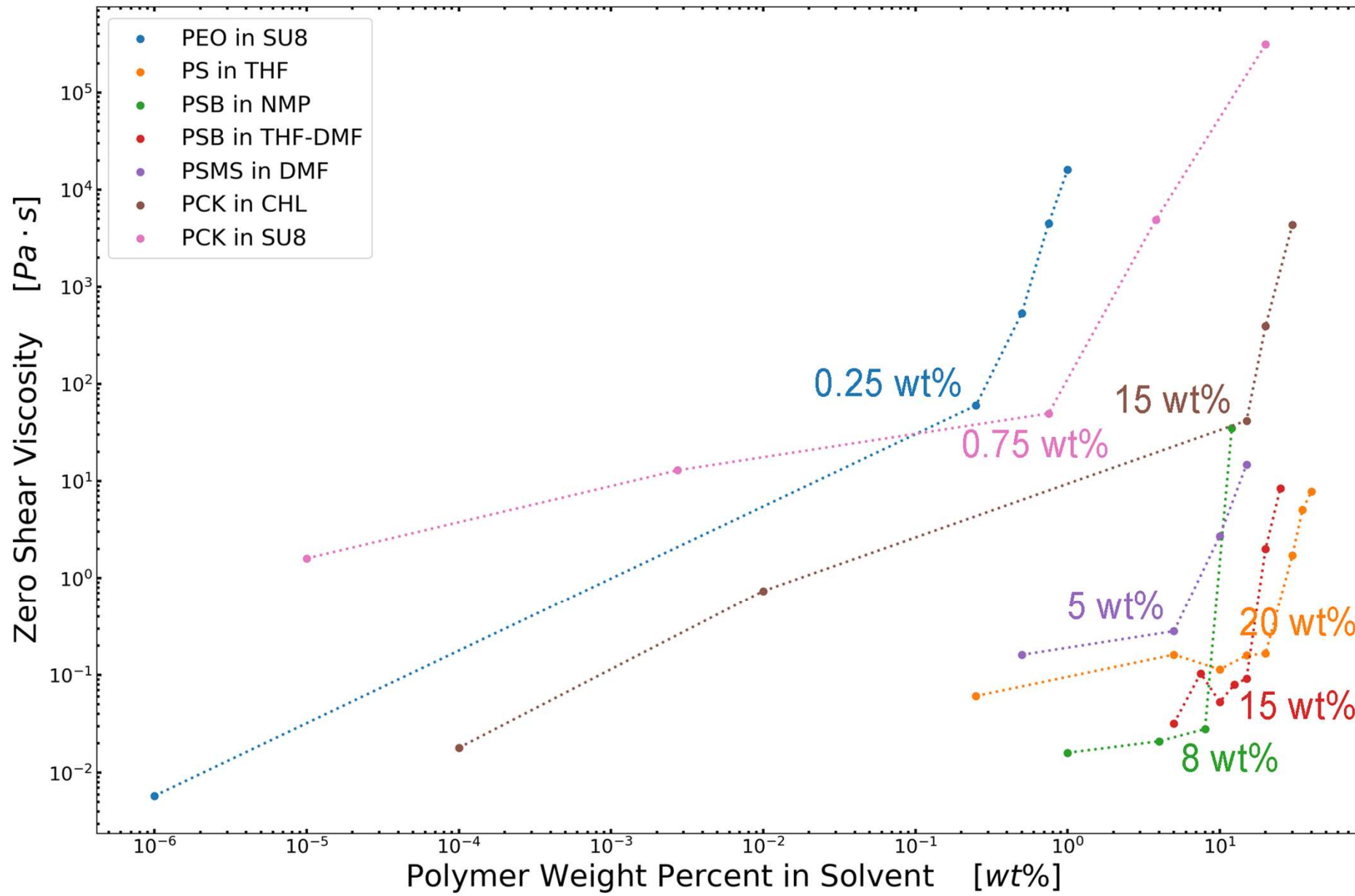
Table 1. Zero-Shear Viscosity and Relaxation Time Calculated for Different PEO Concentrations

	Zero-Shear Viscosity η_0 (Pa·s)	Relaxation Time λ (s)
1% PEO	1.33	0.7
2% PEO	28.70	10.0
3% PEO	111.00	25.0

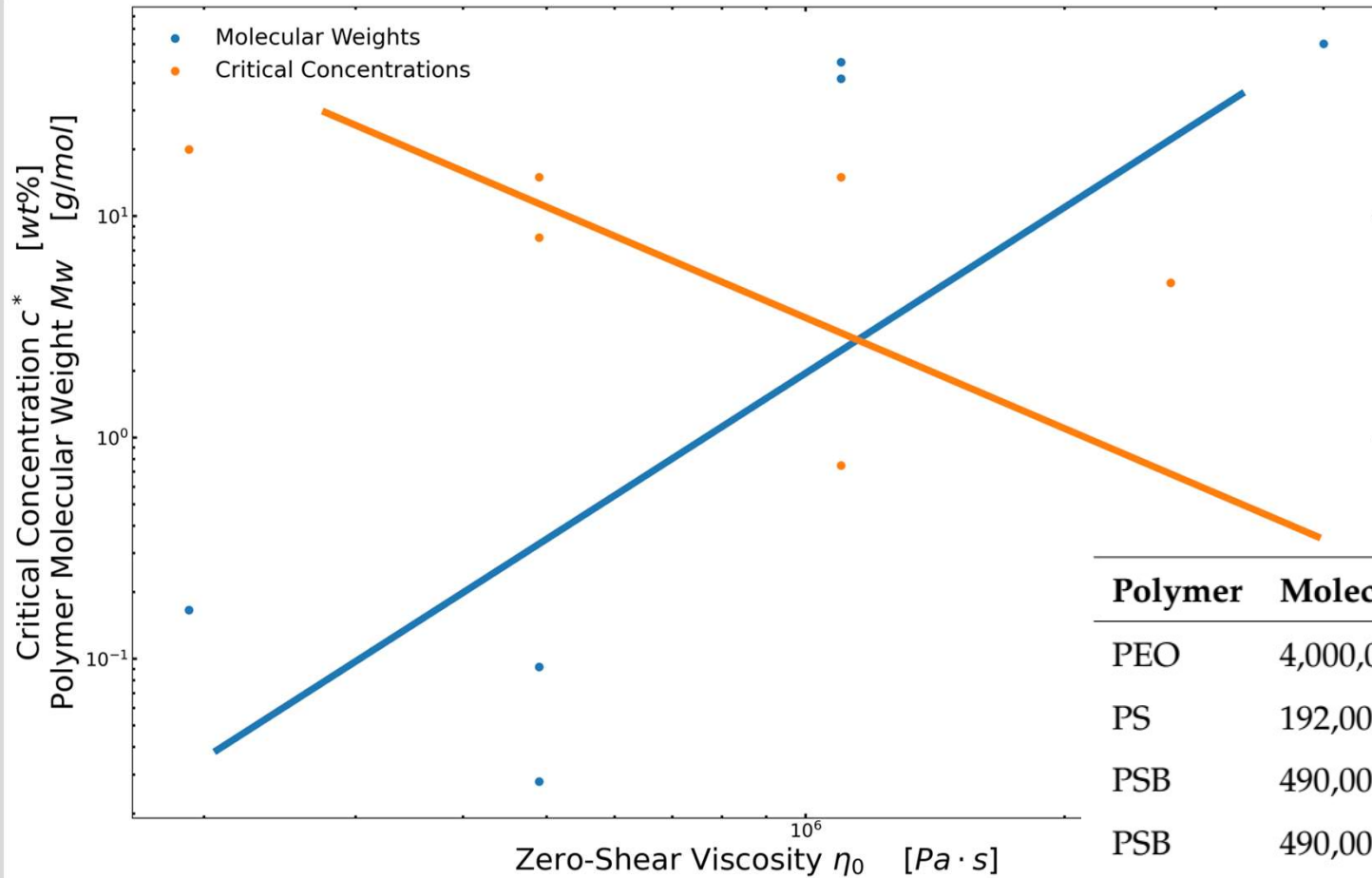
Spinnable/Critical Concentration



Spinnable/Critical Concentration



Conclusion 2.1: Spinnable/Critical Concentration

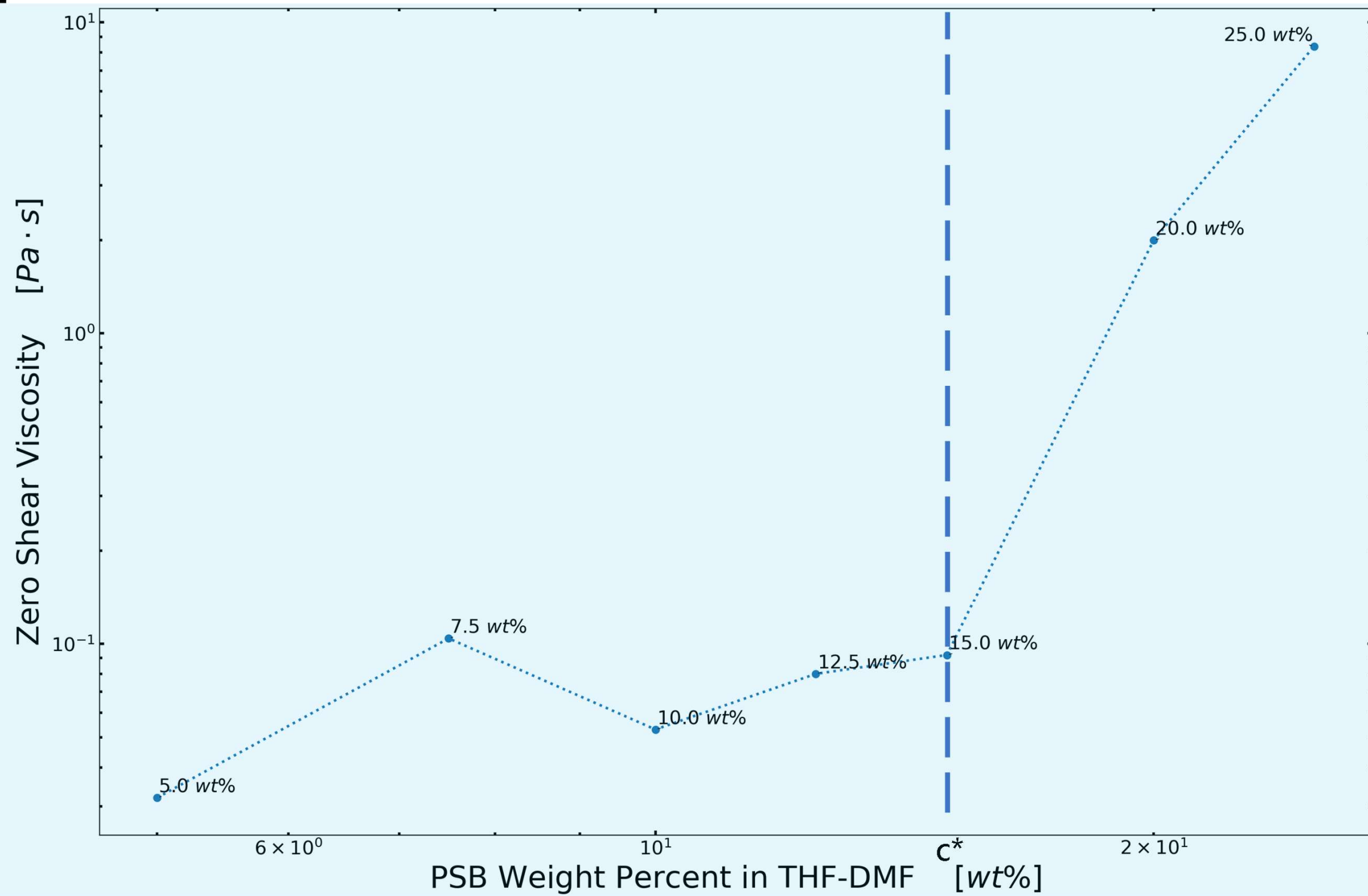


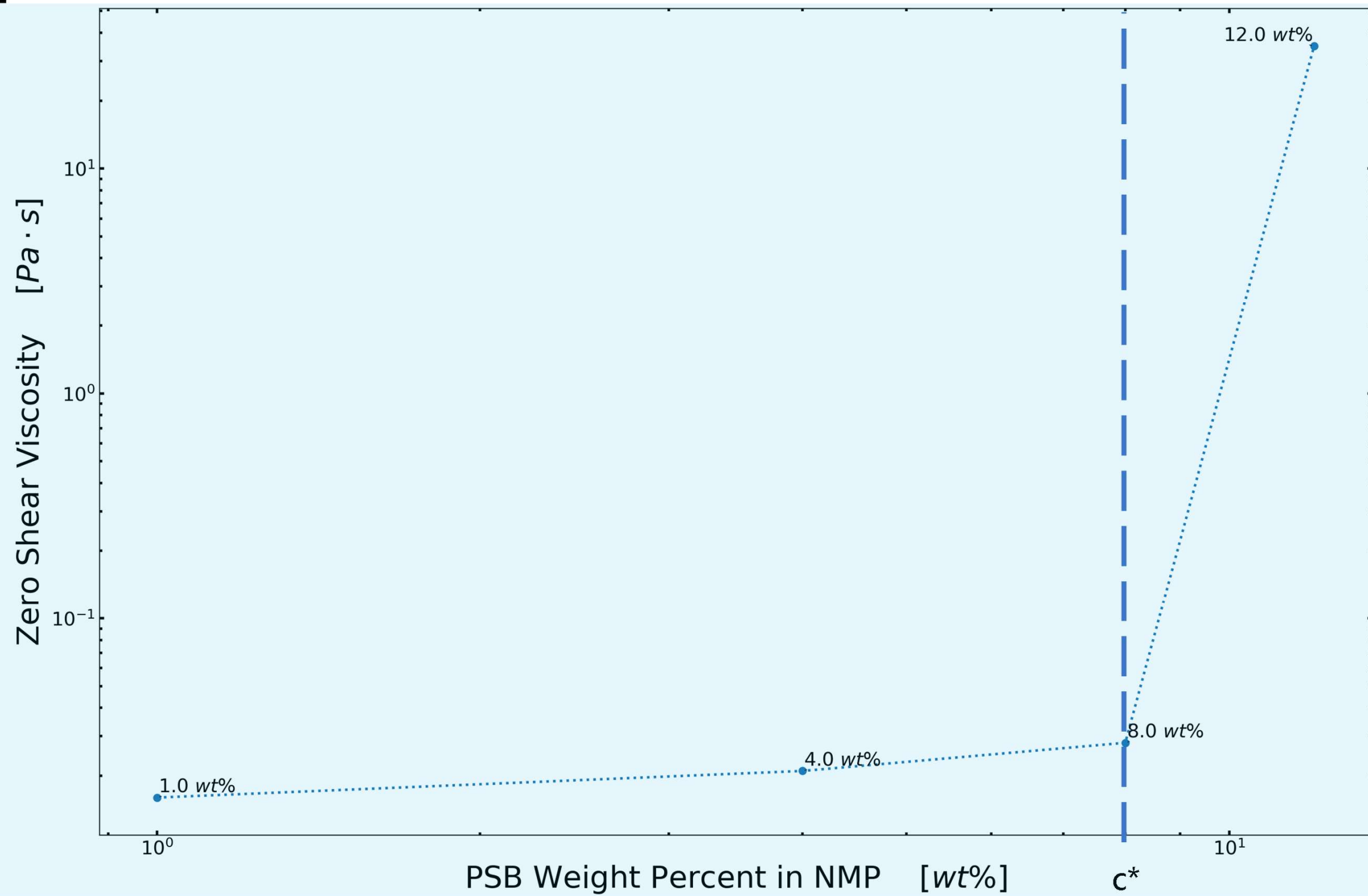
A low molecular weight shall be compensated with higher concentrations to reach a spinnable viscosity.

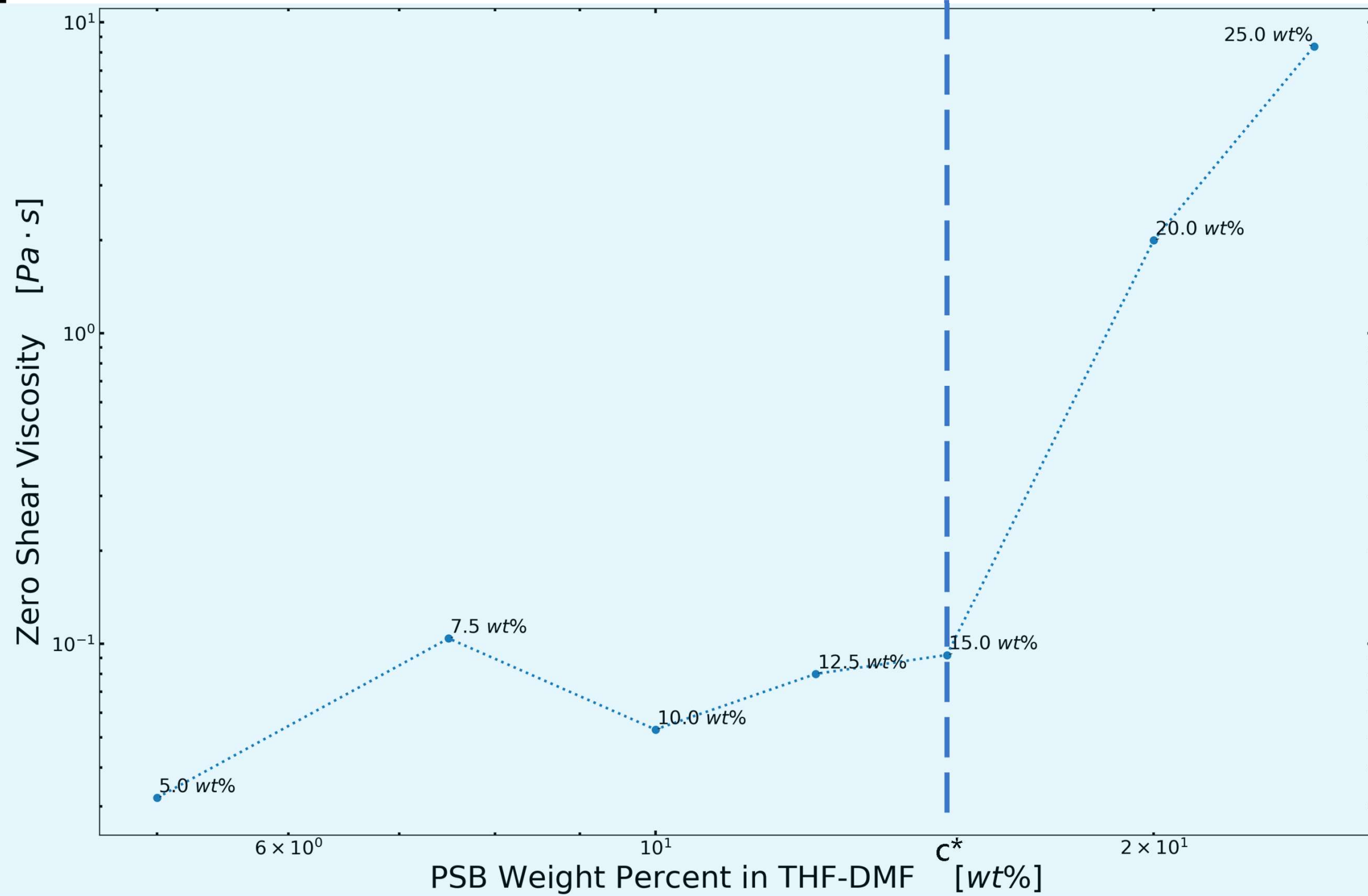
Polymer	Molecular Weight [g · mol]	Solvent	c^* [wt%]	η_0 [Pa · s]
PEO	4,000,000	CPO (SU-8)	0.25	60.022
PS	192,000	THF	20.00	0.166
PSB	490,000	NMP	8.00	0.028
PSB	490,000	THF and DMF	15.00	0.092
PSMS	2,658,076	DMF	5.00	0.282
PVK	1,100,000	CHL	15.00	41.861
PVK	1,100,000	CPO (SU-8)	0.75	49.657

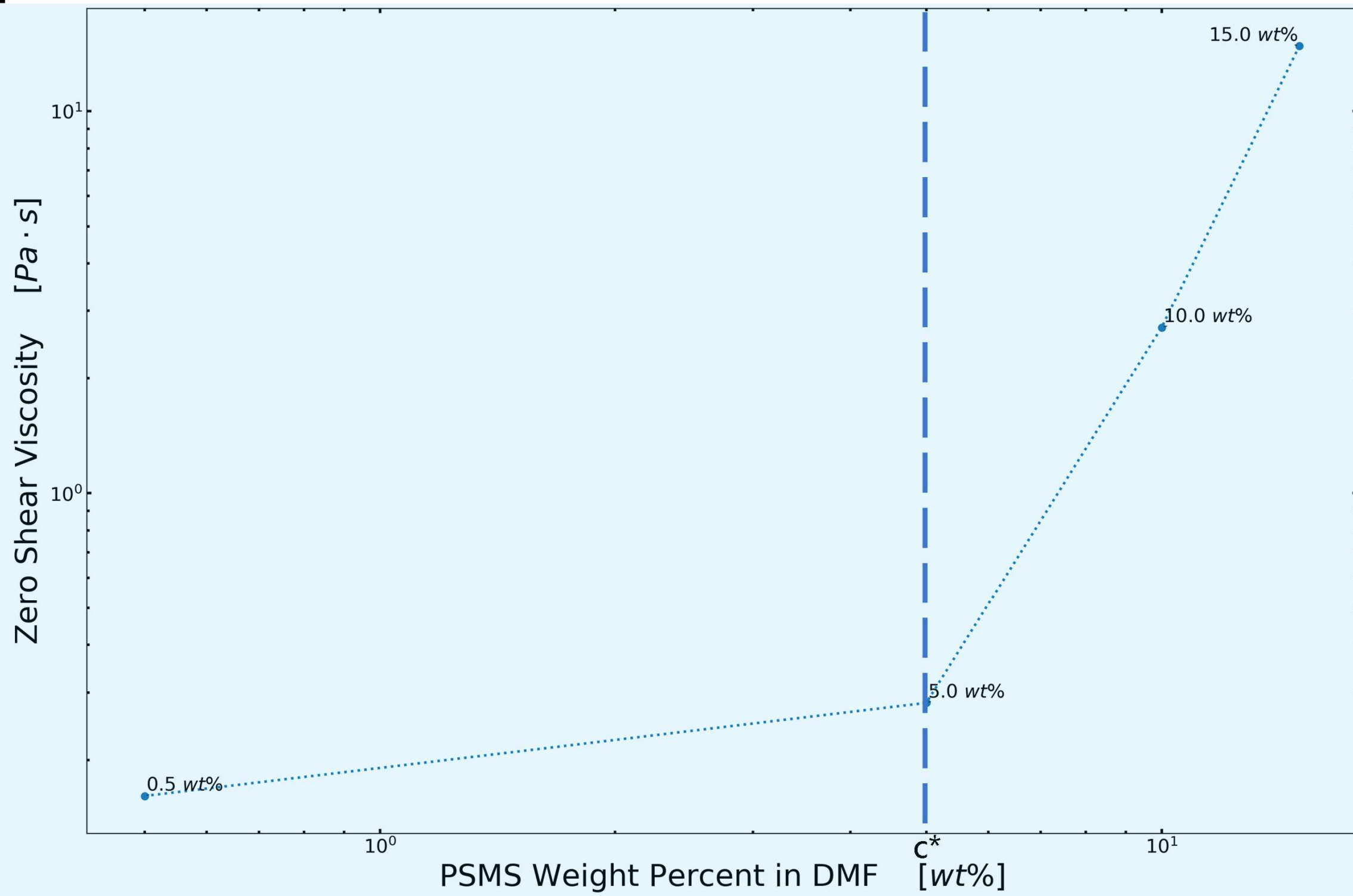
Vu Anh Doan et al. "Interphase transfer of tackifier between poly(butadiene) and poly(styrene-co-butadiene)". In: Journal of Materials Science 48.5 (Mar. 2013), pp. 2046–2052. ISSN: 0022-2461. DOI: 10.1007/s10853- 012- 6974- 1. URL: <http://link.springer.com/10.1007/s10853-012-6974-1>.

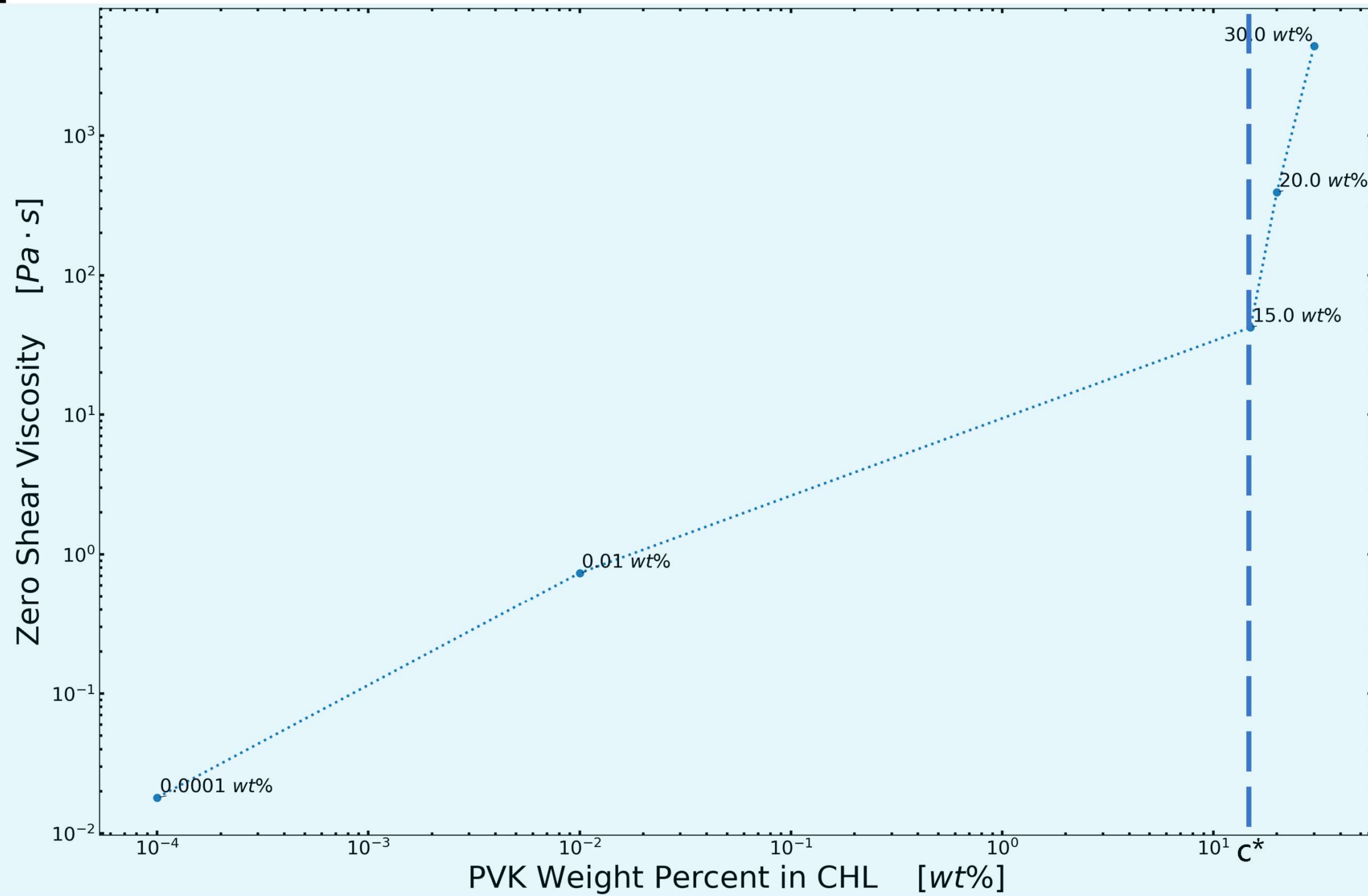
Ralph H. Colby, Lewis J. Fetters, and William W. Graessley. "The melt viscosity-molecular weight relationship for linear polymers". In: Macromolecules 20.9 (Sept. 1987), pp. 2226–2237. ISSN: 0024-9297. DOI: 10 . 1021 / ma00175a030. URL: <https://pubs.acs.org/doi/abs/10.1021/ma00175a030>.

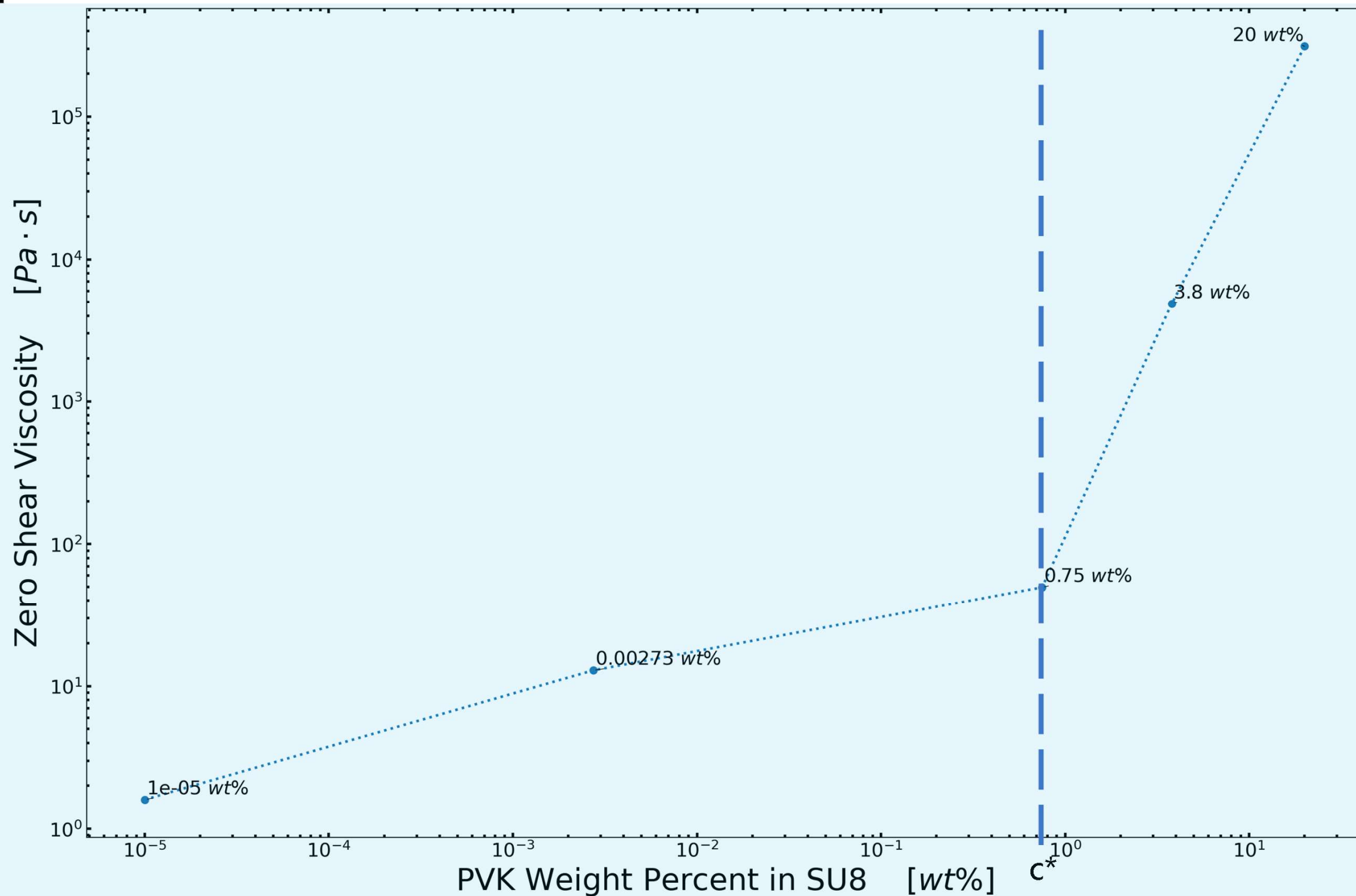






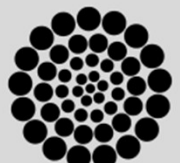






Specific Objective 3. Propose **alternatives** to the SU-8/PEO benchmark formulation for the production of microscopic polymer fibers with potential for the fabrication of carbon nano-wires.

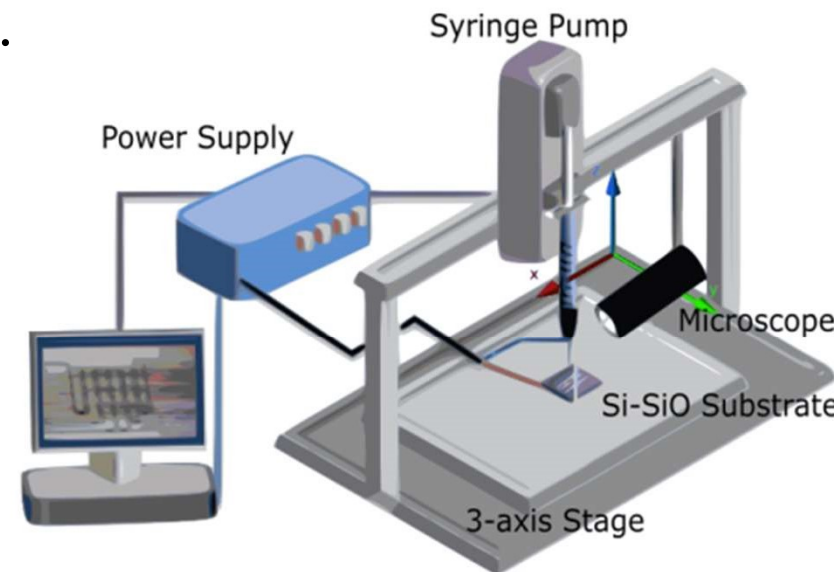
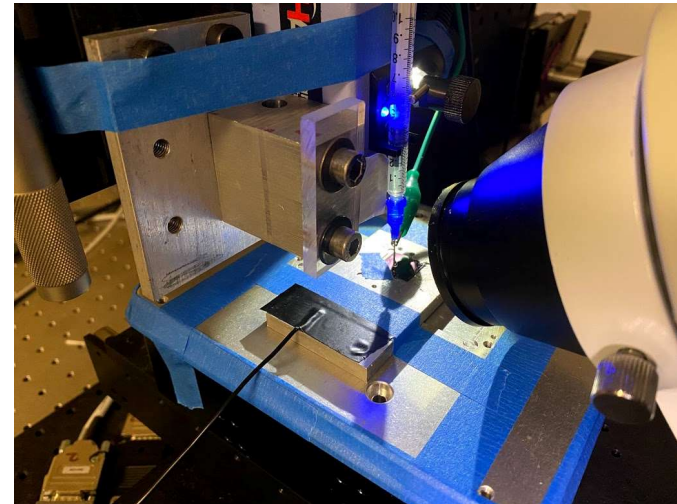
Fabrication & Characterization



Methods: Design of experiments / NFES

Given the results of previous work, the experiments shall reflect:

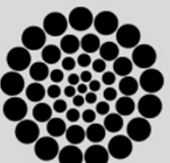
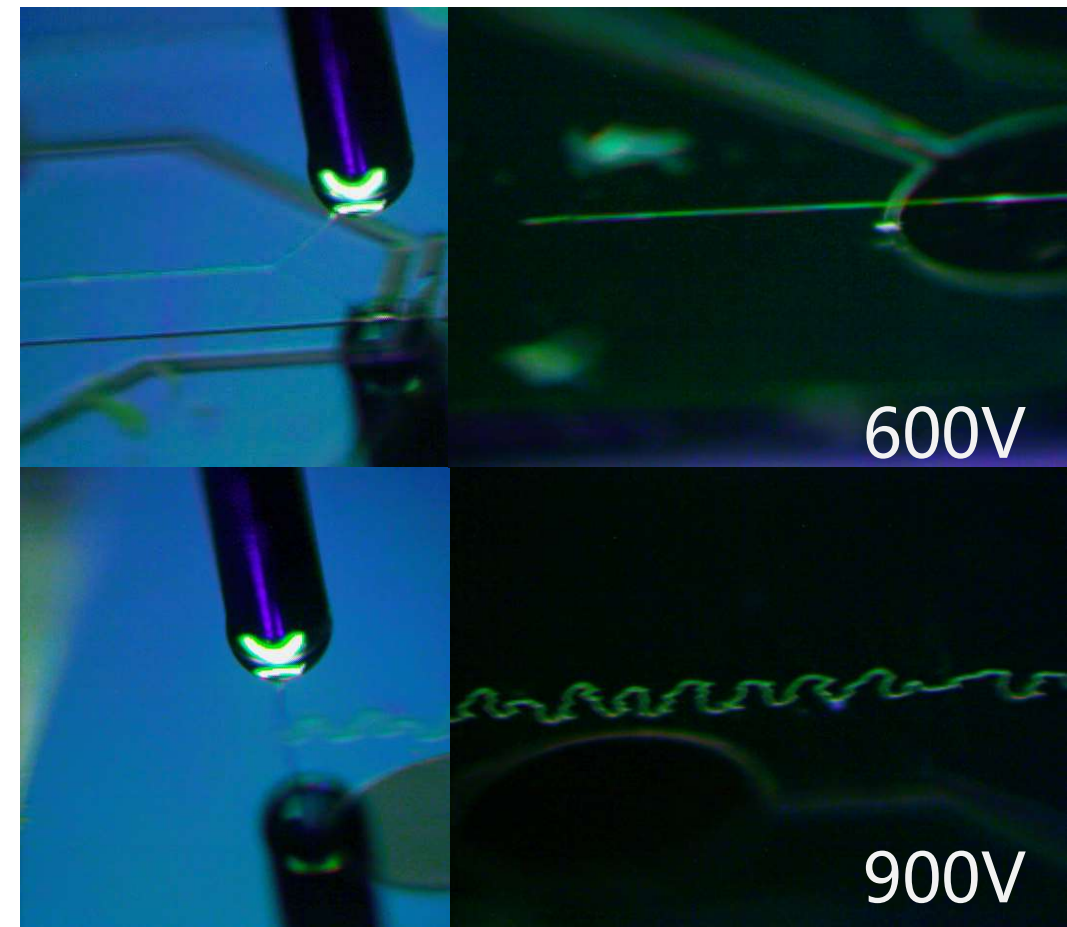
- The SU8-PEO sample set is the control
- The calculated critical concentration were used for each sample set.
- Each sample was electrospun at different applied voltages from 200 to 600V
 - Other process parameters (working distance, stage velocity, flow rate) are to be tuned and remain constant during NFES.



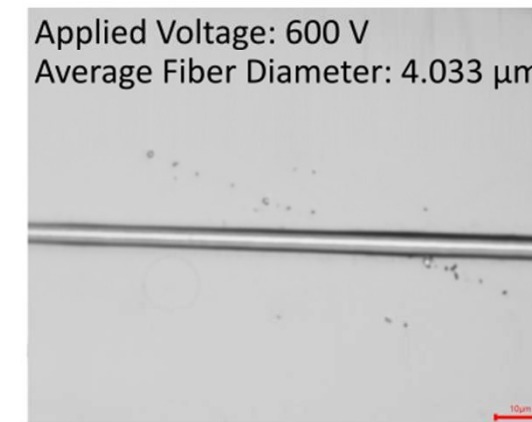
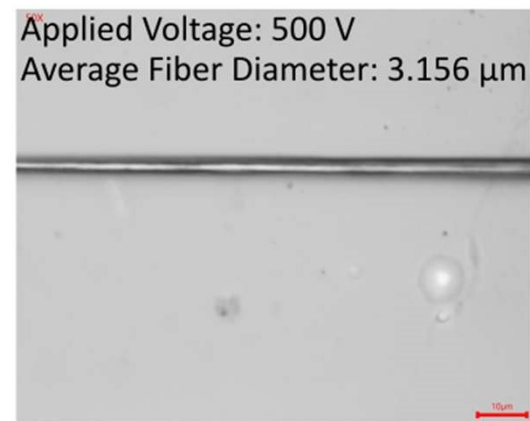
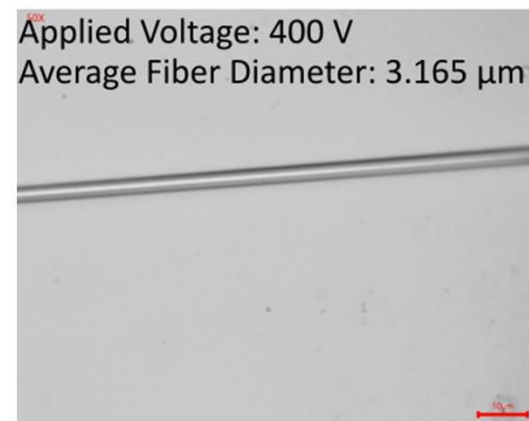
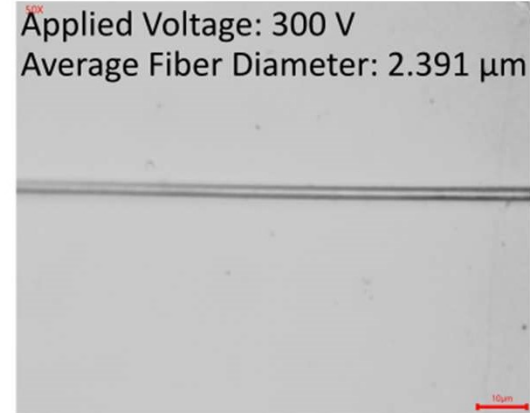
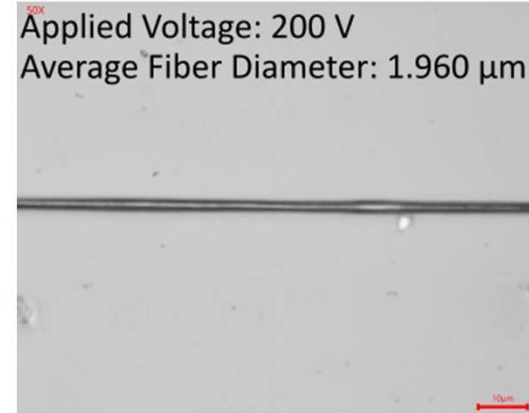
Fabrication: Process Parameters

- Fabrication velocity: 10 mm/s
- Working distance: 0.5 mm
- Applied voltage: 200V to 600V
- Applied current: 10 uA
- Flow rate: 0.04 uL/min
- Spacing: 10um

0.25 wt% PEO in SU-8



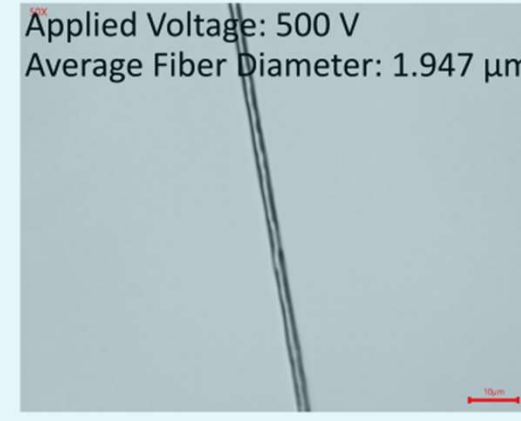
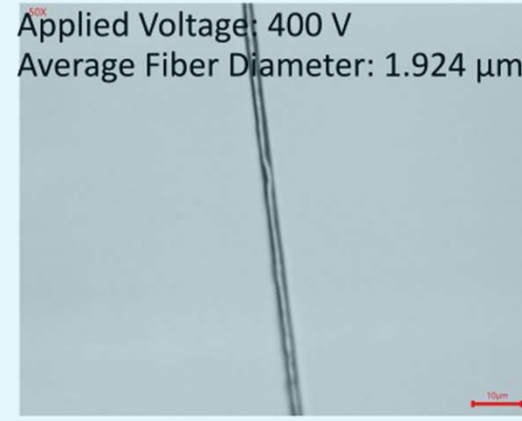
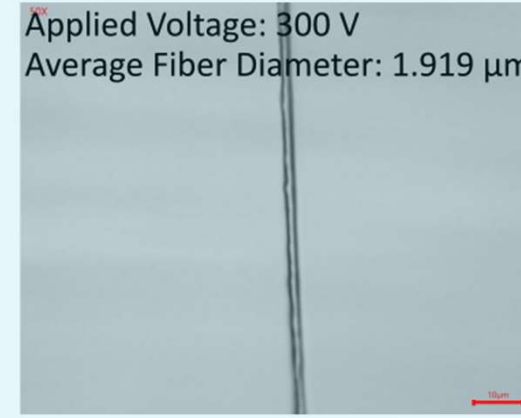
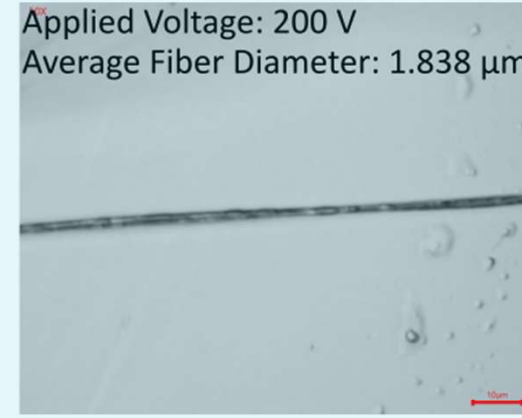
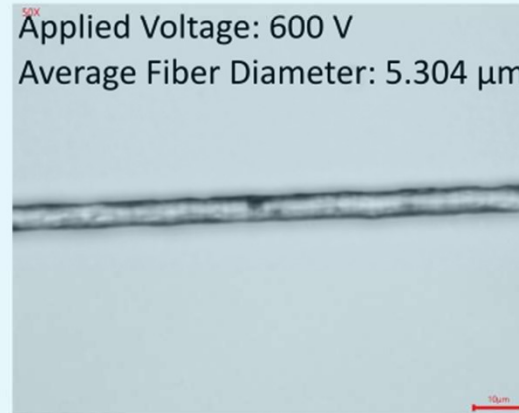
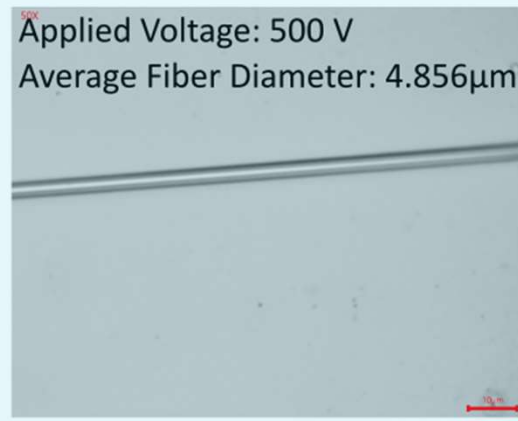
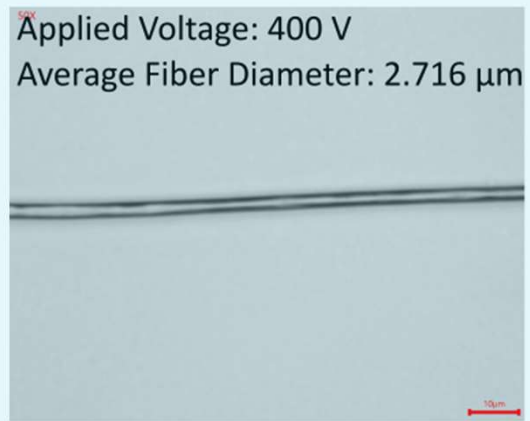
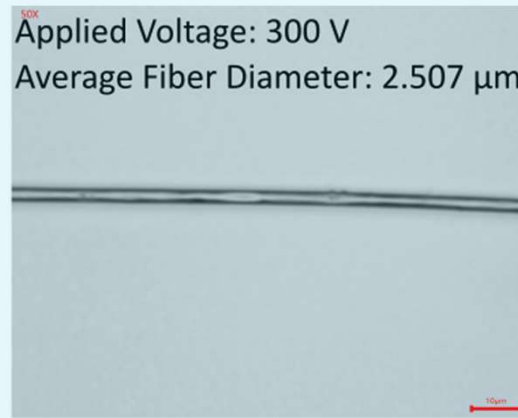
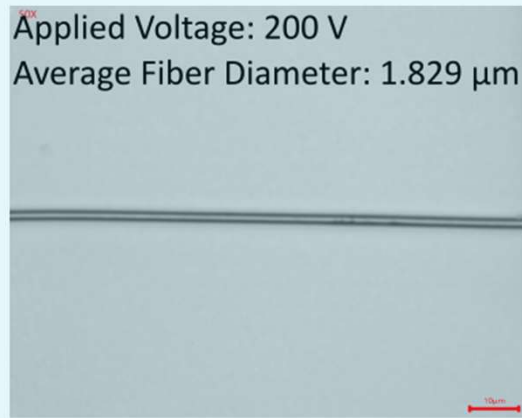
Characterization:



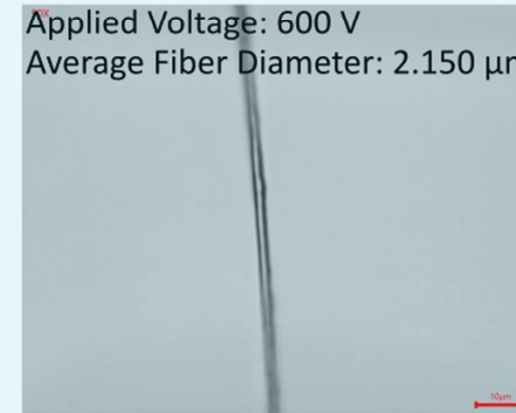
PEO in
SU-8



PS in
THF

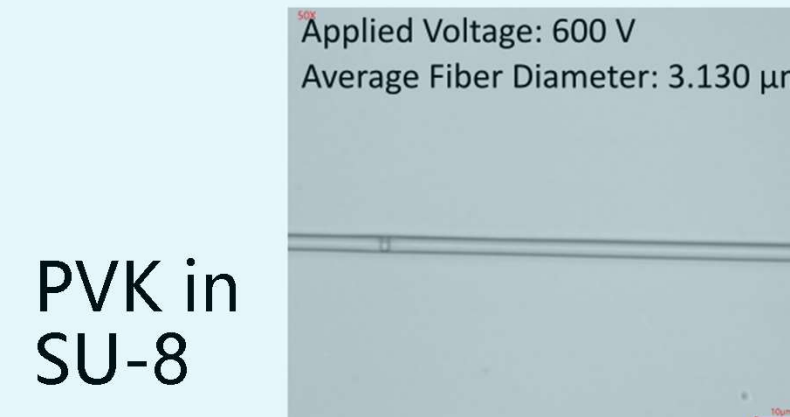
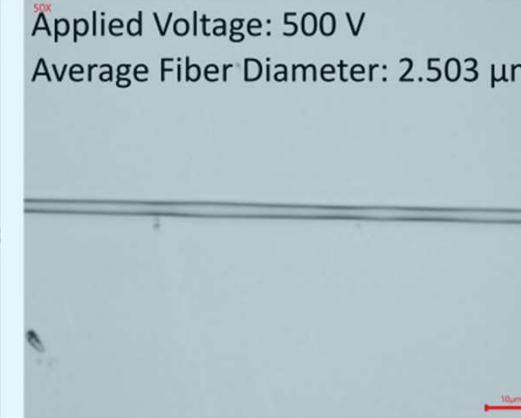
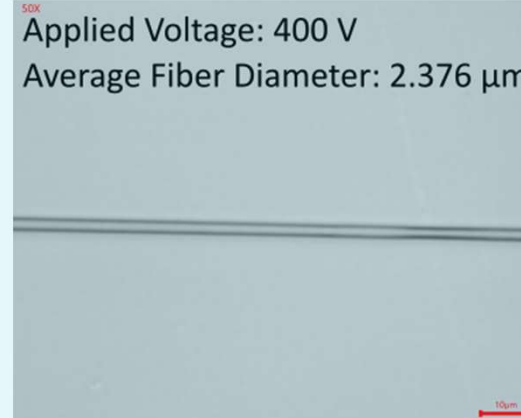
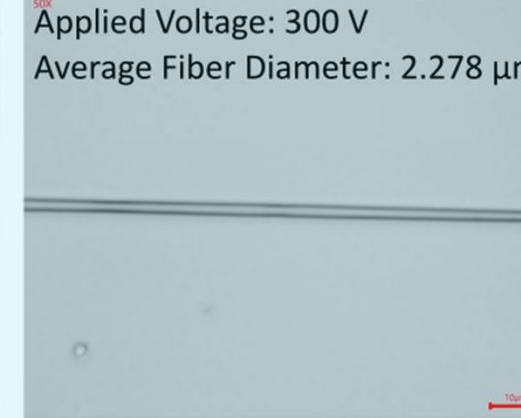
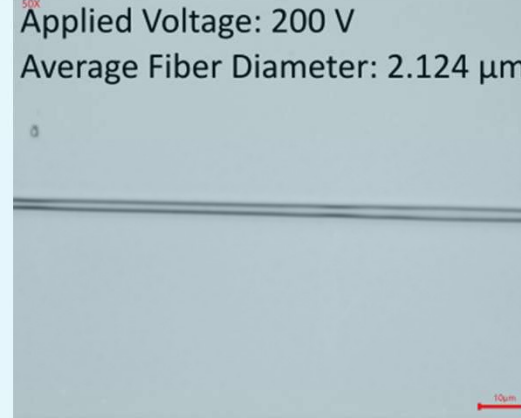
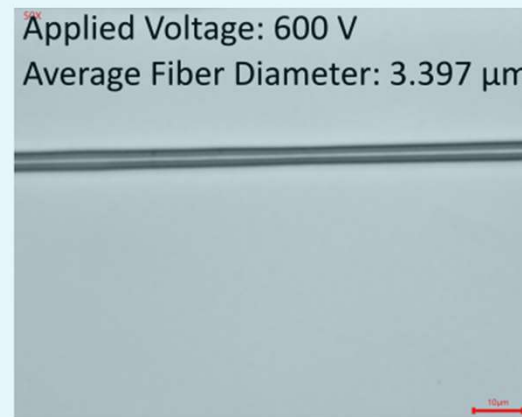
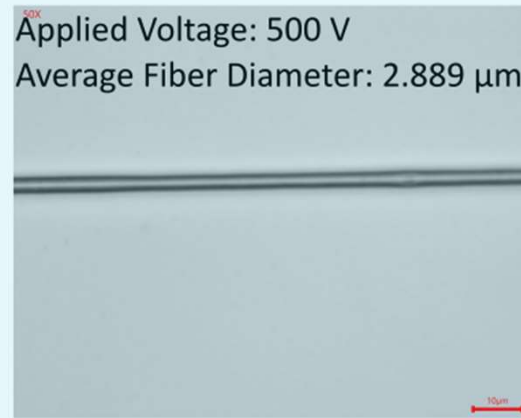
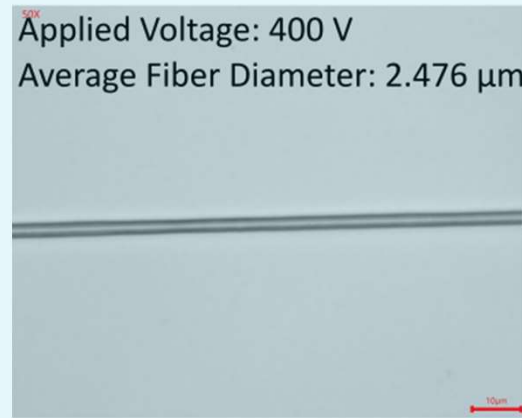
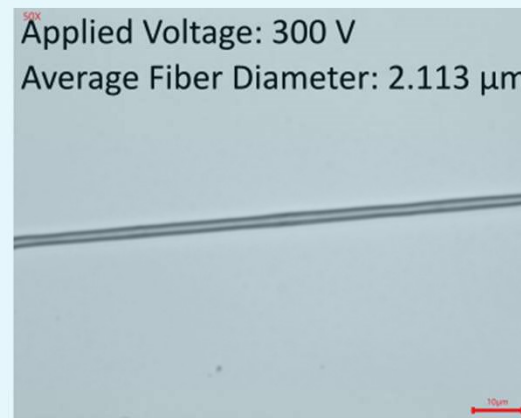
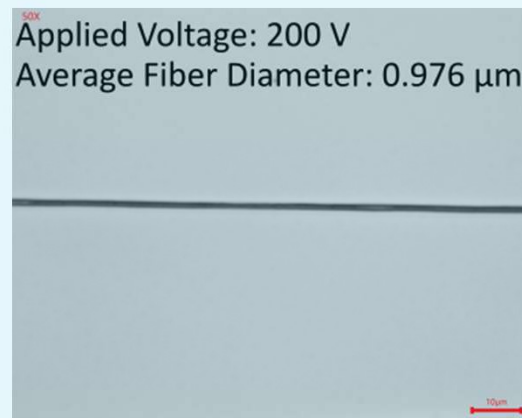


PSB in
THF
and
DMF



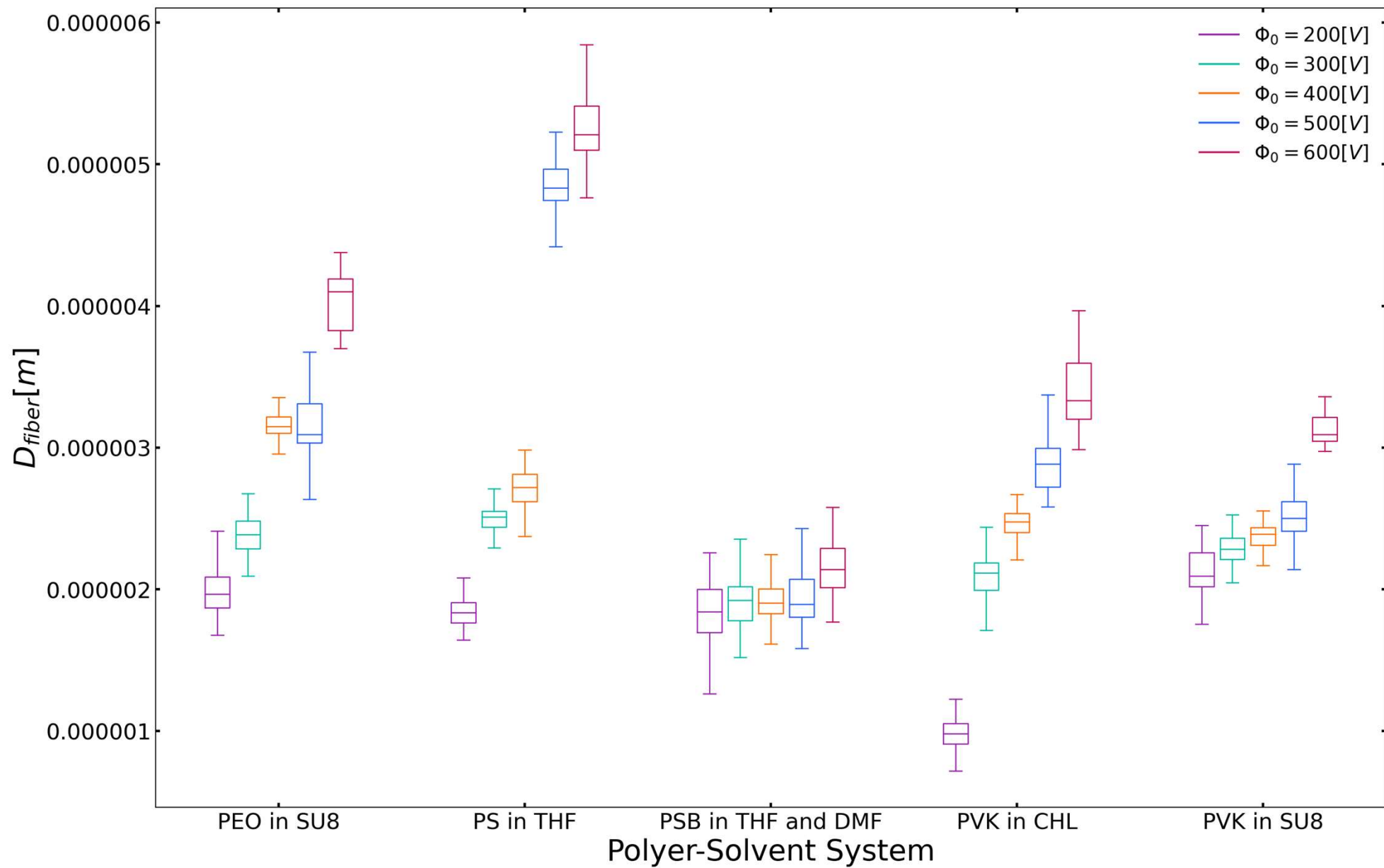


PVK in CHL



PVK in SU-8

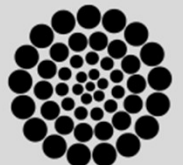
Results: Spinnable solutions



Conclusion 3.1: non-spinnable solutions

Polymer / Solvent	Critical / spinnable concentration	Rationale
Poly(Styrene-co-alpha-Methylstyrene) (PSMS) in N,N-Dimethylformamide (DMF)	5 wt% (and 10, 15 wt%)	Fibres were broken into agglomerates / dust
Poly(Styrene-co-Butadiene) (PSB) in 1-Methyl-2-Pyrrolidinone (NMP)	8.00 wt%	Development of a shell around the drop.

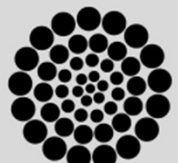
Conclusions & Future Work



Helgeson's Dimensionless analysis

Helgeson's model was thought to work with **far-field electrospinning**, hence the deviation of the NFES data from the model trend.

For an accurate NFES fiber diameter prediction, the **mechanical stresses** introduced by the moving stage shall be considered in the model



Pyrolysis Process

This work verifies the electro-spinnability of four new formulations and one modification to the PEO/SU-8 solution, however **fibers were not carbonized** into carbon structures.

Further work shall **study the pyrolysis process** of the proposed fibers to get carbon structures with good electrical conductivity.

A photo-polymerization process could be introduced before pyrolysis to increase the order of the molecules and achieve carbon with higher conductivity.



Process Parameters

The viscosity-concentration plot is a helpful tool to estimate the critical spinnable concentration of a polymer-solvent system as NFES solutions require specific viscosities to initiate a polymer jet. However there is room for improvement as this method **only considers rheological data.**

Other methods could be adopted to better **tune other process parameters** such as stage velocity, and applied voltage.



Thank You

Tecnológico
de Monterrey

CONACYT

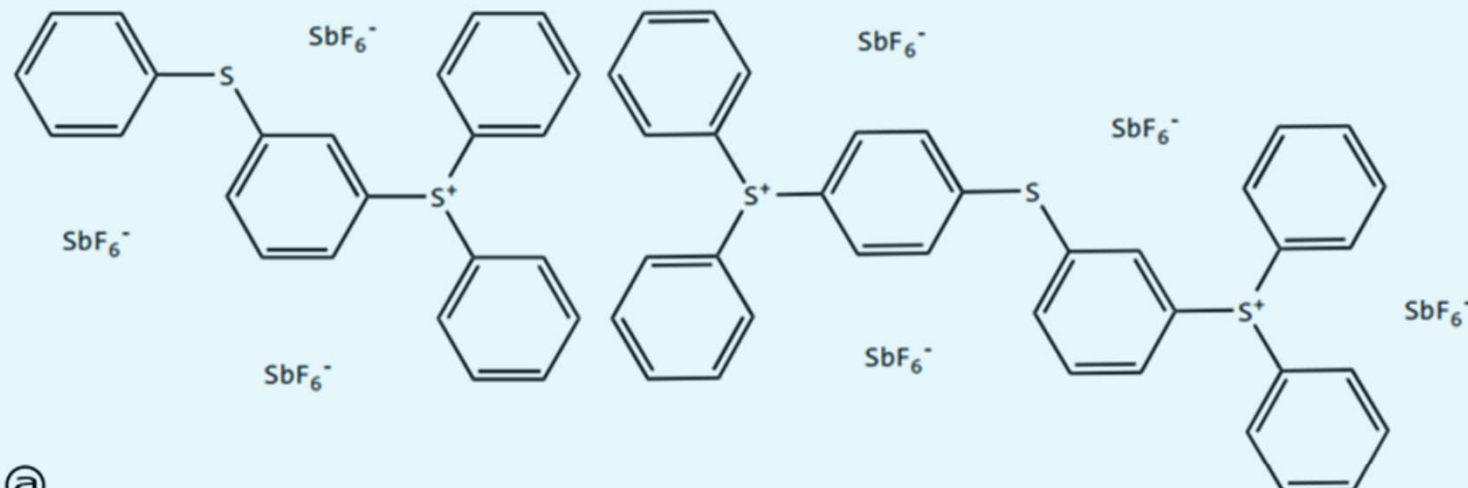
Consejo Nacional de Ciencia y Tecnología



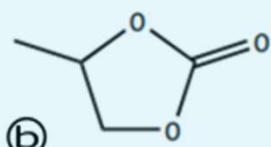


Any Questions?

SU-8 (MicroChem, US)



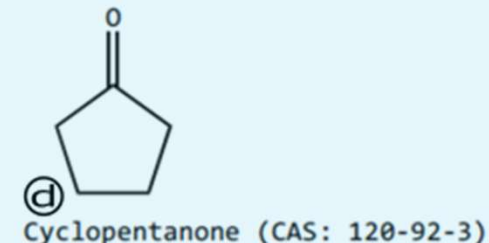
a Mixed Triarylsulfonium/Hexafluoroantimonate Salt (CAS: 89452-37-9)/(CAS: 71449-78-0)



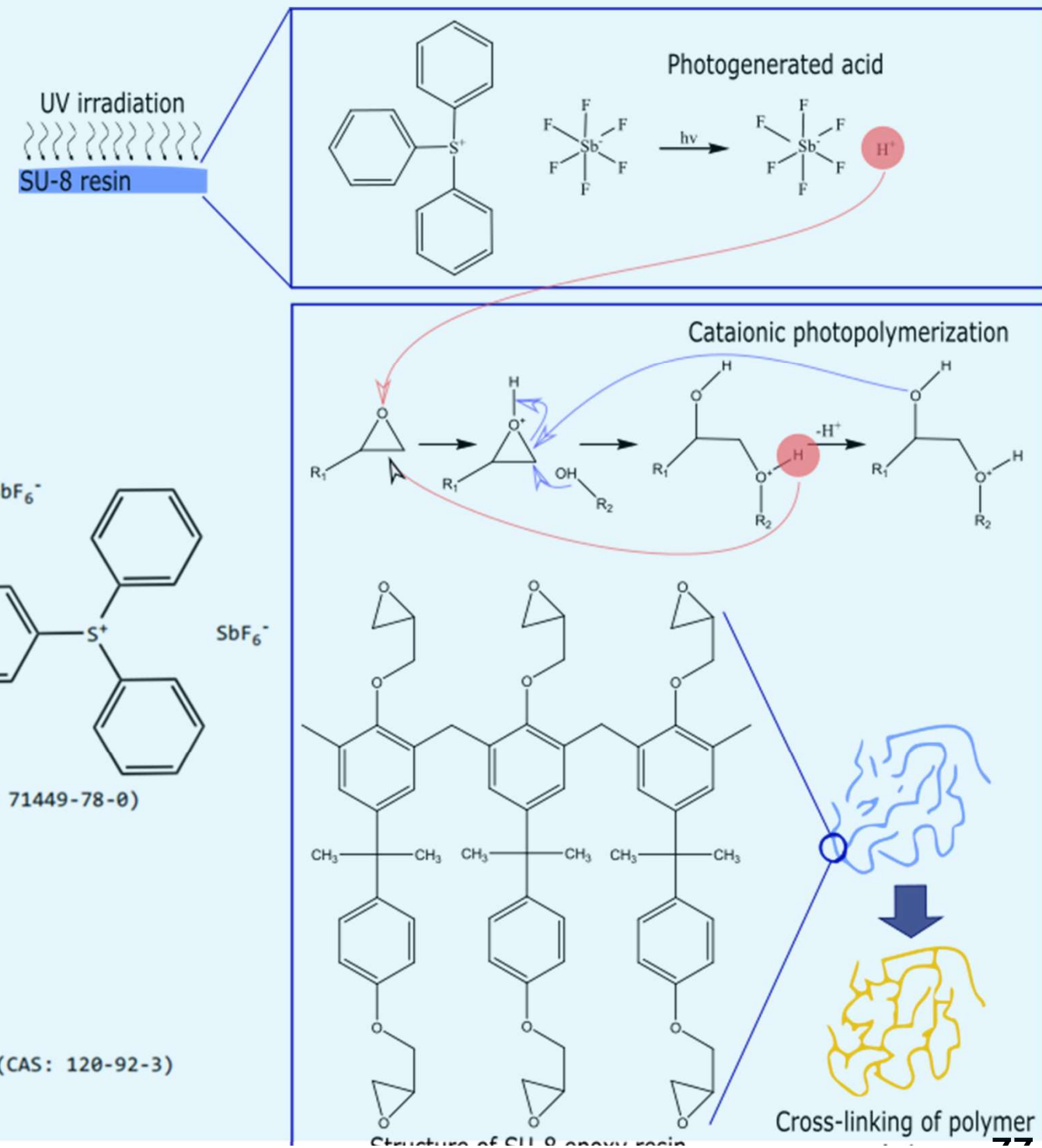
b Propylene Carbonate (CAS: 108-32-7)



c Epoxy Resin (CAS: 28906-96-9)



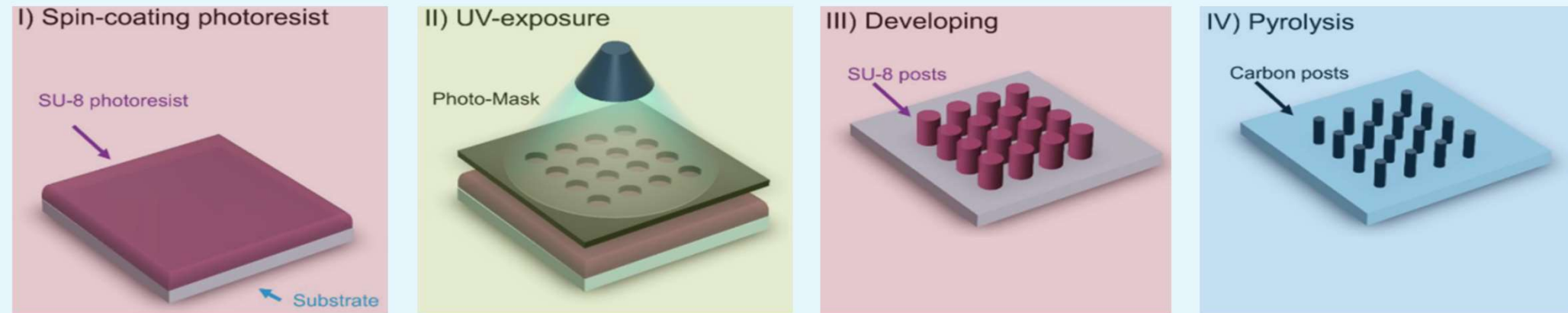
d Cyclopentanone (CAS: 120-92-3)



Carbon nanostructures via Lithography

The production of C-MEMS:

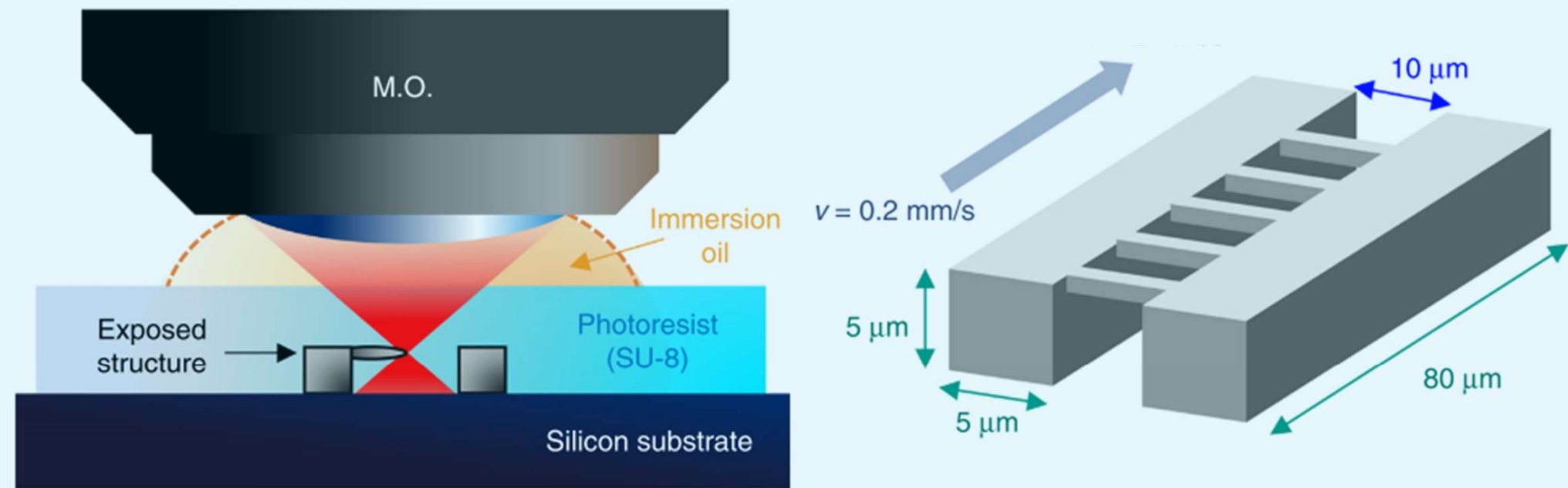
1. Polymer patterning through ~~photolithography~~
electrospinning
2. Carbonization through **pyrolysis**



photolithography
process

- SU-8 Waste
- Physical & Optical Limitations
- Structure Limitations

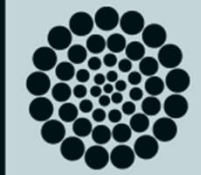
TPP – Two-Photon Polymerization

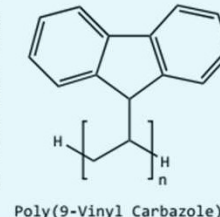
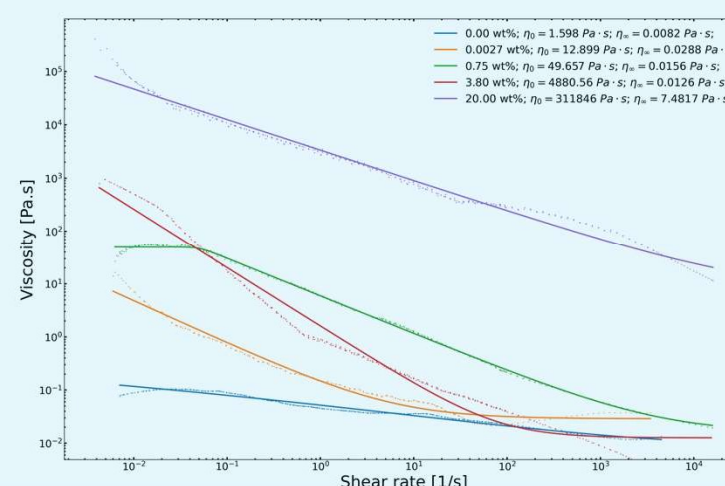
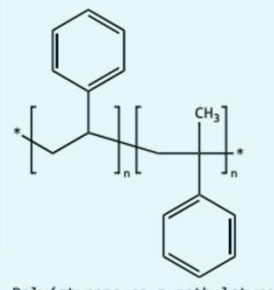
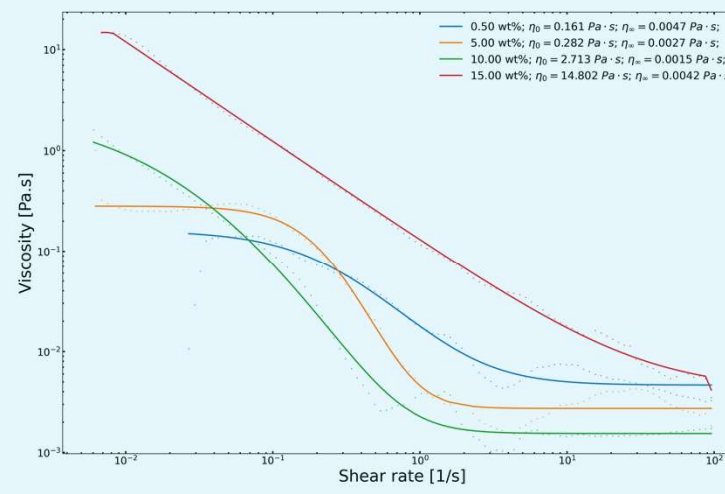
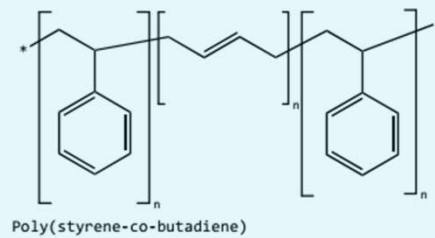
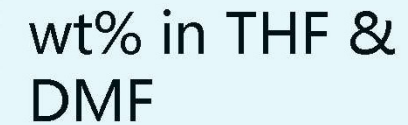
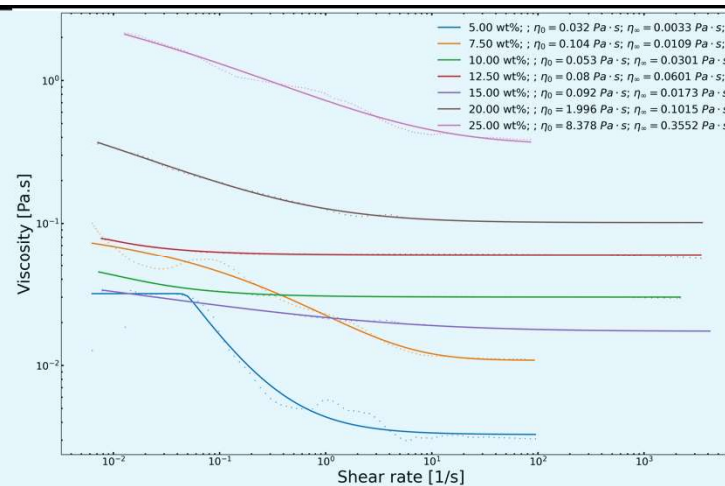
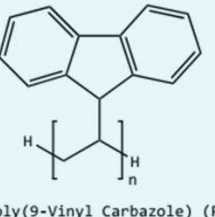
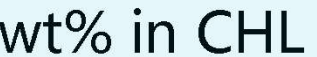
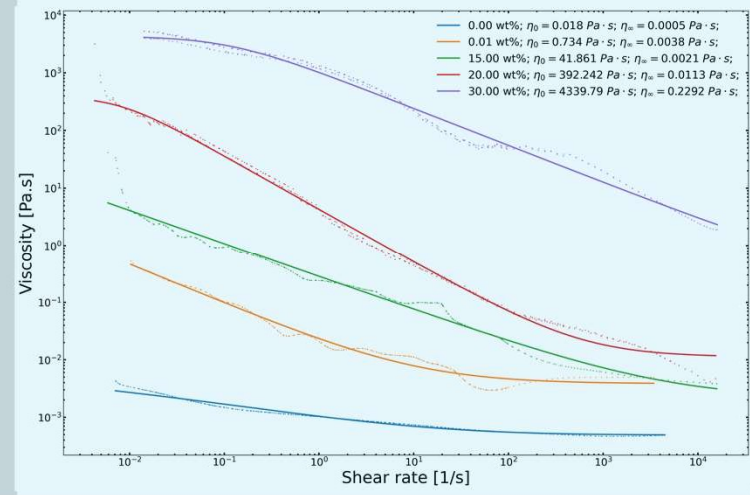
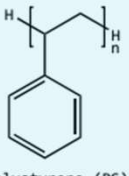
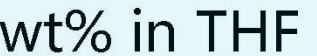
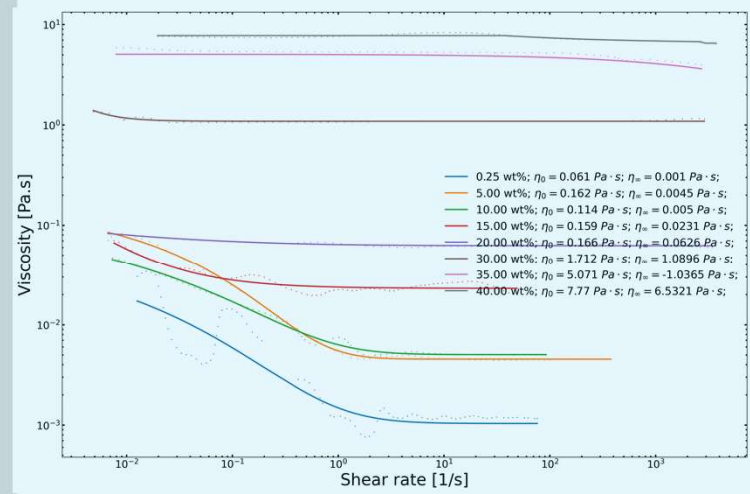
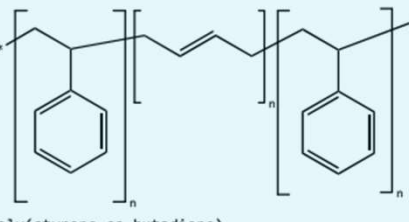
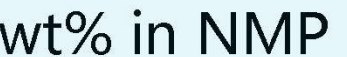
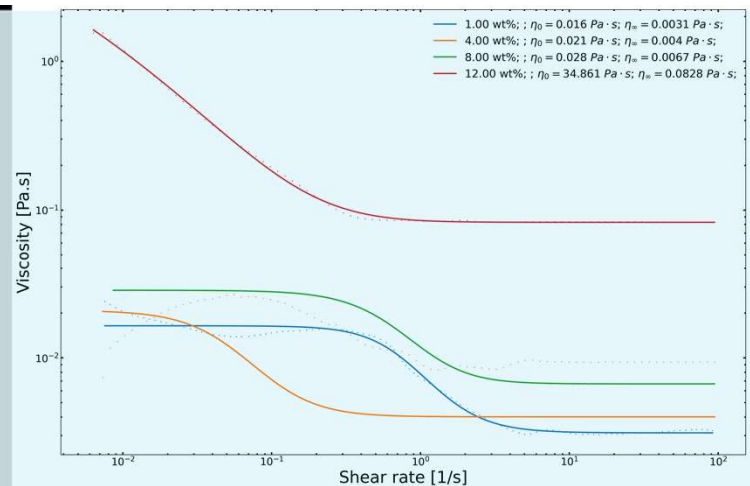


B. Cardenas-Benitez, C. Eschenbaum, D. Mager, J.G. Korvink, M.J. Madou, U. Lemmer, I. De Leon, S.O. Martinez-Chapa, Pyrolysis-induced shrinking of three-dimensional structures fabricated by two-photon polymerization: experiment and theoretical model, *Microsystems Nanoeng.* 5 (2019). <https://doi.org/10.1038/s41378-019-0079-9>.

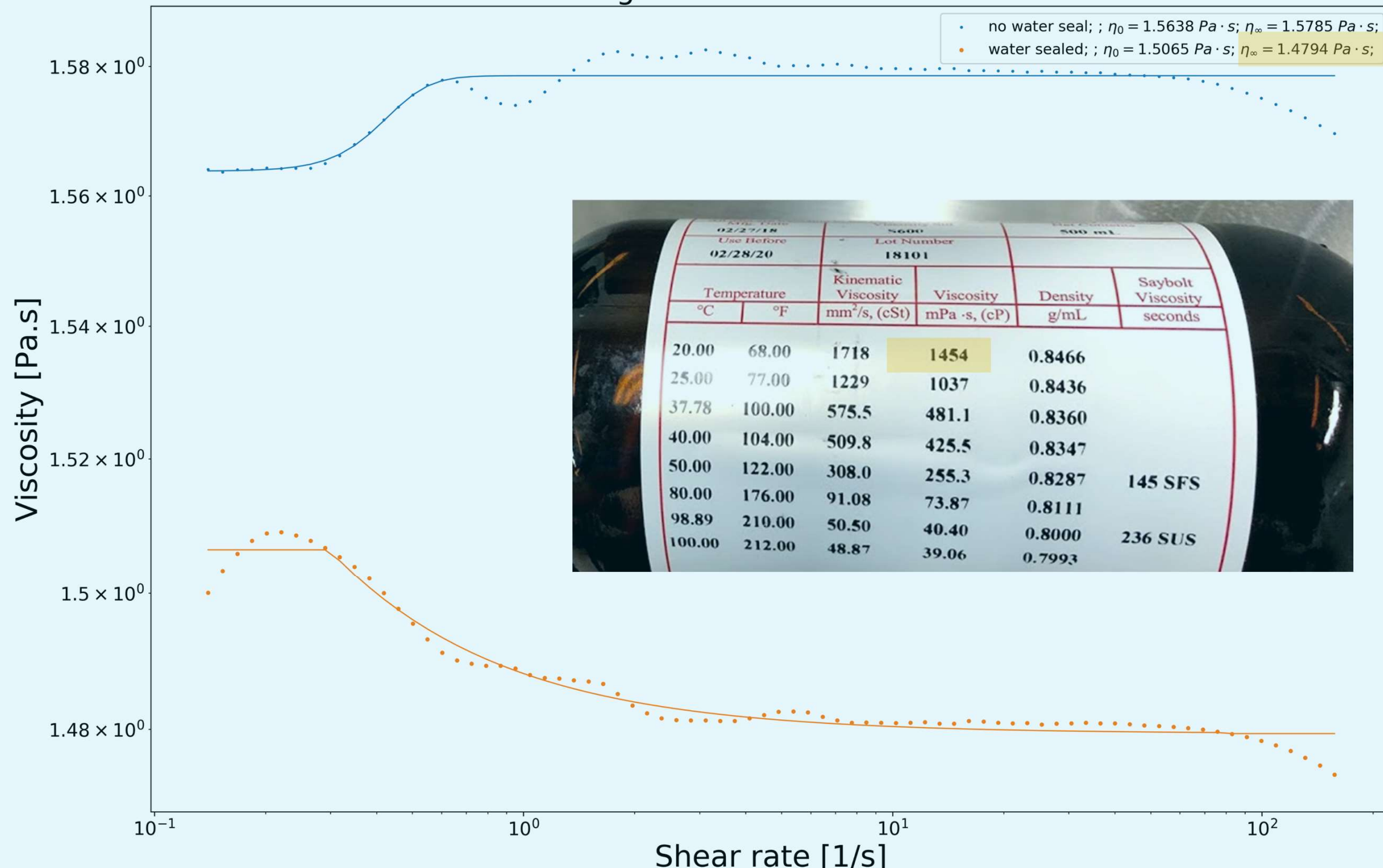
Characterization of the 0.25 wt% PEO Solution

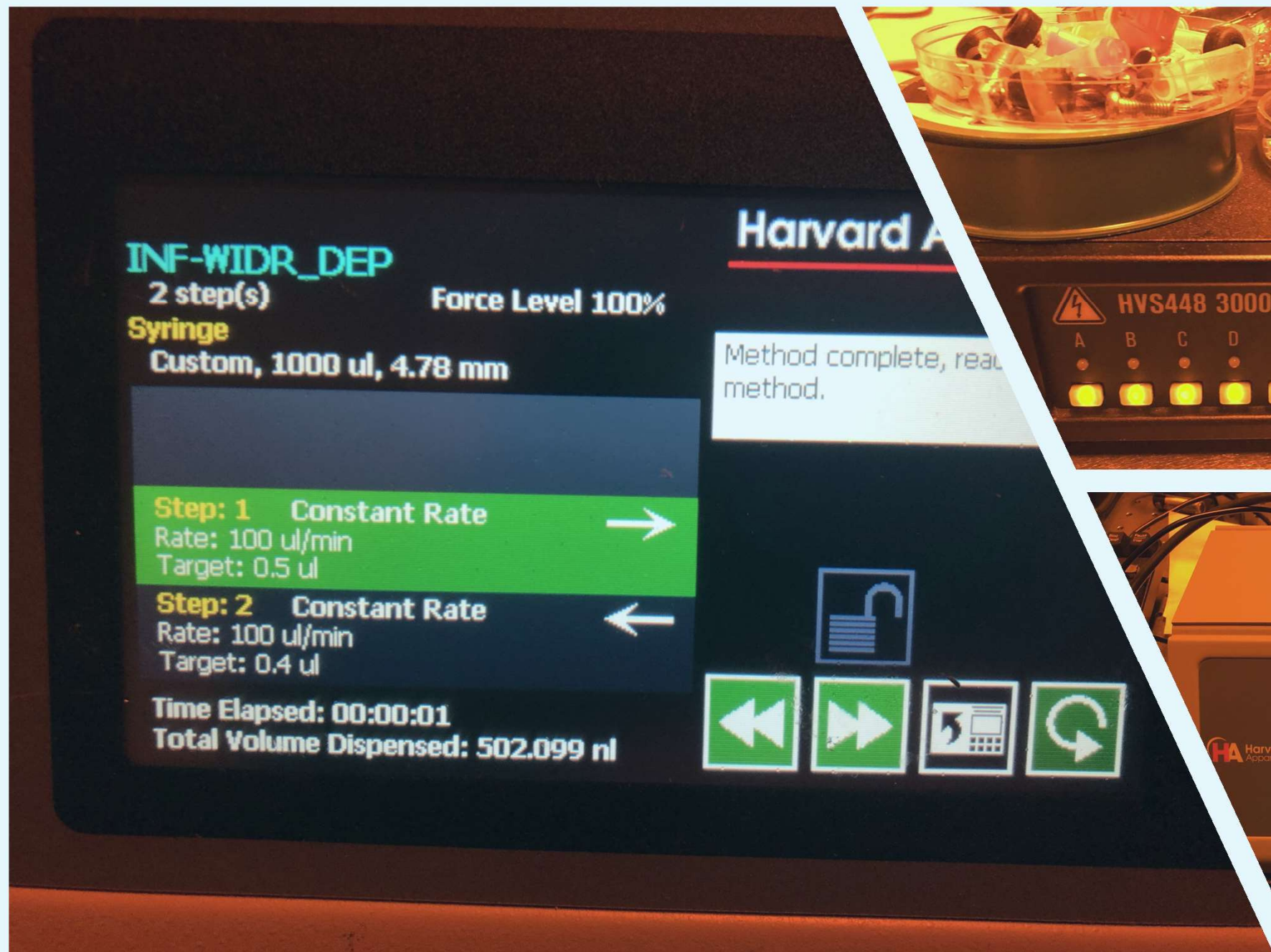


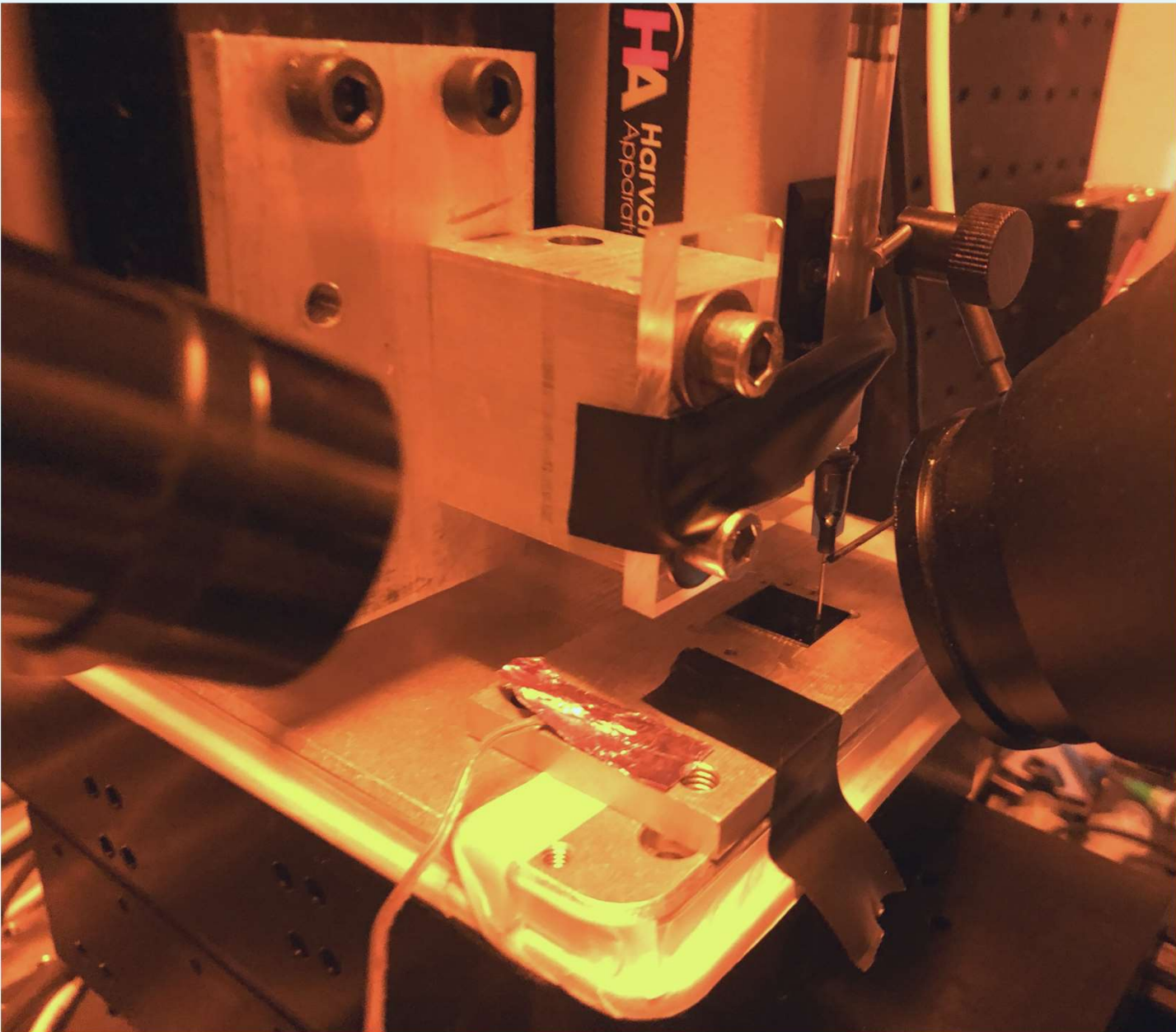
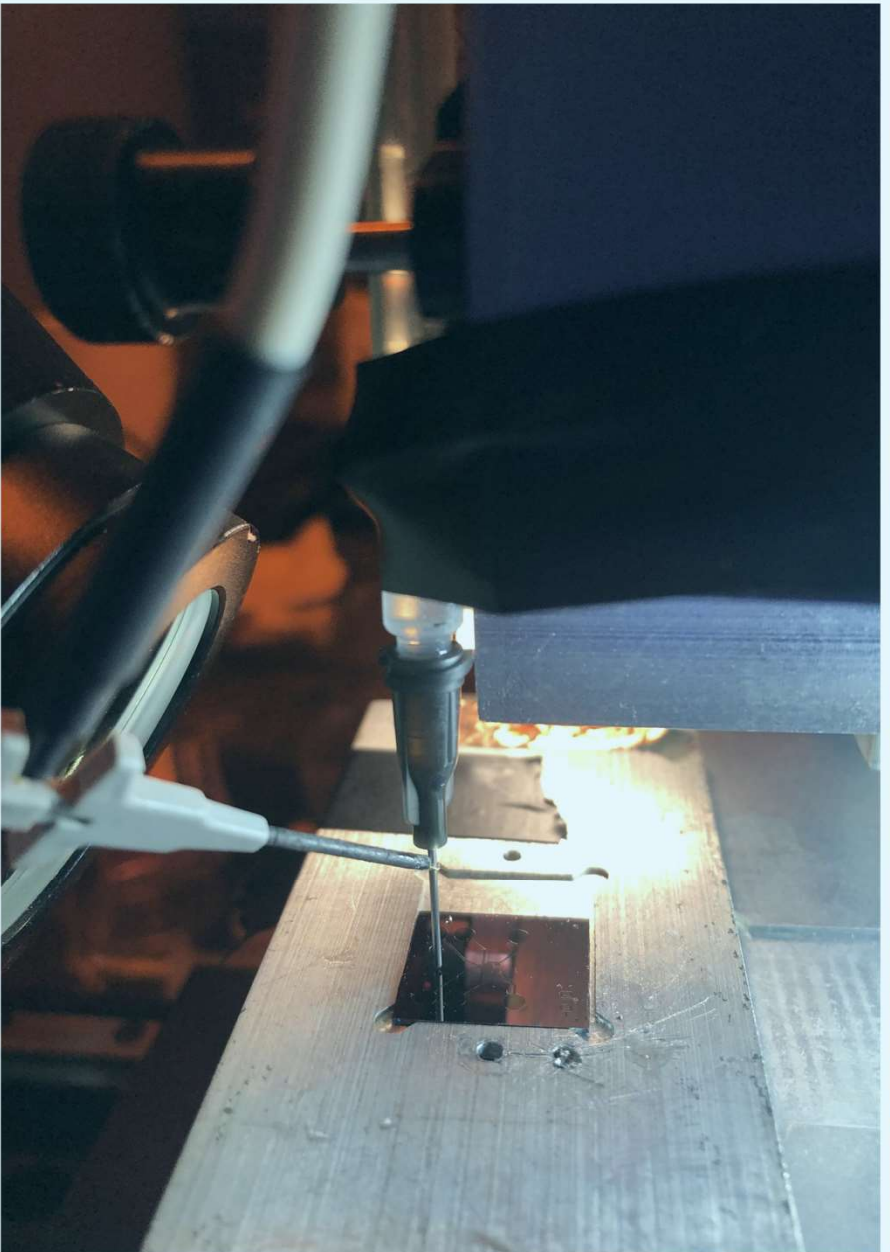




Standard Conforming to ASTM Oil Standard - Water Seal Test







SU-8 (MicroChem, US)

MICROCHEM CORP SU-8 2002 500ML

encompass

Manufacturer: MICROCHEM CORP Y111029

Catalog No.	NC0702370
\$628.71 / Each	
Qty	<input type="text"/> Check Availability
	Add to cart

<https://www.fishersci.com/shop/products/NC0702370/nc0702370#?keyw ord=MICROCHEM+CORP+PHOTORESIST+SU-8>

MICROCHEM CORP SU-8 DEVELOPER 4L

encompass

Catalog No. NC9901158

\$172.90 / Each

INGREDIENTS:

Cyclopentanone (CAS: 120-92-3); 23-78%.
Mixed Triarylsulfonium/ Hexafluoroantimonate Salt;
(CAS: 89452-37-9)/(CAS: 71449-78-0); 1-5%
Propylene Carbonate (CAS: 108-32-7); 1-5%
Epoxy Resin (CAS: 28906-96-9); 25-75%

<https://www.fishersci.com/shop/products/NC9901158/nc9901158#?keyw ord=SU-8++developer>

Materials

Safety Solvents		CAS Number	Presentation
	1-Methyl-2-pyrrolidinone (NMP)	872-50-4	anhydrous, 99.5% 328634-100ML 328634-1L
	Dichloromethane (Methylene chloride)	75-09-2	anhydrous, ≥99.8%, 40-150 ppm amylene as stabilizer 270997-100ML 270997-1L
	Dimethylacetamide (DMAc)	127-19-5	anhydrous, 99.8% 271012-100ML 271012-1L
250 ml	Dimethylformamide (DMF)	68-12-2	anhydrous, 99.8% 227056-100ML 227056-1L
1 L	Tetrahydrofuran (THF)	109-99-9	anhydrous, ≥99.9%, inhibitor-free 401757-1L
	Dihydrolevoglucosenone (Cryene)	53716-82-8	807796-100ML 807796-1L
Polymers			
	Polystyrene (PS)	9003-53-6	average Mw 192,000 430102-1KG
	Poly(styrene-co-butadiene)	9003-55-8	butadiene 4 wt. %, melt index 6 g/10 min (200°C/5kg) 430072-1KG
	Poly(styrene-co- α -methylstyrene)	9011-11-4	457205-250G
	Polybenzimidazole (PBI)	26985-65-9	rod, diam. 9.5 mm, L 25 mm, black GF31259527-1EA
	Polyaniline (PANI / emeraldine salt)	25233-30-1	average Mw >15,000, powder (Infusible), 3-100 μ m particle size 428329-5G
	Polyvinylcarbazole (PVK)	25067-59-8	average Mw ~1,100,000, powder, 182605-5G

title:

- <a point>
- <another point>

<content> <**key concept**> <**key concept**>

